Iron-oxides and Iron-citrate as new photocatalysts in solar inactivation of Escherichia coli in water: Mechanistic aspects

PAR

Cristina del Socorro LONFAT

EPFL

ÉCOLE POLYTECHNIQUE
FÉDÉRALE DE LAUSANNE

Suisse
2015

A Helena y Valentin

Remerciements

Je crains qu'il soit difficile de mentionner ici toutes les personnes qui, à leur manière et d'une façon ou d'une autre, m'ont apporté leur soutien tout au long de la réalisation de cette étude. Je leur en suis profondément reconnaissante et ai en particulier une pensée pour :

Mon directeur de thèse, M. le Professeur César Pulgarín, qui m'a intégré à son équipe et fait confiance pour effectuer ce doctorat, en me prodiguant toujours de précieux conseils et en ne cessant de stimuler mes réflexions par ses riches connaissances ;

Ces remerciements s'adressent également aux membres du jury de cette thèse, Mme le Professeur Chantal Guillard, M. le Dr Andrzej Sienkiewicz, M. le Professeur Sixto Malato et M. le Professeur François Golay, qui malgré des emplois du temps fort chargés ont bien voulu se consacrer à la lecture et à l'évaluation de cette présente analyse ;

Je me souviens également que mes premiers pas dans la recherche sur la photocatalyse à l'EPFL ont été guidés par le Dr Juan Kiwi, qui a grandement facilité mon adaptation dans ce domaine de recherche ;

Mon directeur de mémoire de master à l'Université de Valle M. le Professeur Luis Norberto Benitez m'a quant à lui ouvert un chemin vers la Suisse que j'ai fini par adopter, tout en me rappelant à la Colombie au cours de ces fréquents allers-retours ;

Je ne saurais non plus oublier le Dr Jose Fernando Barona et ses enrichissantes discussions scientifiques ;

Je citerais également ma collègue et amie Juliette Ndounla, d'une rare gentillesse et bonne humeur et le Dr Sami Rtimi, toujours disposé à répondre à mes questions et à m'aider pour mes présentations – je vous souhaite le meilleur pour la suite! Mes autres collègues et amis de l'EPFL, Paula Osorio, Laura Suarez, Dr Stefanos Giannakis, Stefanos Papoutsakis, María Munoz, Natalia de la Cruz, Jessie Madrazo, Céline Henzelin-Nkubana ou encore Mariluz Bagnoud se reconnaîtront également et me rappelleront toujours aux bons moments passés ensemble ;

Enfin et surtout, je tiens à saluer ma famille en Colombie, ma maman Socorro pour toute sa tendresse, ainsi que mon papa Silvio, ma sœur Rocio et mon frère Alex pour leurs encouragements qui m'ont toujours accompagné malgré la distance.

Sans oublier bien sûr ma belle-famille, Coralie, Jean-Luc et Linette (la « gardienne du vendredi » !) et mes deux amours.

Bonne lecture.

Abstract

This study addresses the bacterial inactivation mechanisms by photo-Fenton process at near-neutral pH, focusing on iron-oxides and iron-citrate as photocatalysts for solar water disinfection and using *E. coli* as a bacteria model.

Cell envelope damage during bacterial inactivation by photo-Fenton using $FeSO_4$ as catalyst at near-neutral pH and TiO_2 photocatalysis were investigated and provided the evidence for lipid peroxidation and cell permeability. TiO_2 photocatalysis induced significant cell membrane damage, in contrast to the near-neutral photo-Fenton process, but the inactivation kinetics for both disinfection processes was similar. Electron spin resonance (ESR) suggested a higher efficiency of photo-generation of reactive oxygen species (ROS) in the presence of TiO_2 photocatalyst compared with the photo-Fenton system at near-neutral pH. The bactericidal effect of Fe^{3+}/hv seems possible due to the adsorption of Fe^{3+} ions on the bacterial cell wall followed by photosensitization of iron-bacteria exciplexes oxidizing the cell membrane. In contrast, the effect of Fe^{2+}/hv was associated with diffusion into the cell giving raise to intracellular dark Fenton's reactions. We suggest that cell envelope damage might not necessarily be a unique pathway in bacterial inactivation by near-neutral photo-Fenton treatment. In particular, the enhancement of an internal (photo)-Fenton process by the synergistic action of UVA and the external Fenton's reactants appears to be an important contribution to bacterial inactivation.

Bacterial inactivation by the heterogeneous photo-Fenton process was carried out *via* iron (hydr)oxide particles, *i.e.* hematite, goethite, wüstite and magnetite, at near-neutral pH. Photocatalysis by iron (hydr)oxides were investigated in the absence or presence of H_2O_2. We found that, the iron (hydr)oxides act as photocatalytic semiconductors and catalysts in the heterogeneous photo-Fenton process with the exception of magnetite, which needs H_2O_2 as electron acceptors. Furthermore, no bacterial reactivation and/or growth were observed after photo-Fenton treatment. Similar antimicrobial activity was induced for the photocatalytic semiconducting action of hematite and goethite. Additionally, a delayed disinfection effect was observed to continue in the dark period for the photo-assisted wüstite-based treatment. ESR measurements confirmed that $HO^{\bullet}$ and $O_2^{\bullet-}$ radicals were the principal ROS produced by iron (hydr)oxide particles under light in the absence or presence of H_2O_2. Natural organic

matter (NOM) and inorganic substances did not interfere with the photocatalytic semiconducting action of hematite during bacterial inactivation, but enhanced bacterial inactivation mediated by hematite used as the photo-Fenton reagent. Our results demonstrated, for the first time, that low concentration of iron (hydr)oxides (0.6 mg/L relative to the Fe content) under sunlight, acting both as semiconductors or catalysts of the heterogeneous photo-Fenton process at near-neutral pH, may serve as a disinfection method for waterborne bacterial pathogens.

Bacterial inactivation by the homogeneous photo-Fenton process was carried out using Fe–citrate complex as a source of iron. The efficiency of the homogeneous photo-Fenton process using Fe–citrate complex strongly improved bacterial inactivation as compared with the $FeSO_4$ and goethite as sources of iron at near-neutral pH. The bacterial inactivation rate increased in the order of goethite $<$ $FeSO_4$ $<$ Fe-citrate, which agreed with the $HO^{\bullet}$ radicals detected by ESR. Encouraging results were also obtained while applying this treatment for bacterial inactivation in natural water samples at pH 8.5. No bacterial reactivation and/or growth were observed after photo-Fenton treatment showing that Fe–citrate–based photo-Fenton process efficiently inactivate bacteria using a low iron concentration of Fe–citrate (Fe–citrate concentration: 0.6 mg/L relative to the Fe content), while avoiding precipitation of ferric hydroxides.

The application of the photo-Fenton process at near-neutral pH is a potential promising technique for bacterial inactivation, due to its simplicity, the use of the natural energy that provides the sun, the low concentration of reagents and does not produce toxic waste.

Keywords*: Solar disinfection, near-neutral photo-Fenton, bacterial inactivation, semiconductors, iron oxides, iron citrate, $HO^{\bullet}$ radicals.*

Résumé

Cette étude porte sur la compréhension des mécanismes d'inactivation bactérienne par la réaction Fenton photo-assistée (ci-après photo-Fenton) à pH proche du neutre. Elle se concentre en particulier sur les oxydes de fer et les citrates de fer comme photocatalyseurs dans la désinfection de l'eau sous radiation solaire, utilisant *E. coli* comme modèle de bactérie.

Les dommages sur l'enveloppe cellulaire pendant l'inactivation bactérienne par la réaction photo-Fenton en utilisant $FeSO_4$ comme catalyseur et la photocatalyse au TiO_2 ont été évalués et fournissent des preuves de la peroxydation lipidique et de la perméabilité cellulaire. La photocatalyse au TiO_2 induit une importante altération de la membrane cellulaire, contrairement au procédé photo-Fenton à pH proche du neutre, même si la cinétique d'inactivation des deux procédés de désinfection est similaire. La résonance de spin électronique (RSE) suggère une meilleure efficience de la photo-génération d'espèces réactives de l'oxygène (EROs) en présence de TiO_2 par rapport au système photo-Fenton à pH proche du neutre. L'effet bactéricide du $Fe^{3+}/h\nu$ semble possible grâce à l'adsorption des ions Fe^{3+} à la paroi cellulaire suivie par la photosensibilisation des complexes fer-bactéries oxydant la membrane cellulaire. En revanche, l'effet de $Fe^{2+}/h\nu$ a été associé à la diffusion dans la cellule bactérienne, intensifiant ainsi la réaction de Fenton intracellulaire. Ces résultats suggèrent que les dommages de l'enveloppe cellulaire pourraient ne pas être nécessairement une voie unique dans l'inactivation bactérienne par le processus photo-Fenton à pH proche du neutre. En particulier, l'augmentation d'un processus (photo)-Fenton intracellulaire par l'action synergique de la lumière et les réactifs de Fenton externe semble être importante dans l'inactivation bactérienne.

L'inactivation bactérienne par le procédé photo-Fenton hétérogène a été réalisée avec des particules d'(hydr)oxyde de fer, *i.e.* hématite, goethite, wustite et magnétite, à pH proche du neutre. La photocatalyse avec des (hydr)oxydes de fer a été évaluée en l'absence et en la présence de H_2O_2. Nous avons constaté que les (hydr)oxydes de fer agissaient comme des semi-conducteurs photocatalytiques et catalyseurs dans le procédé photo-Fenton hétérogène, à l'exception de la magnétite qui a besoin de H_2O_2 comme accepteurs d'électrons. Par ailleurs, aucune réactivation et/ou croissance bactérienne n'a été observée après le traitement photo-

Fenton. Une activité antimicrobienne similaire a été induite en utilisant l'hématite et la goethite comme semi-conducteurs photocatalytiques. En outre, un effet de désinfection après l'exposition (retardée) a été observé à l'obscurité dans le cas de traitement de wustite sous illumination. Les résultats de RSE ont prouvé que les radicaux $HO^{\bullet}$ et $O_2^{\bullet-}$ étaient les principales espèces réactives de l'oxygène produites par les particules d'(hydr)oxyde de fer sous radiation solaire en l'absence ou en présence de H_2O_2. La matière organique naturelle (MON) et les substances inorganiques présentes dans l'eau n'interfèrent pas avec l'action semi-conductrice de l'hématite pendant l'inactivation bactérienne, mais améliorent cette activité antibactérienne lorsque l'hématite est utilisée comme catalyseur de la réaction photo-Fenton. Nos résultats ont démontré, pour la première fois, que de faible concentration d'(hydr)oxydes de fer (0.6 mg/L par rapport au contenu du fer) sous illumination, agissant à la fois comme des semi-conducteurs photocatalytiques ou des catalyseurs du processus photo-Fenton hétérogène à pH proche du neutre, peuvent servir de méthode de désinfection des bactéries pathogènes d'origine hydrique.

L'inactivation bactérienne par le procédé photo-Fenton homogène a été réalisée en utilisant le complexe Fe-citrate (citrate de fer) comme source de fer. Ce procédé a fortement amélioré l'inactivation bactérienne comparativement aux cas où la goethite et le $FeSO_4$ étaient utilisés comme sources de fer à un pH proche du neutre. Le taux d'inactivation bactérienne a augmenté dans l'ordre suivant : goethite $< FeSO_4 <$ Fe-citrate. Ces résultats concordent de surcroît avec le taux des radicaux $^{HO^{\bullet}}$ détecté par RSE au cours des traitements. Des résultats encourageants ont également été obtenus lors de l'application de ce traitement pour l'inactivation bactérienne sur des échantillons d'eau naturelle à pH 8,5. Aucune réactivation et/ou croissance bactérienne n'a été observée après le traitement photo-Fenton. Ceci démontre que le procédé photo-Fenton à base de Fe-citrate inactive efficacement les bactéries en utilisant une faible concentration du complexe (Fe-citrate: 0.6 mg/L par rapport au contenu du fer), tout en évitant la précipitation des hydroxydes ferriques.

L'application du procédé photo-Fenton à un pH proche du neutre est donc une technique prometteuse pour l'inactivation bactérienne, non seulement par sa simplicité mais aussi parce qu'elle permet d'exploiter la lumière solaire, ne nécessite pas une grande quantité de réactifs et ne génère pas de déchet toxique.

Mots-clés: désinfection solaire, photo-Fenton à pH proche du neutre, inactivation bactérienne, semi-conducteurs, oxydes de fer, citrate de fer, radicaux $HO^{\bullet}$.

Table of contents

List of figures

List of tables

List of symbols

AOP: Advanced oxidation processes

AFM: Atomic force microscopy

CFU/mL: Colony Forming Units per millilitre

CPC: Compound Parabolic Collector

°C: Degree Celsius

DBP: Disinfection by-product

DMPO: 5,5-dimethylpyrroline N-oxide

DNA: Deoxyribonucleic acid

Ebg: Band-gap energy

E. coli: *Escherichia coli*

e^-_{cb}: Conduction band electron

EDDS: Ethylenediamine-N,N'-disuccinic acid

EDTA: Ethylenediaminetetraacetic acid

ESR: Electron spin resonance

HPLC: High performance liquid chromatography

h: Hours

H_2O_2: Hydrogen peroxide

h^+_{vb}: Valence band hole

hv: light

ICP-ES: Inductively Coupled Plasma Emission Spectrometer

IEP: Isoelectric point

IR: Infrared range

K: Acidity constant

k: Rate constants

kJ/L: Kilojoules per liter

L: liter

LPS: lipo-polysaccharide

LB: Luria-bertani

LMCT: Ligand-to-metal charge transfer

λ: Wavelength

MDA: Malondialdehyde

MDG: Millennium Development Goal

Min: Minutes

mg/L: Milligrams per litter (ppm)

NHE: Normal hydrogen electrode

nm: nanometers

NOM: Natural organic matter

NTU: Nephelometric turbidity units

$^1O_2$: Singlet oxygen

$O_2^{\bullet-}$: Superoxide anion

$HO^{\bullet}$: Hydroxyl radical

ONPG: Ortho-nitrophenyl-β-D-galactoside

OS: Oxidative stress

PBS: Phosphate buffered saline

PET: Polyethylene terephthalate

pK_a: Acid dissociation constant

PS: Photosensitizer

Pyrex: Name for thermal shock resistant borosilicate laboratory glassware

PZC: Points charge zero

ROS: Reactive oxygen species

SEM: Scanning electron microscopy

SODIS: Solar disinfection

SOD: Superoxide dismutase

spp.: Species

TEMPOL: 4-hydroxy-2,2,6,6-tetramethylpiperidine 1-oxyl

THM: Trihalomethanes

TiO_2: Titanium dioxide

VB: Valence band

UV-A: Ultraviolet Radiation, where $\lambda = 320 - 400$ nm

UV-B: Ultraviolet Radiation, where $\lambda = 280 - 320$ nm

UNICEF: The United Nations Children's Fund

W/m^2: Watt per square meter

WHO: World Health Organization

1. Introduction and overview

1.1. Drinking water scarcity and household water treatment technologies

The availability of safe drinking water is a high priority issue for health and life quality, yet this need goes unmet for millions of people across the world on a daily basis. It is estimated that 768 million people are living without access to safe source for drinking-water in 2011 (UNICEF and WHO, 2013), with the main problem being microbial contamination (WHO, 2011). Some of the areas most affected by water scarcity are rural areas of developing countries as Sub-Saharan Africa, Southeast Asia, and South America (UNICEF and WHO, 2012). This lack of safe drinking water leads to a high risk of waterborne diseases, such as cholera, typhoid fever, hepatitis A and dysentery, as well as other diarrheal diseases (WHO, 2011). In 2013, 1600 children under the age of 5 dying each day as a result of diarrhea (WHO/UNICEF, 2013). These deaths are preventable with access to clean water, but capital costs and maintenance requirements for large-scale treatment systems are prohibitive and challenging to implement in remote or distributed communities.

In developing countries, particularly in small communities and rural areas, chlorine disinfection is often the only treatment available for drinking water. However, chlorine disinfection has not always been successfully implemented in rural areas because of financial problems that result in intermittent disinfection, bad dosification or poor operation and maintenance. Additionally, in the presence of natural organic matter (NOM), chlorination leads to the formation of disinfection by-products (DBPs) such as trihalometanes (THMs) (Bekbölet and Balcioglu, 1996). The concentration of such compounds depends on both the level of NOM in water and the dosing of chlorine. As a consequence, in communities where the disinfection process is not carried out in optimal conditions, the chemical risk due to generation of DBPs is high. In this sense, there is an urgent need for innovative low cost and safe drinking water treatments, requiring a small energy input, using local human resources and low maintenance cost.

One of the recommended methods by the World Health Organization (WHO) for household drinking water treatment or for the treatment during an emergency situation, where people do not have access to an alternative method to obtain safe drinking water is SODIS (Solar Disinfection) (WHO, 2007). SODIS is a simple, low-cost treatment convenient for sunny regions. Its principle is based on a synergistic effect of thermal and optical parameters of the solar radiation which lethally inactivates the water microorganisms. 1 to 2 L of water of low turbidity (< 30 NTU) are filled up in PET (polyethylene terephthalate) bottles or plastic bags and exposed during about 6 h of mid-latitude midday summer sunshine (Wegelin *et al.*, 1994; Byrne *et al.*, 2011) or up to two days under cloudy weather (Meierhofer and Wegelin, 2002). This treatment is strongly temperature dependent and treated volume is limited to 1-2 liters. Also bacterial re-growth is sometimes observed during water cooling and storing (Mäusezahl *et al.*, 2009).

This thesis study an alternative processes which might overcome some of the disadvantages of SODIS addressing the reduction of biological risks of raw water. The alternative method is known as photo-Fenton process at near-neutral pH. More scientific details about this technology are presented in section 1.4.

1.2. Solar disinfection

The solar irradiance incident on the outer earth atmosphere is approximately 1368 W/m^2 this value varies with position within the elliptical sidereal orbit of the Earth as it orbits the Sun. Water vapour, carbon dioxide, ozone and oxygen, in addition to pollutants in the atmosphere, scatter and absorb solar irradiation. The typical cloudless atmosphere in summer at the equator, receives a solar irradiance at ground level on the equator of 1120 W/m^2. Thus we have 1.12 kJ/m^2 of optical energy available in each second to inactivate whatever microbial pathogens present in water exposed to sunlight. This value reduces as latitude increases away from the equator (McGuigan *et al.*, 2012).

Solar radiation is filtered by the earth's atmosphere; the part reaching the earth surface includes the wavelengths from 290 to 4000 and is divided into three bands: ultraviolet radiation (290-400 nm), visible light (400-760 nm), and infrared radiation (760-4000 nm) (Peter Schroeder and Krutmann, 2010).

The ultraviolet (UV) part of the sunlight is directly responsible for a part of the bacterial inactivation (Smith *et al.*, 1987; Reed, 2004). UV light is subdivided in three bands according to their energy and ability to cause cellular damage. UV-A (320 to 400 nm), due to its lower energy, is the less harmful UV light. UVB (280 to 320 nm) is typically the most destructive form of UV light, because it has enough energy to damage biological tissues. UVC (100 to 280 nm) is almost completely absorbed by the atmosphere. In nature, UVC is never found, however, UVC lamps can be used to purify water be of their strong germicidal effect.

The inactivation of microorganisms by UV irradiation results primarily from the absorption of light by the DNA resulting in dimerization of thymine bases. These thymine dimers obstruct the conformation of the double helix and interfere with normal DNA replication (Harris *et al.*, 1987).

Although the UV-A wavelengths bordering on visible light are not sufficiently energetic to directly modify DNA bases, they play an important role in formation of reactive oxygen species (ROS) in water such as singlet oxygen ($^1O_2$), superoxide anion ($O_2^{\bullet-}$), hydroxyl radical ($HO^\bullet$) or hydrogen peroxide (H_2O_2). Photons of light are absorbed by endogenous photosensitizers (PS) within cells such as porphyrins, flavins, cytochromes and quinones, NADH/NADPH, and others (Hartman and Eisenstark, 1978; Curtis *et al.*, 1992; Rajendran *et al.*, 2004) which become electronically excited and react with neighboring oxygen molecules leading to the production of intracellular ROS. Once formed, these ROS can cause damage to DNA; oxidations of amino acids in proteins; oxidations of poly-unsaturated fatty acids in lipids (Reed *et al.*, 2000). Additionally, sunlight can be absorbed by natural exogenous photosensitizers present in surface waters (humic acids (Curtis *et al.*, 1992; Paul *et al.*, 2004), fulvic acids (Cory *et al.*, 2008)) and or other dissolved natural organic material (Haag and Hoigné, 1985; Canonica *et al.*, 1995; Sandvik *et al.*, 2000; Zhan *et al.*, 2006; Zhan, 2009) which in turn can react with oxygen to produce ROS, which can exert a disinfecting effect (Whitelam and Codd, 1982). A strong synergistic effect has been observed between optical and thermal inactivation processes for water temperatures exceeding 45 °C (McGuigan *et al.*, 1998).

The bactericidal effect of solar radiation was scientifically reported for the first time by Downes and Blunt, (1877). Almost a century later Acra *et al.*, (1980) re-introduced this effect and proposed the practical application of sunlight for the disinfection of oral re-hydration solution. According to these results, they concluded that sunlight might be able to provide a

low-cost, sustainable, and simple method for treating contaminated drinking water in developing countries with consistently sunny climates (Acra *et al.*, 1989). This process is broadly known today as SODIS.

The synergetic (thermal and physical) inactivation of SODIS is strongly dependant on the local immediate climatic conditions and the volume and shape of the used recipient. This is due to the fact that the infra-red (IR, wavelenght from 780 nm to 500 µm) solar radiation is significantly attenuated by clouds, optical inactivation does limit the volumes that can be treated at a time because the penetration of UV-A radiation decreases exponentially with the water depth and can be scattered by turbidity. Moreover, the process does not remove natural or anthropogenic chemical pollutants contained in the water. In consequence, the control of the required exposure time or turbidity for a given weather condition and water source can overburden some households, leading to under exposure, regrowth and limited acceptance among the population (Mäusezahl *et al.*, 2009).

In order to overcome the climatic and volumetric dependency of SODIS, the physical improvement of SODIS has been assessed during the past 20 years. Tested physical improvement include: agitation (Reed *et al.*, 2000; Khaengraeng and Reed, 2005), aluminum foil, black painted back, (Kehoe *et al.*, 2001), the possibility of adding an artificial photosensitizers, *e.g.* methylene blue (Wegelin *et al.*, 1994; Acra and Ayoub, 1997) or a photocatalyst *e.g.* TiO_2 (Rincon *et al.*, 2001; Marugan *et al.*, 2008; Malato *et al.*, 2009) or rose bengal (Jiménez-Hernández *et al.*, 2006).

1.3. Heterogeneous solar photocatalysis

The heterogeneous solar photocatalytic process consists of making use of the near ultraviolet of the solar spectrum (wavelength shorter than 400 nm), to photo-excite a semiconductor catalyst in contact with water in the presence of oxygen. Some semiconductor catalysts can absorb above 400 nm (*e.g.*, Fe_2O_3, CdS, *etc.*) (Malato *et al.*, 2009).

Semiconductors (*e.g.*, TiO_2, Fe_2O_3, ZnO, CdS, ZnS, *etc.*) can act as sensitizers for light-induced processes due to their electronic structure, which is characterized by a filled valence band (VB) and an empty conduction band (CB). The two bands are separated by an energy gap particular to each semiconductor referred to as the band-gap (Ebg). When the semiconductor is illuminated with light ($h\nu$) of greater energy than that of the band gap, an

electron is promoted from the VB to the CB, thus leaving a positive hole in the valence band. The valence band holes are powerful oxidants depending on the semiconductor and pH (Mills and Le Hunte, 1997).

An interesting feature of the semiconductor such as TiO_2 or Fe_2O_3 is the amphoteric character of their surface. Depending of the pH, a variation in the superficial charge can be observed. In aqueous media, the surface has water molecules adsorbed and alcohol groups M-OH giving the amphoteric character to TiO_2 and Fe_2O_3. The points charge zero (PZC) on TiO_2 (anatase or rutile) and Fe_2O_3 are around 6-7. This means that at pH below this value, the M-OH groups will be protonated, charging positively the surface and allowing the adsorption of negatively charged molecules or surfaces. In contrast, beyond the PZC, the alcohol groups will be deprotonated, charging negatively the surface and allowing the adsorption of positively charged species.

For oxidation reactions to occur, the VB must have a higher oxidation potential than the reactant under consideration. The redox potential of the VB and the CB of different semiconductors varies between +4.0 and -1.5 Volts versus Normal Hydrogen Electrode (NHE). Therefore, by careful selection of the semiconductor photocatalyst, a wide range of species can be treated *via* these processes.

1.3.1. Mechanism of the photocatalytic action of TiO_2

Hydroxyl radical is considered as the main oxidant, responsible for inactivating microorganisms (Ireland *et al.*, 1993; Cho *et al.*, 2004a; Veréb *et al.*, 2013). Indeed, after absorption of near ultraviolet radiation at $\lambda < 387$ nm, electron/hole pairs (Eq. (1.1)) separated between the CB and VB are generated (Malato *et al.*, 2009), as shown in Figure 1-1.

$$TiO_2 + h\upsilon \; \rightarrow \; TiO_2 \; (e^- + h^+) \hspace{4cm} (1.1)$$
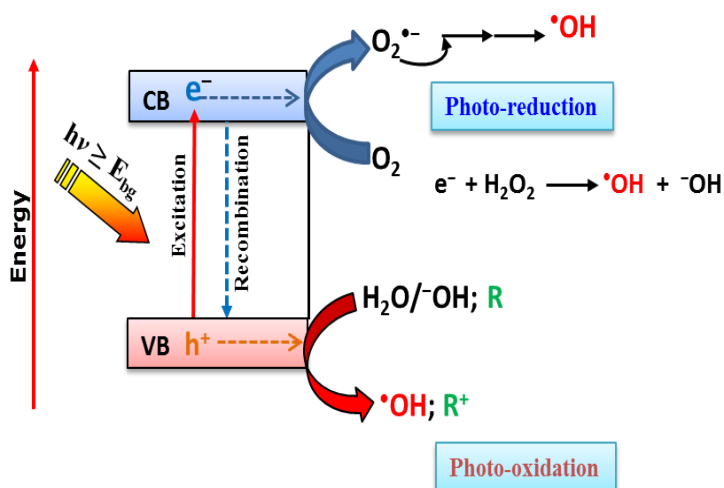
Figure 1-1: TiO_2 semiconductor photocatalysis process: scheme showing some photochemical and photophysical events that might be taking place on an irradiated semiconductor particle.

The different events that take place once the UV light has been absorbed by TiO_2 particles and the subsequent electrons (e^-_{CB}) and holes (h^+_{VB}) have been generated and partially separated, are summarized in Equations 1.2 to 1.9 and in Figure 1-1. Three oxidation reactions have been experimentally investigated: electron transfer from adsorbed organic (Eq. (1.2)), H_2O (Eq. (1.3)), and OH^- (Eq. (1.4)) adsorbed on the catalyst surface. Reactions 1.3 and 1.4 appear to be of great importance in oxidative degradation processes, most probably due to the high concentration of OH^- and H_2O adsorbed on the TiO_2 surface.

$$TiO_2\ (h^+) + R_{ad} \rightarrow TiO_2 + R_{ad}^{\bullet+} \tag{1.2}$$

$$TiO_2\ (h^+) + H_2O \rightarrow TiO_2 + HO^{\bullet} + H^+ \tag{1.3}$$

$$TiO_2\ (h^+) + OH^- \rightarrow TiO_2 + HO^{\bullet} \tag{1.4}$$

To avoid recombination, an electron acceptor must be present. Molecular oxygen is generally the acceptor species in an electron transfer reaction with the photocatalyst CB (Eq. (1.5)). Superoxide anion or its protonated form can dismutate (Eqs. (1.6)-(1.8)) to yield hydrogen peroxide or peroxide anion (Nosaka *et al.*, 2002). It has also been shown that hydrogen peroxide addition considerably enhances the photodegradation rate, most probably *via* reaction 1.9, or by surface-catalyzed dismutation of H_2O_2 (Pichat *et al.*, 1995).

$$TiO_2\,(e^-) + O_2 \rightarrow \; TiO_2 + O_2^{\bullet -} \tag{1.5}$$

$$O_2^{\bullet -} + H^+ \rightarrow \; HO_2^{\bullet} \tag{1.6}$$

$$2\,HO_2^{\bullet} \rightarrow H_2O_2 + O_2 \tag{1.7}$$

$$O_2^{\bullet -} + \; HO_2^{\bullet} + H^+ \rightarrow H_2O_2 + O_2 \tag{1.8}$$

$$TiO_2\,(e^-) + H_2O_2 \; \rightarrow \; TiO_2 + \; HO^{\bullet} \; + \; OH^- \tag{1.9}$$

1.3.2. Photocatalytic disinfection of water

Solar disinfection with TiO_2 is a consequence of both direct action of the light on the microorganisms and the photocatalytic action of the excited TiO_2 particles. Photocatalytic inactivation has been explained by the attack of radicals photogenerated at the surface of the catalyst like $O_2^{\bullet -}$, $HO_2^{\bullet}$ and $HO^{\bullet}$ (Rengifo-Herrera *et al.*, 2009; Veréb *et al.*, 2013). In recent years, photocatalytic disinfection in water by TiO_2 has widely been studied (Gumy *et al.*, 2006b; Benabbou *et al.*, 2007; Guillard *et al.*, 2008; Foster *et al.*, 2011; Robertson *et al.*, 2012; Thabet *et al.*, 2013) and its bactericidal activity and its killing mechanism have been well-documented (Sun *et al.*, 2003; Gogniat *et al.*, 2006; Liu *et al.*, 2010; Benabbou *et al.*, 2011; Pigeot-Rémy *et al.*, 2011; Pigeot-Rémy *et al.*, 2012).

Saito and co-workers (1992) reported for the first time that the bacterial death was caused by a significant disorder in cell permeability and by the decomposition of cell wall. Since then, more evidence that outer membrane damage occurs was described by Sunada and co-workers (1998; 2003) who studied *Escherichia coli* and found that the endotoxin, an integral component of the outer membrane, was destroyed under photocatalytic conditions when TiO_2 was used. Other authors have found also evidence for disruption of the cell wall, cell membrane and leakage of the cell contents (Maness *et al.*, 1999; Kiwi and Nadtochenko, 2004; Dalrymple *et al.*, 2011). These results were obtained by indirect measures (permeability of the membrane); direct measures (membrane components) and/or direct observation (SEM and AFM microscopy). Lipid peroxidation reaction was proposed as the first evidence as the underlying mechanism of the death of *E. coli* (Maness et al., 1999; Kiwi and Nadtochenko, 2004; Dalrymple et al., 2011).

1.4. Solar photo-Fenton processes

In 2006, Rincon et Pulgarín, (2006) tested the effect of Fe^{3+} and H_2O_2 on the photocatalytic disinfection of water compared to the one by TiO_2. During some control experiments, they observed that by an initial near-neutral pH (6.5), Fe^{3+}/H_2O_2 (0.3 mg/L and 10 mg/L, respectively) systems had almost a strong bactericidal effect as TiO_2 system under irradiation and a stronger effect in the dark. Furthermore, they observed that only the addition of either Fe^{3+} or H_2O_2 alone to a basic SODIS system does enhance the inactivation rates. Rincon et Pulgarín, (2006) concluded that the presence of Fe^{3+} under light accelerates *E. coli* inactivation due to the photo-activation of iron aquo-complexes under UV and visible light. This SODIS enhancement by the simultaneous addition of iron salts ($Fe^{2+ \text{ or } 3+}$) and H_2O_2 (Moncayo-Lasso *et al.*, 2009) or by taking advantage of iron naturally present in environmental waters with the addition only of H_2O_2 (Sciacca *et al.*, 2010; Bandala *et al.*, 2012; Soboleva *et al.*, 2012) is known as the photo-Fenton process.

1.4.1. The Fenton processes

The Fenton reagent is a system containing a mixture of ferrous iron (Fe^{2+}) or ferric iron (Fe^{3+}) and H_2O_2. The Fenton reaction refers basically to the generation of $HO^\bullet$ aided by the activation of H_2O_2 by Fe^{2+} (Eq. (1.10)) (Fenton, 1894; Haber and Weiss, 1934; Sychev and Isak, 1995; Malato *et al.*, 2009). It has been largely studied for the treatment of bio-recalcitrant wastewater from industry or agriculture at low pH (2.5-3.0) (Pignatello *et al.*, 2006; Kenfack *et al.*, 2009).

$$Fe^{2+} + H_2O_2 \rightarrow Fe^{3+} + HO^\bullet + OH^- \qquad k = 53 - 76 \text{ M}^{-1} \text{ s}^{-1} \qquad (1.10)$$
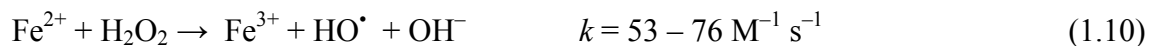
The rate constant k depends on pH and other factors. To achieve a catalytic system, Fe^{2+} needs to be regenerated from Fe^{3+} and this can take place in the presence of H_2O_2 leading to the generation of $HO_2^\bullet$ and H^+ (Eq. (1.11)) (Sychev and Isak, 1995; Pignatello *et al.*, 2006; Malato *et al.*, 2009):

$$Fe^{3+} + H_2O_2 \rightarrow Fe^{2+} + HO_2^\bullet + H^+ \qquad k = 1 - 2 \ 10^{-2} \text{ M}^{-1} \text{ s}^{-1} \qquad (1.11)$$
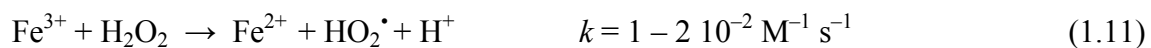
But as the rate constant k for the reduction of Fe^{3+} by H_2O_2 to Fe^{2+} is of several magnitudes lower than its oxidation from Fe^{2+} in Eq. (1.10) (Haber and Weiss, 1934; Sychev and Isak, 1995; Gernjak et $al.$, 2004), this reaction is the limiting step for the Fenton process. In addition to equations (1.10) and (1.11) and in the absence of other interfering ions and organic substances, the following catalytic reactions (Eqs. (1.12)-(1.15)) have to be regarded, k have been reported by Sychev and Isak, (1995).

$$Fe^{2+} + HO_2^{\bullet} \rightarrow Fe^{3+} + OH^{-} \qquad k = 75 - 150 \ 10^4 \ M^{-1} \ s^{-1} \qquad (1.12)$$

$$Fe^{2+} + HO^{\bullet} \rightarrow Fe^{3+} + OH^{-} \qquad k = 25 - 58 \ 10^7 \ M^{-1} \ s^{-1} \qquad (1.13)$$

$$Fe^{3+} + HO_2^{\bullet} \rightarrow Fe^{2+} + O_2 + H^{+} \qquad k = 33 - 210 \ 10^4 \ M^{-1} \ s^{-1} \qquad (1.14)$$

$$Fe^{3+} + O_2^{\bullet-} \rightarrow Fe^{2+} + O_2 \qquad k = 50 - 190 \ 10^7 \ M^{-1} \ s^{-1} \qquad (1.15)$$
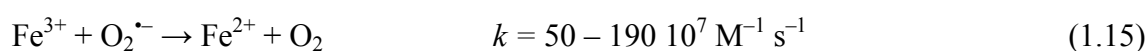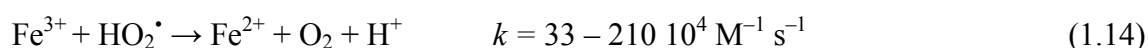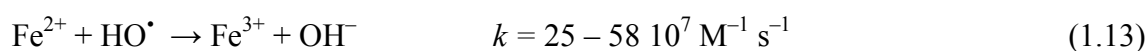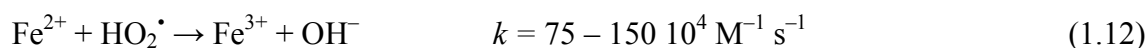
The Fenton reagent is strongly enhanced by solar radiation. The enhancement of the Fenton kinetic under light illumination is known as photo-Fenton. The photo-Fenton reaction typically gives faster rates and a higher degree of mineralization than the thermal or dark reaction and can take advantage of light in the solar spectral region because of the photo-activity of some iron aquo/organo-complexes (Kiwi et $al.$, 2000; Malato et $al.$, 2009). Therefore, the photo-Fenton process is of a general increasing interest of the scientific community for drinking water disinfection.

1.4.2. The photo-Fenton process

Ferrous iron, in the absence of any other complexing agent, has the tendency to rapidly become oxidized and form different aqua-Fe^3 species depending on the pH of the medium. At $2.8 < pH < 3$, the predominant form is $[Fe(H_2O)_5(OH)]^{2+}$, which exhibits significant photoactivity in the UV–vis radiation, and allows for Fe^{2+} regeneration when illuminated by solar radiation (Eq. (1.16). The regenerated Fe^{2+} reacts again with H_2O_2, perpetuating the formation of $HO^{\bullet}$ in the photo-Fenton process (Pignatello et $al.$, 2006; Malato et $al.$, 2009).

$$[Fe(H_2O)_5(OH)]^{2+} + h\nu \rightarrow Fe^{2+} + HO^{\bullet} + H^{+} \qquad (1.16)$$
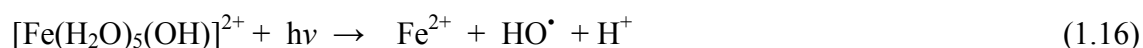
At pH above 3, the hexaquo complex undergoes extensive hydrolysis to produce Fe^{3+}-hydroxy complexes, until the reactions are ended in precipitation of amorphous ferric hydroxides (Eq. (1.17).

$$Fe^{3+} \rightarrow Fe(OH)^{2+} \rightarrow Fe(OH)_2^{+} \rightarrow Fe_2(OH)_2^{4+} \rightarrow\rightarrow Fe_2O_3{:}nH_2O_{(s)} \qquad (1.17)$$
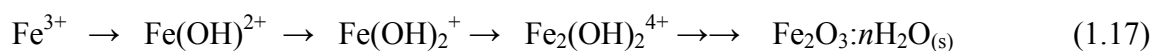
1.4.3. Photo-Fenton process at neutral pH

As the pH of most natural waters is in the neutral region, successful application of the photo-Fenton process requires acidification and constant monitoring of the pH. To avoid this limitation, the use of iron oxides particles and iron-chelating agents as the sources of iron, which catalyze the decomposition of H_2O_2 are being considered. (He *et al.*, 2002; Cho *et al.*, 2004b; Garrido-Ramírez *et al.*, 2010; Papoutsakis *et al.*, 2015a; Ruales-Lonfat *et al.*, 2015).

1.4.3.1. Iron oxides used in heterogeneous photo-Fenton process

Several kinds of heterogeneous catalysts, including iron oxides (He *et al.*, 2002; Matta *et al.*, 2007; Xue *et al.*, 2009), iron-immobilized materials (Lv *et al.*, 2005; Shin *et al.*, 2008; Mazille *et al.*, 2010), clays and carbon materials (Tabet *et al.*, 2006; Chueca *et al.*, 2012), *etc.*, are used as the iron source in heterogeneous Fenton or photo-Fenton processes for the oxidation of organic compounds at neutral pH values. The iron species present in such catalysts is quite stable in the structure or interlayer and the iron sludge could be prevented.

The most common iron oxide particles involved in heterogeneous Fenton and photo-Fenton reactions are iron (hydr-)oxides because they are abundant in both natural and engineered systems. Many investigations have demonstrated the effectiveness of this process for water treatment purposes. These studies have shown that iron-bearing minerals, namely goethite, hematite, magnetite and ferrihydrite can catalyze the oxidation of organic pollutants by H_2O_2 over a pH range from 3 to 7 (Kwan and Voelker, 2003; Lee *et al.*, 2006; Matta *et al.*, 2007).

Degradation of organic substrates (*e.g.*, phenol, nalidixic acid, pesticide mixtures, *etc.*) demonstrated that the iron oxides have synergistic photocatatalytic activity at neutral pH. Iron oxides can participate in the photo-Fenton reactions (Eqs. (1.18) – (1.20)) (S.Sunglin., 1998) and photocatalytic reaction (Eq. (1.21)) occurring on the iron oxide surfaces. In all the above equations, $> Fe^{2+}$ and $> Fe^{3+}$ are iron species in the solid phase or at the solid-liquid interface. The mechanism occurring in photo-Fenton reaction with oxides involving semiconductor photocatalysis are presented in section 3.1.

Several investigations have suggested that the oxidation of organic pollutants take place *via* HO$^\bullet$ radicals generated on the particle surface (Gurol and Lin, 2002; Kwan and Voelker, 2003; Lee *et al.*, 2006).

$$> Fe^{3+} + H_2O_2 \rightarrow > Fe^{2+} + H^+ + HO_2^\bullet \qquad (1.18)$$

$$> Fe^{2+} + H_2O_2 \rightarrow > Fe^{3+} + OH^- + HO^\bullet \qquad (1.19)$$

$$> Fe^{3+}L_n + hv \rightarrow > Fe^{2+} L_{n-1} + L_{OX}^{\bullet+} \qquad (1.20)$$

(L: complexing agent or polycarboxylic acid)

$$Fe_2O_3 + hv \rightarrow Fe_2O_3 (e^- + h^+) \qquad (1.21)$$

1.4.3.2. Iron complex used in homogeneous photo-Fenton processes

Homogeneous photo-Fenton process at neutral pH could be carried out using iron-complexing ligands. The use of organic iron-complexing ligands has recently been gaining interest as a means of enhancing the performance of photo-Fenton photocatalytic systems. Compared with Fe^{3+}-aqua complexes, Fe^{3+}-organic ligand complexes maintain their solubility at a wider pH range, limiting the need for acidification and pH control (Pignatello *et al.*, 2006). Additionally, can exhibit higher absorbance in the UV–vis region and can be photochemically reactive via participation in ligand-to-metal charge transfer (LMCT) transitions Eq. (1.22). This assures the turnover of Fe^{2+} which is essential for homogeneous photo-Fenton process.

$$[Fe^{3+}L] + hv \rightarrow [Fe^{3+}L]^* \rightarrow Fe^{2+} + L^\bullet \qquad (1.22)$$
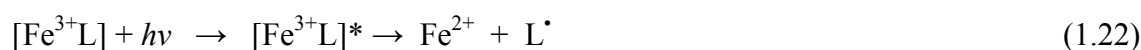
(L: complexing agent or polycarboxylic acid)

The ligand can be any Lewis base able to form a complex with ferric iron (OH$^-$, H$_2$O, HO$_2^-$, Cl$^-$, R-COO$^-$, R-OH, R-NH$_2$ etc.).

The carboxylate group [R-C(O)O-] is one of the most common functional groups of the dissolved organic compounds present in natural waters (Faust and Zepp, 1993). Poly-carboxylates, which contains molecules that have more than one carboxylate functional group, such as citrate, malonate, and oxalate are common constituents of precipitation, fog and surface waters and soil solutions. Poly-carboxylates can form strong complexes with Fe^{3+} and enhance the dissolution of iron in natural water through photochemical processes. Moreover, such poly-carboxylate complexes undergo rapid photochemical reactions under sunlight irradiation leading to the formation of oxidative species (Faust and Zepp, 1993; Panias *et al.*, 1996).

Faust et al., (1993) declared that Fe^{3+}- poly-carboxylates complexes undergo LMCT process upon irradiation generate Fe^{2+}, $O_2^{\bullet -}/HO_2^{\bullet}$, H_2O_2 and $HO^{\bullet}$ in atmospheric water drops and surface waters. It is also found that the efficiency of the Fe^{3+}-poly-carboxylates photoreduction reaction in solution depends strongly on: pH, the initial Fe to poly-carboxylates ratio, and the quantum yield are in the order as: oxalate > tartrate > malate > citrate > isocitrate > succinate > formate at acidic pH (Abrahamson et al., 1994).

Among the most well studied ligands are citrate (Katsumata et al., 2006; Silva et al., 2007; N. Seraghni, 2012; de Lima Perini et al., 2013) and oxalate (Balmer and Sulzberger, 1999; Nogueira et al., 2005; Batista and Nogueira, 2012) which have been the most commonly used ligands in photo-Fenton processes applied for removal of organic chemicals in aqueous solutions. The improved efficiency is mainly due to the high quantum yield of Fe^{2+} in the presence of ligands, and hence increased generation of $HO^{\bullet}$ (Chen et al., 2007). Besides citrate and oxalate, other ligands including EDDS (ethylenediamine-N,N'-disuccinic acid) (Klamerth et al., 2013; Papoutsakis et al., 2015a; Papoutsakis et al., 2015b), humic acids (Farré et al., 2007; Klamerth et al., 2011) have been used to complex iron in modified photo-Fenton systems.

Citric acid is ubiquitous in nature and it has key biological functions. The tricarboxylic acid and its salts are used in a wide variety of industrial applications (e.g., in soft drinks and effervescent salts, as an antioxidant in foods, as a sequestering agent for metal ions, as a cleaning and polishing agent for metals, as a mordant in dyeing). Most of these applications arise from the affinity of citrate for metal ions (Gautier-Luneau et al., 2005).

Ferric citrate complex is a good alternative for iron solubilization in the photo-Fenton processes. Although its photolysis shows a lower quantum yield for Fe^{2+} generation than that observed for ferrioxalate, citrate is less toxic (Sillanpaa and Pirkanniemi, 2001; Liang et al., 2004; Silva et al., 2007), has higher cumulative stabilization constants (log β = 14.29) (Feng et al., 2012), is readily available and can be used at higher pH values than oxalate (up to pH 9.0) (Abrahamson et al., 1994). Ferric citrate complexes have been successfully implemented for the photo-Fenton treatment at near-neutral pH conditions and with using artificial or solar light towards degradation of organic compounds in polluted waters (Zepp et al., 1992; Sun and Pignatello, 1993; Katsumata et al., 2006; Silva et al., 2007; Trovó and Nogueira, 2011).

There is some discrepancy in the literature concerning the ferric citrate species dominant in solution at different pHs (Abrahamson et al., 1994; Quici et al., 2007). According to Field,

(1974) and Nansheng, (1998), the main Fe^{3+}–citrate species include Fecit, $FeHcit^+$, $FeOHcit^-$, and $Fe_2(OH)_2(cit)_2^{2-}$. Figure 1-2 illustrates the fraction of Fe^{3+} species in the Fe^{3+}–cit aqueous solution based on the data from stability constants of Fe^{3+}–cit and Fe^{3+}–hydroxo species as a function of pH (Chen *et al.*, 2011). At low pH, Fecit is the predominant species. With increasing pH (pH > 4), $FeOHcit^-$ and $Fe_2(OH)_2(cit)_2^{2-}$ become the main species gradually.
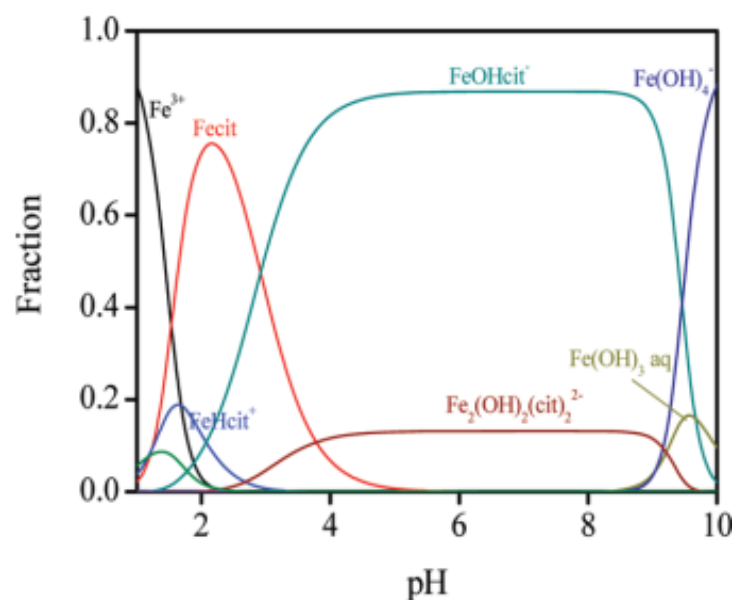
Figure 1-2: The fraction of Fe^{3+} species based on the stability constants of Fe^{3+}–cit and Fe^{3+}–hydroxo species as a function of pH.

Francis et Dodge, (1993) reported that ferric iron formed a bidentate complex with citric acid at neutral pH, $[Fe^{3+}(OH)_2cit]^{2-}$ involving two carboxylic acid groups with iron : citrate molar ratio 1:1 (Figure 1-3). In contrast, ferrous iron formed tridentate complex with citric acid, $[Fe^{2+}cit]^-$, involving two carboxylic acid groups and the hydroxyl group. However, oxidation and hydrolysis of the ferrous iron resulted in the formation of a tridentate ferric-citrate complex, $[Fe^{3+}OHcit]^-$.
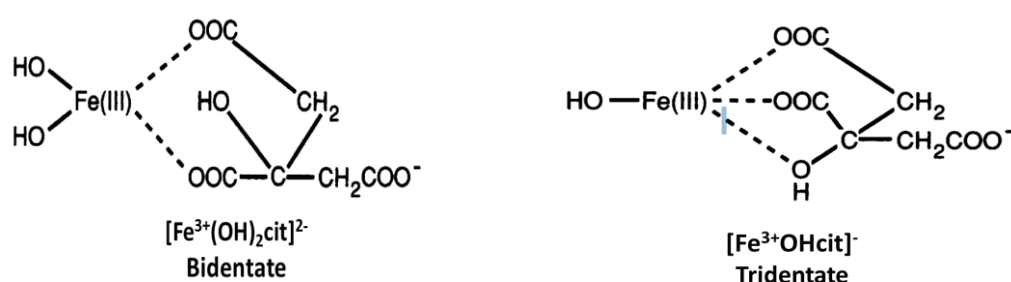
Figure 1-3: Schematic representation of the structures of the ferriccitrate complexes at neutral pH.

1.4.3.3. Siderophores as iron ligands

The interest in biological siderophores as iron ligands has increased in recent years. Siderophores are one species of low-molecular weight, high-affinity Fe^{3+}-chelating ligands. More than 500 types of siderophores have been reported in the last three decades. Siderophores are excreted by plants or micro-organisms under conditions of iron stress to scavenge and transport iron. Various fungi and heterotrophic bacteria cultured under conditions of limited iron levels have been found to produce siderophores that form complexes with high stability constants (Hutchins *et al.*, 1999; Amin *et al.*, 2009). The photoreactivity of siderophores is primarily determined by the chemical structure of their Fe^{3+}-binding groups, namely, hydroxamate and catecholate moieties. Hydroxamate groups are photochemically resistant regardless of Fe^{3+} complexation. Catecholate siderophores are susceptible to photooxidation and undergo light-induced ligand oxidation and reduction of Fe^{3+} to Fe^{2+} (Barbeau *et al.*, 2003).

It is widely accepted that the solubilization of iron-bearing mineral phases is a key function of siderophores. Borer *et al.*, (2005) reported that siderophores greatly accelerate light-induced dissolution of crystalline iron oxides such as lepidocrocite and goehite in suspensions at pH 6. Recently, the use of Fe^{3+}-siderophore complexes in a Fenton (Wang *et al.*, 2013) and photo-fenton (Wang *et al.*, 2015) process at near-neutral pH was investigated for degradation of pollutant organic.

1.4.4. The photo-inactivation mechanism

1.4.4.1. Characterization of some reactive oxygen species

ROS are chemically-reactive molecules containing oxygen. They are highly reactive, some due to the presence of unpaired valence shell electrons. In living cells, such oxidation products are formed during normal metabolic processes and have important roles in cell signaling. Cells contain a variety of biomolecules, which are potential targets for oxidation by various types of ROS, like the $HO^{\bullet}$ and $O_2^{\bullet-}$, and molecules like H_2O_2, hypochlorous acid (HClO) as well as singlet oxygen ($^1O_2$) an electronically excited state of molecular oxygen. Additional environmental stresses (*e.g.* UV or heat exposure) can dramatically increase ROS levels. This can result in significant damage to cell structures that cumulate into a situation known as oxidative stress (OS). In living cells, OS occurs when the level of pro-oxidants, *i.e.* ROS exceeds the ability of the cell to respond through its antioxidant defense. Proteins

comprise about 70% of the dry weight of cells and, because of their abundance, are major targets for OS-induced damages (Davies, 2005).

 Numerous studies have shown that $^1O_2$ can oxidize a variety of organic substances including biologically important compounds, such as amino acids (Zepp *et al.*, 1977) or other parts of proteins (Davies, 2003; Rengifo-Herrera *et al.*, 2009). The bacterial membranes (lipids) are the most likely target for the often exogenously produced singlet oxygen and oxygen radicals (Curtis *et al.*, 1992) leading to enhanced permeability and serious damage of the cells.

$O_2^{\bullet-}$ itself is relatively little reactive. When generated exogenously $O_2^{\bullet-}$ is sufficiently long living to diffuse into the cells but this process is slowed because $O_2^{\bullet-}$ is charged (Imlay, 2008). However, $O_2^{\bullet-}$ produced endogenously is responsible for the oxidation of [4Fe-4S] cluster present in cells, the subsequent release of Fe^{2+} and the simultaneous formation of H_2O_2 allowing the generation of toxic $HO^{\bullet}$ *via* intracellular Fenton reactions (Kellogg and Fridovich, 1975; Gutteridge, 1982; Imlay, 2003; Fridovich, 2011).

$HO^{\bullet}$ reacts at, or close to, a diffusion-controlled rate of 6 x 10^9 $M^{-1}s^{-1}$. Hence, any formed $HO^{\bullet}$ will react with whatever is present at its formation site and directly damage all biological molecules, including DNA (Halliwell and Gutteridge, 1992), leading to the oxidation of lipids affecting the structural and functional integrity of the membranes (Kellogg and Fridovich, 1975). If produced inside the cells, they will attack the biomolecules, especially DNA.

H_2O_2 on its own is little reactive, but has the ability to attack the cellular membrane, initiating lipid peroxidation chains that increase membrane permeability and affect the viability of the cells (Halliwell and Chirico, 1993). However, H_2O_2 penetrates membranes and diffuse into cells whenever it is present in the extracellular habitat (Imlay, 2008). The presence of H_2O_2 in the cell can led to serious damage because of its ability to react with metal ions (*e.g.* Fe^{2+}) generate highly toxic $HO^{\bullet}$ (Gutteridge, 1982; Imlay, 2003, 2008).

1.4.4.2. Pathway of the photo-oxidative stress

The biological targets of ROS ($^1O_2$, H_2O_2, $O_2^{\bullet-}$ as well as $HO^{\bullet}$) and other radicals are DNA, RNA, proteins and lipids (Cabiscol *et al.*, 2000). Oxygen dependent are probably the major component of optical bacterial damage because of the ROS induced membrane lipid peroxidation and DNA damage (Reed, 2004). Free radicals attack membrane lipids (Gourmelon *et al.*, 1994b) such as the phospholipids chains (Gutteridge, 1982) or polyunsaturated fatty acids, initiating lipid peroxidation chains (Cabiscol *et al.*, 2000). Lipid

peroxidation is a complex process characterized by three distinct phases: a slow induction period, a rapid autocatalytic phase and a slow termination phase (Gutteridge, 1982). Lipid peroxidation results in a decrease of the membrane fluidity altering the membrane properties and disrupting membrane-bound proteins (Cabiscol *et al.*, 2000). It action can also lead to increase membrane permeability, disruption of transmembrane ion gradients and finally inactivation (Reed, 2004). The attack of polyunsaturated fatty acids acts as an amplifier, more radicals are formed, and the polyunsaturated fatty acids are degraded to a variety of products. Some of them are aldehydes, which are on their turn very reactive and can damage molecules, such as proteins. When proteins are exposed to reactive oxygen species, modifications of amino acid side chains occur and, consequently, the protein structure is altered (Cabiscol *et al.*, 2000).

1.4.4.3. Oxidative stress through intracellular Fenton

Under UV-A and visible light, iron concentrations can be enhanced inside the cells. Hoerter et al., (1996), (2005) have shown that enterobactin is an endogenous chromophore for UV-A and contributes to cell lethality under radiation in the solar spectrum *via* the destruction of its ligand, releasing Fe^{2+} into the cytoplasm of *E. coli* bacteria to catalyze the production of highly reactive hydroxyl radicals and other toxic oxygen species *via* the Haber-Weiss reaction. Pourzand et al., (1999) have shown that the UV-A radiation also increases the level of intracellular reactive iron pools *via* the proteolysis of ferritin. UV-A radiation also breaks down heme-containing proteins in the microsonial membrane to release free heme as an additional photosensitizing component (Tyrrell *et al.*, 2000). Imlay, (2008) described that during the oxidative-stress, $O_2^{\bullet-}$ could penetrate in the active sites of enzymes containing iron-sulfur clusters ($[4Fe-4S]^{2+}$). $O_2^{\bullet-}$ then binds the critical iron atom and oxidizes the cluster to a redox state that is unstable (Eq. (1.23)), the produced $[4Fe-4S]^{3+}$ then releases Fe^{2+} and is left in an inactive $[4Fe-4S]^{+}$ form (Eq. (1.24)). The $[4Fe-4S]^{2+}$ cluster can also be oxidized by H_2O_2 leading to the release of Fe^{3+} and the oxidation of the cluster by $O_2^{\bullet-}$ leads simultaneously also to the generation of cellular H_2O_2 (Imlay, 2003, 2008):

$$[4Fe-4S]^{2+} + O_2^{\bullet-} + 2H^+ \rightarrow [4Fe-4S]^{3+} + H_2O_2 \tag{1.23}$$

$$[4Fe-4S]^{3+} \rightarrow [4Fe-4S]^{+} + Fe^{2+} \tag{1.24}$$
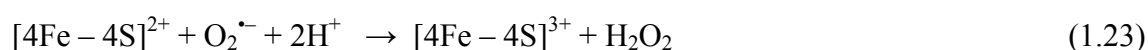
Besides the Fe^{2+} release from iron-sulfur cluster, $O_2^{\bullet-}$ can also reduce and liberate Fe^{3+} from ferritin (Henle and Linn, 1997). The generated H_2O_2 and Fe^{2+} can through the Fenton reaction

lead to the generation of highly reactive HO$^{\bullet}$ radical which will damage/oxidize the cell DNA (Gutteridge, 1982; Henle and Linn, 1997).

1.4.5. Some applications of the photo-Fenton at near-neutral pH

The photo-Fenton process at near-neutral pH and very low reagent concentration was tested for the elimination of NOM from river water (Murray and Parsons, 2004; Moncayo-Lasso *et al.*, 2009; Ruales-Lonfat *et al.*, 2013). Simultaneous to organic oxidation it was also observed that the process significantly enhanced the solar inactivation of some pathogenic bacteria (Moncayo-Lasso *et al.*, 2009). The enhancing effect of the photo-Fenton process for photo-inactivation of *E. coli* in drinking water at near-neutral pH was for the first time reported by Rincón and Pulgarin, (2006). Subsequently, the enhancement of bacterial photo-inactivation *via* photo-Fenton at near-neutral pH was reported at lab scale, pilot scale and in natural waters at reagents' concentrations in the micro to millimolar range (Moncayo-Lasso *et al.*, 2009; Sciacca *et al.*, 2010; Spuhler *et al.*, 2010). The Table 1-1 summarizes the state of art concerning microorganism inactivation by photo-Fenton process at near-neutral and neutral pH conditions.

Table 1-1: State of art concerning microorganism inactivation by photo-Fenton process at near-neutral and neutral pH conditions.

Microorganisms	Main objectives	References
E. coli –K12	The enhancing effect of the photo-Fenton process for photo-inactivation of *E. coli* in drinking water at near-neutral pH was for the first time reported. The evaluation of the solar treatment in order to assess its effectiveness in reducing bacterial load by photo-Fenton system and the durability of the different disinfection systems (post irradiation events) were studied.	(Rincón and Pulgarin, 2006)
E. coli –K12	Field experiments with a large solar compound parabolic collector (CPC) reactor under solar radiation are reported. The bacterial cultivability was monitored for photocatalytic systems such as sunlight/TiO$_2$, sunlight/TiO$_2$/Fe^{3+}, sunlight/Fe^{3+}/H$_2$O$_2$ (photo-Fenton system). The study focuses on the durability of the different disinfection systems during 24 h after stopping of the field scale phototreatment.	(Rincón and Pulgarin, 2007a)

E. coli –K12	Field disinfection of water in a large solar photoreactor was conducted at ''natural'' temperature of 35 °C by different photocatalytic processes. The following topics were addressed in this study: (a) bacterial inactivation by sunlight in the presence and absence of TiO_2, (b) the influence of iron addition on the TiO_2 photo-assisted disinfection process, (c) bacterial inactivation by photo-Fenton system, (d) the durability of the different disinfection systems.	(Rincón and Pulgarin, 2007b)
E. coli –K12	A heterogeneous iron supported catalyst (A woven inorganic silica fabric loaded with Fe-ions) was tested under simulated solar light during bacterial inactivation at ''natural'' pH and in the presence of a low concentration of H_2O_2.	(Moncayo-Lasso *et al.*, 2008)
E. coli –K12	Bacteria inactivation and natural organic matter oxidation in river water was simultaneously conducted *via* photo-Fenton using low concentrations of Fe^{3+} and H_2O_2 at "natural" pH in a solar CPC reactor.	(Moncayo-Lasso *et al.*, 2009)
E. coli –K12	Systematic study, investigating the effect of Fe^{2+}, Fe^{3+} and H_2O_2 on the photo-inactivation of *E. coli* in Mili-Q water and mineral water enriched with resorcinol, a model NOM. A mechanistic interpretation of iron catalyzed solar water disinfection was proposed, which illustrates the possible pathways involved in photo-inactivation of *E. coli* in the presence of the photo-Fenton reagent.	(Spuhler *et al.*, 2010)
E. coli –K12	The fixation and photocatalytic performance of iron oxide on different polymer films previously functionalized by different methods was studied. The ability of these photocatalysts in organic pollutants degradation and bacterial inactivation was described.	(Mazille *et al.*, 2010)
Wild *Salmonella* sp. and total coliforms	Comparative disinfection effect at natural neutral pH of (i) the addition of H_2O_2 in the dark, (ii) SODIS process as it is known, and (iii) SODIS adding H_2O_2 on wild coliforms and Salmonella sp. contained in water of the urban dams in Ouagadougou, Burkina Faso. Water containing dissolved iron (0.3 mg/L).	(Sciacca *et al.*, 2010)
Virus (MS2 coliphage)	Virus inactivation by iron- and copper catalyzed Fenton systems was studied in natural systems at near neutral pH. The influence of H_2O_2 and metal concentrations, $HO^\bullet$ production, and sunlight on inactivation was investigated.	(Nieto-Juarez *et al.*, 2010)
Wild *Salmonella* sp. and total coliforms	Evaluation of disinfection efficiency of the photo-Fenton process during solar irradiation using natural surface water with high turbidity in a CPC solar photoreactor.	(Sciacca *et al.*, 2011)
Dreissena Polymorpha (zebra mussel)	Titanium dioxide solar photocatalysis and neutral photo-Fenton were checked for disinfestation of zebra mussel from irrigation facilities. Bench scale experiments performed in a solar photo-reactor was also evaluated.	(Bernabeu *et al.*, 2011)
Enterococcus Faecalis, (Gram-positive microorganism)	The effect of temperature on bacterial inactivation using the photo-Fenton reaction at initial near-neutral pH with resorcinol was studied.	(Ortega-Gómez *et al.*, 2012)

E. coli, Salmonella, Shigella,	The effect of the simultaneous presence of organic compounds – resorcinol and hydroquinone and bacteria cells on the degradation of organics and inactivation of bacteria in water by heterogeneous photocatalysis on TiO_2 and near-neutral photo-Fenton systems was studied. The effect of the presence of chemical substances that interact strongly or weakly with TiO_2 surfaces, such as resorcinol and hydroquinone, respectively, and those that can be found in natural waters, on the photocatalytic inactivation of bacteria cells was also evaluated.	(Moncayo-Lasso *et al.*, 2012)
Fusarium Solani	The efficiency of the solar photo-Fenton reaction and solar H_2O_2/UV–vis to disinfect simulated municipal effluents at pH of about 8, polluted with spores in solar bottle reactors under natural solar conditions was assessed.	(Polo-Lopez *et al.*, 2012)
Total bacteria and total coliforms	A modified photo-Fenton treatment for the degradation of micro pollutants and disinfection in municipal wastewater treatment plant effluents at a neutral pH was developed. Photo-Fenton experiments were performed in a pilot compound parabolic collector (CPC) solar plant. Complexation of Fe by ethylenediamine-N,N′-disuccinic acid (EDDS) leaded to stabilization and solubilisation of Fe.	(Klamerth *et al.*, 2012)
Fusarium solani E. coli	The effectiveness of three solar treatments; Fe^{3+}/sunlight, H_2O_2/sunlight, and solar photo-Fenton at near-neutral pH was evaluated and compared for disinfection of water.	(García-Fernández *et al.*, 2012)
E. coli, enterococcus faecalis, and pseudomonas aeruginosa.	The inactivation of three different kinds of bacteria usually present in municipal wastewater treatment effluents using a coagulation–flocculation–decantation (CFD) process combined with photo-Fenton treatment at pH 5 was evaluated under artificial solar irradiation.	(Rodriguez-Chueca *et al.*, 2013)
Enterococcus Faecalis	The aim of this research was to study the effect of the water matrix on the bacterial inactivation process by solar photo-Fenton at initial neutral pH. Saline solution, saline solution with resorcinol and a simulated secondary effluent from a municipal wastewater treatment plant.	(Ortega-Gómez *et al.*, 2013)
E. coli –K12	Borosilicate and PET bottles were comparatively studied, as photo-Fenton reactors for *E. coli* inactivation under simulated solar irradiation and natural sunlight.	(Ruales-Lonfat *et al.*, 2013)
Virus (MS2 coliphage)	The bacteriophage MS2 inactivation during heterogeneous Fenton-like processes catalyzed by iron (hydr)oxide particles at circumneutral pH was studied. The effect of the different particle types, H_2O_2 and sunlight on inactivation was studied. Both physical removal of viruses from solution *via* adsorption onto particles as well as true inactivation were considered.	(Nieto-Juarez and Kohn, 2013)
Total coliforms/*E. coli* and Salmonella spp.	The inactivation of bacteria in natural waters from the Sahelian wells having different pH 4.9 and 6.3 and a natural iron content of 0.07 mg/L was studied under Fenton reagent and photo-Fenton processes.	(Ndounla *et al.*, 2013)

E. coli, spores of sulphite-reducing clostridia (SRC), somatic coliphages (SOMCPH) and F-specific RNA bacteriophages (FRNA).	The disinfection of a real secondary effluent from a Municipal Wastewater Treatment Plant using added H_2O_2, TiO_2 and photo-Fenton under natural solar irradiation in Compound Parabolic Collector photo-reactors was studied. For this purpose, the microbial indicators in real wastewater effluents were tested before and throughout the different solar treatments in order to: (i) determine the inactivation of these microbial indicators, (ii) determine the indicator removal efficiency of the technologies studied, and (iii) evaluate the feasibility of these disinfection technologies for water reclamation.	(Agulló-Barceló *et al.*, 2013)
phytophthora capsici zoospores	The capacity of photo-Fenton to zoospores in distilled water at small scale under natural solar radiation was studied. Photo-Fenton process efficiency was evaluated using two different iron sources, ferrous sulphate (Fe^{2+}) and ferric nitrate (Fe^{3+}). In addition, the separated effects of H_2O_2, Fe^{2+} and Fe^{3+} over spores under natural solar radiation and in the dark were also evaluated.	(Polo-López *et al.*, 2013)
Total coliforms/*E. coli* and Salmonella spp.	Impact of irradiance vs. dose on the efficiency of the photo-Fenton process was evaluated for bacterial inactivation in well water naturally containing dissolved and solid iron forms (*e.g.* iron oxides). Well water was treated in the compound parabolic collector (CPC) under direct solar radiation.	(Ndounla *et al.*, 2014)
Total coliforms/*E. coli* and Salmonella spp.	Effect of the dry or rainy season on photo-Fenton disinfection of natural water from two different wells (W1, pH: 4.6–5.1) and (W2 pH: 5.6–5.7) was carried out at Ouagadougou–Burkina Faso, West Africa. Well water was treated in the compound parabolic collector (CPC) under direct solar radiation.	(Ndounla and Pulgarin, 2014)
E. coli –K12	For the first time was investigated cell envelope damage during *E. coli* inactivation by the near-neutral photo-Fenton system and compares the underlying mechanisms with the photo-catalytic action of TiO_2. Bacterial inactivation by homogeneous and heterogeneous photo-Fenton systems at near-neutral pH was comparatively studied.	(Ruales-Lonfat *et al.*, 2014)
wild enteric *E. coli* and total coliform	This study analyses the use of the solar photo-Fenton treatment in compound parabolic collector photo-reactors at neutral pH for the inactivation of bacteria present in secondary effluents of a municipal wastewater treatment plant. Control experiments were carried out to find out the individual effects of mechanical stress, pH, reactants concentration, and UV-A radiation as well as the combined effects of UV-A-Fe and UV-A-H_2O_2.	(Ortega-Gómez *et al.*, 2014b)
Enterococcus Faecalis	The role of an organic molecule as resorcinol (considered as a model of NOM) on the disinfection process by solar photo-Fenton at neutral pH was investigated.	(Ortega-Gómez *et al.*, 2014a)
E. coli and enterococcus sp.	The efficiency of the Fenton processes induced by electromagnetic fields at near neutral pH (pH 5) to remove bacteria added in simulated wastewater effluents was evaluated. Several iron sources, ferric chloride, magnetite and clay were evaluated in the presence and absence of hydrogen peroxide and electromagnetic fields.	(Rodríguez-Chueca *et al.*, 2014a)

E. coli and *E. faecalis.*	The effectiveness of a solar photo-Fenton system at near neutral pH for the removal of fecal bacteria in urban wastewater effluents was investigated. Several concentrations of ferrous sulfate (2.5–10 mg-Fe^{2+}/L) and hydrogen peroxide (5–50 mg/L) were tested in solar CPC under natural sunlight. Solar photo-Fenton processes at pH 5 and pH 3 were compared. Furthermore, the influence of precipitated and dissolved iron on the efficiency of the photo-Fenton process at near-neutral pH values was also evaluated.	(Rodríguez-Chueca *et al.*, 2014b)
Fusarium Spores	The efficiency of the solar-driven photo-Fenton with Fe^{2+} and Fe^{3+}, heterogeneous photocatalysis (TiO_2) and solar photoassisted H_2O_2 treatment for inactivating spores in distilled water, simulated municipal wastewater effluent, and real municipal wastewater effluents was investigated.	(Polo-López *et al.*, 2014)
E. coli –K12	The disinfection ability of four iron (hydr)oxides semiconductors, *i.e.* (hematite, goethite, wüstite and magnetite), in aqueous media under solar light illumination, at near-neutral pH of 6.5, in the absence or presence of H_2O_2 was investigate.	(Ruales-Lonfat *et al.*, 2015)
Virus (MS2 coliphag and Echovirus)	The inactivation of virus by solar photo-Fenton at near neutral pH in carbonate buffer solution matrix was evaluated. The effects of reactant concentration (H_2O_2, Fe^{2+}, Fe^{3+}) and solar irradiance on the photo-Fenton process were studied. In order to validate the efficiency of the photo-Fenton process at near neutral pH, the photocatalytic treatment was carried out in natural water (Lake Geneva, Switzerland) and with a human virus (Echovirus). Finally, a conceptual mechanistic interpretation was proposed.	(Ortega-Gómez *et al.*, 2015)

1.4.6. The studied bacteria

Bacteria are prokaryotic microorganisms, which mean that they lack a nucleus enclosed by a nuclear membrane. Bacterial cells mostly range in size from 0.5 to 5 microns. Based on the different ability of their cell wall components to be stained by the Gram stain, bacteria are often divided into two classes: Gram-positive and Gram-negative.

The bacteria selected for this study was the Gram negative *Escherichia coli* (*E. coli*), a representative bacteria of the Enterobacteriaceae family, which is the most common pathogenic bacteria family found in water.

These Gram-negative bacteria inhabit the intestinal tract of humans and warm-blooded animals. Their presence in water samples is almost always indicative of faecal pollution and the possible existence of other enteric pathogens such as Salmonella spp., Yersinia spp., Shigella spp., *etc*. These enteric bacteria are responsible for slight gastrointestinal diseases.

However, depending on the strain virulence, severe illness or death can occur (Rodriguez-Chueca *et al.*, 2013).

E. coli has been taken as a model for bactericide studies as model microorganism, and it DNA, metabolism, structure and composition, morphology, behavior under different nutrient media, pathogenicity, types, strains, has been extensively reported (Malato *et al.*, 2009).

The envelope of *E. coli* bacteria is composed of two membranes, the inner and outer membranes, which are separated by the periplasm that contains a thin peptidoglycan layer (Figure 1-4) (Doerrler, 2006).

The outer membrane (or cell wall) is about 6 to 18 nm. It consists of 50% lipopolysaccharides (LPS), 35% phospholipids, and 15% lipoproteins. Together, the outer membrane and peptidoglycan provide mechanical protection to maintain intact the cell morphology (Michael T. Madigan *et al.*, 2003). LPS works as a selective permeability barrier for *E. coli* and other Gram-negative bacteria (Raetz and Whitfield, 2002). Removing LPS molecules increases the permeability of cell wall. Unlike the outer membrane and the periplasm, the inner membrane (or cytoplasmic membrane) is absolutely vital for bacteria. In addition to its selective permeability properties, the cytoplasmic membrane has a respiratory function through the electron transport and oxidative phosphorylation. With a width of approximately 8 nm, its loss of integrity leads to bacteria death.

In the case of iron the bacteria is provided for with receptor, transporter and energy-transducing proteins ensure that there is a sufficient supply of iron-containing compounds, such as siderophores (Faraldo-Gomez and Sansom, 2003). The membrane proteins mediate the uptake of the siderophores that are known as ferrichrome, enterobactin and ferric citrate from *E. coli* (Braun, 2001).

The reactive oxygen species, $O_2^{\bullet-}$, and H_2O_2 are naturally generated during bacteria respiration by way of Haber–Weiss (Eq. (1.25)) or the Fenton reaction (Eq. (1.10))

$$H_2O_2 \;+\; O_2^{\bullet-} \;\rightarrow\; O_2 + HO^{\bullet} \;+\; OH^- \hspace{3cm} (1.25)$$

However, *E. coli* also produces the enzyme superoxide dismutase (SOD) to dismutate the $O_2^{\bullet-}$ to O_2 and H_2O_2 (Eq. (1.26)), and the enzyme catalase to reduce the intracellular concentration of H_2O_2 and convert it to H_2O and O_2 (Eq. (1.27)) (Eisenstark, 1998).

$$2O_2^{\bullet-} + 2H^+ \xrightarrow{\text{SOD}} O_2 + H_2O_2 \qquad\qquad (1.26)$$

$$H_2O_2 + H_2O_2 \xrightarrow{\text{CATALASE}} 2H_2O + O_2 \qquad\qquad (1.27)$$
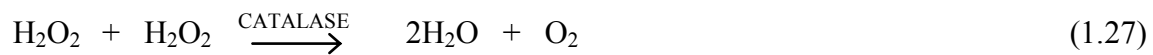
In addition, bacteria cells as *E. coli* have protection and recovery mechanisms to overcome the effects of UV radiation and oxidative stress that involve endogenous proteins, such as the anti-oxidant enzymes, DNA repair enzymes and DNA-integrity proteins.
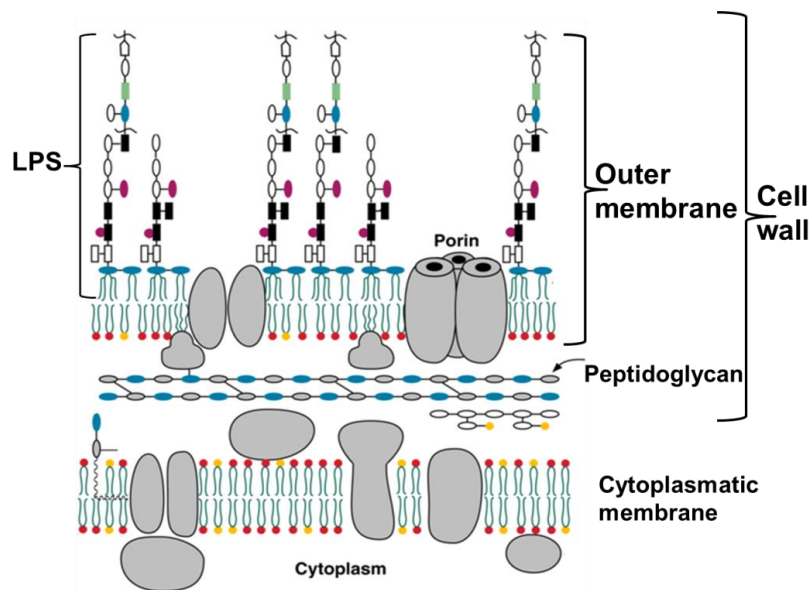
Figure 1-4: Schematic representation of the *E. coli* cell envelope. LPS: lipo-polysaccharide (Raetz and Whitfield, 2002).

2. Aims and outline of the thesis

The overall objective of this research work is to contribute to an in-depth understanding of the bacterial inactivation mechanism by photo-Fenton process at near-neutral pH, using iron-oxides and iron-citrate as photocatalysts in water disinfection.

The following specific tasks were carried out:

- To evaluate the cell envelope damage during bacterial inactivation by the near-neutral photo-Fenton system and to compare the underlying mechanisms with the photo-catalytic action of TiO_2.
- To investigate the disinfection ability of four different iron (hydr)oxides particles in aqueous media under solar light illumination, at near-neutral pH, in the absence/presence of H_2O_2 in heterogeneous photo-Fenton processes.
- To assess the efficacy of the Fe-citrate complex during bacterial inactivation by homogeneous photo-Fenton process at near-neutral and alkaline pH in water.
- To quantify the ROS generated by heterogeneous and homogeneous photo-Fenton processes.
- To evaluate the efficiency of the heterogeneous and homogeneous photo-Fenton processes at natural pH in real-world condition, *i.e.* in natural water samples.
- To conduct post irradiation experiments in order to assess if bacterial reactivation and/or growth takes place in heterogeneous and homogeneous photo-Fenton processes.

The thesis is organized in six chapters:

The introductive chapter 1 addresses household level water treatments and presents solar photocatalysis and solar photo-Fenton processes.

Chapter 3 presents a comparative study of cell envelope damage during bacterial inactivation by photo-Fenton at near-neutral pH and TiO_2 photocatalysis addressing lipid peroxidation and

cell permeability change. Additionally, the bactericidal effect of Fe^{3+}/hv and Fe^{2+}/hv was evaluated.

Chapter 4 presents the photocatalytic disinfection of four different commercially available iron (hydr)oxides semiconductors in the absence or presence of H_2O_2. The reactive oxygen species (ROS) generated by iron (hydr)oxides during heterogeneous photocatalysis and/or photo-Fenton treatments were quantified and the effect of NOM on hematite mediating the disinfection was investigated.

Chapter 5 presents the first evidence of Fe–citrate–based photo-Fenton chemistry for the inactivation of *E. coli* at near-neutral and alkaline pH conditions, using low iron concentration. The effects of the solution pH and Fe-citrate concentrations on *E. coli* inactivation were investigated. Furthermore, the photo-Fenton processes mediated by Fe-citrate complex, $FeSO_4$ and goethite were compared. The $HO^{\bullet}$ radicals formation during the photo-disinfection was monitored. Finally, the efficiency of the Fe–citrate–based photo-Fenton process was evaluated in natural water samples from Lake Geneva (Switzerland) at pH 8.5.

Chapter 6 presents the short version of the chapters 3-5 and suggest a mechanistic model for bacterial inactivation in the presence of Fenton's reagent.

Chapter 7 presents the conclusions and an outlook for water disinfection by photo-Fenton process at near-neutral pH.

3. Deleterious effect of near-neutral photo-Fenton system on *Escherichia coli*. Comparison with photo-catalytic action of TiO$_2$ during cell envelope disruption.

3.1 Introduction

Harmful microorganisms are a major problem in drinking water that can cause severe health problems for humans. Hence, developing innovative water disinfection methods is a continuous need. Recently, the photo-Fenton ($Fe^{2+/3+}/H_2O_2/hv$) system at near-neutral pH under solar light was found to be an effective option for disinfection of bacteria present in water (Rincón and Pulgarin, 2006, 2007a; Moncayo-Lasso *et al.*, 2009). Fenton's reagent action is based on the reaction of H_2O_2 with $Fe^{2+/3+}$, thus resulting in the formation of hydroxyl radicals and other highly oxidative species in aqueous media (Eqs. (3.1) and (3.2)). However, the Fenton process is limited by the Fe^{2+} regeneration of Fe^{3+} (Eq. (3.2)). This drawback is partially countered by photo-Fenton reactions. In fact, Fe^{3+}-hydroxy complexes undergo photo-reduction under ultraviolet A (UV-A) and visible radiation, thus regenerating Fe^{2+} *via* ligand-to-metal charge transfer (LMCT) and contributing to an additional pathway of $HO^{\bullet}$ production (Eq. (3.3)) (Cieśla *et al.*, 2004).

$$Fe^{2+} + H_2O_2 \rightarrow Fe^{3+} + HO^{\bullet} + OH^- \qquad k = 53 - 76\ M^{-1}s^{-1} \qquad (3.1)$$

$$Fe^{3+} + H_2O_2 \rightarrow Fe^{2+} + HO_2^{\bullet} + H^+ \qquad k = 1 - 2\ x\ 10^{-2}\ M^{-1}s^{-1} \qquad (3.2)$$

$$Fe(OH)^{2+} + hv \rightarrow Fe^{2+} + HO^{\bullet} \qquad\qquad\qquad\qquad (3.3)$$

$$[Fe(COO-R)]^{2+} + hv \rightarrow Fe^{2+} + CO_2 + R^{\bullet} \qquad\qquad (3.4)$$
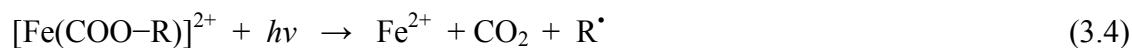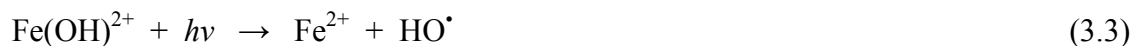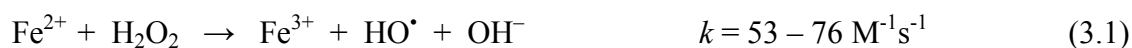
Until now, the process pH was generally perceived as the limiting factor for photo-Fenton systems, because $Fe(OH)^{2+}$ the most photo-active Fe^{3+}-hydroxy complex is predominant at low pH (~2.8). At near-neutral pH, zero-charge ferrous complexes [$Fe(OH)_2$] formed, are very sensitive to oxidation and instantaneously form solid ferric (hydr)oxide compounds such as magnetite, goethite, lepidocrocite, or feroxyhyte. The type of precipitated ferric compounds depends on physico-chemical conditions such as acidity, redox conditions, temperature, ionic strength, presence of organic or inorganic ligands and bacterial activity (Jolivet *et al.*, 2004). In waters containing dissolved organic matter (DOM), Fe^{3+} may complex with certain of these organic compounds. The Fe^{3+}-organo complexes are stable at neutral pH, circumventing the need for the low pH of the standard photo-Fenton process. The photolysis of these Fe^{3+}-organo complexes, which generally have a high molar absorption coefficient in UV-A and visible light, leads to the regeneration of Fe^{2+} and the formation of a ligand radical (Feng and

Nansheng, 2000) (Eq. 2.4). Both Fe^{2+} and organic radicals react with O_2, leading to the formation of ROS ($O_2^{\cdot-}$, $HO^{\cdot}$, H_2O_2) (Faust and Zepp, 1993; Wu and Deng, 2000).

Over the past few years, interest has grown in the application of near-neutral photo-Fenton treatment to inactivate larvae of freshwater mollusc (zebra mussel) (Bernabeu *et al.*, 2011) and other types of microorganisms such as fungi (García-Fernández *et al.*, 2012), virus (Nieto-Juarez *et al.*, 2010) and *Enterococcus faecalis* (Ortega-Gómez *et al.*, 2012). However, the mechanism underlying the photocatalytic inactivation process has not been investigated in detail. Numerous studies on elucidating the mechanism of photo-killing of bacterial cells using TiO_2 concluded that cell envelope damage is the first and perhaps a major step for microbial inactivation. Sunada *et al.*, (2003) proposed that bacterial death is caused by a significant disorder in cell permeability and the decomposition of the cell wall (Saito *et al.*, 1992). More specifically, Maness *et al.*, (1999), Pulgarin *et al.*, (2012) and Pigeot-Rémy *et al.*, (2011), concluded that TiO_2 photocatalysis promotes the peroxidation of the phospholipids in the membrane. More recently, Dalrymple *et al.*, (2011) reported that lipid peroxidation processes are crucial to *E. coli* inactivation using TiO_2 suspension and UV-A light sources.

For the first time, this study investigates cell envelope damage during *E. coli* inactivation by the near-neutral photo-Fenton system and compares the underlying mechanisms with the photo-catalytic action of TiO_2. The production of malondialdehyde (MDA) was used as an index to assess cell membrane damage by lipid peroxidation, and the ortho-nitrophenyl-β-D-galactoside (ONPG) test was used as an index of cell permeability. To confirm the effect of both types of photo-oxidative treatment on the bacterial wall, lipopolysaccharide (LPS), an essential compound of the cell wall of *E. coli*, was used as a model. Finally, lipid peroxidation during photo-assisted Fe^{2+}/Fe^{3+} treatment and its correlation with bacterial inactivation were assessed.

3.2 Materials and methods

3.2.1 Chemicals

This study used the commercial mixed-phase TiO_2–based photocatalyst, Degussa P25 (Frankfurt, Germany) as a high-activity model photocatalyst. Degussa P25 is composed of anatase and rutile crystallites (typical reported ratio of 75:25), having irregular shapes and average particle sizes of 20–30 nm. The specific surface area of TiO_2 particles is 50 m^2/g. The

reactants used for the Fenton process were ferrous sulphate heptahydrate ($FeSO_4 \cdot 7H_2O$) (Riedel-de Haën 99-103.4%), iron chloride ($FeCl_3 \cdot 6H_2O$) (Fluka, Buchs, Switzerland) and hydrogen peroxide (H_2O_2) 30% w/v (Riedel de Haën, Darmstadt, Germany). The lipopolysaccharide (LPS) FITC from *E. coli* 055:B5 (Code F8666) and ortho-nitrophenyl-*β*-D-galactoside (ONPG) were purchased from Sigma Aldrich and used without further purification. LPS was dissolved in ultrapure water (0.4 mg/mL). With a lower concentration, no malondialdehyde (MDA) signal was detected using high performance liquid chromatography (HPLC). All solutions were prepared immediately prior to irradiation using ultrapure water.

3.2.2 Analytical methods

3.2.2.1 Dissolved iron

Dissolved iron ($Fe^{2+/3+}$) was measured using the Ferrozine method as described previously (Spuhler *et al.*, 2010). Total dissolved iron was measured using an Inductively Coupled Plasma Emission Spectrometer (ICP-ES) (Shimadzu) ICPE-9000. Samples were filtered (0.25 μm) and kept in acid solution previous to the determination. The detection limit of ICP-ES used for this experiment was 0.2 μg/L.

3.2.2.2 Analysis of H_2O_2 concentration

The concentration of H_2O_2 was monitored using a titanium (IV) oxysulfate solution *via* a spectrophotometric method at 410 nm (modified method DIN 38 402 H15). The titanium (IV) oxysulfate method has a 0.1 mg/L detection limit.

3.2.2.3 Electron spin resonance spectroscopy (ESR)

Electron spin resonance spectroscopy (ESR) in combination with spin-trapping were used to monitor the formation of ROS, in other words, hydroxyl ($HO^{\bullet}$) and superoxide ($O_2^{\bullet-}$) radicals, generated by either the near-neutral photo-Fenton processes or under the photo-catalytic action of TiO_2 particles. A commercial spin trap, 5,5-dimethyl-1-pyrroline-N-oxide (DMPO), from Sigma–Aldrich (Buchs, Switzerland) was used to trap ROS. DMPO was purified before use through distillation on activated charcoal. Then, a stock solution of 0.5 M DMPO in ultrapure water was stored at –20 $^{\circ}$C.

The following reagents studying the photo-generation of ROS using the near-neutral photo-Fenton system: 0.6 mg/L of iron (FeSO$_4$) and 10 mg/L of H$_2$O$_2$. To study the formation of ROS under the photo-catalytic action of TiO$_2$, the aqueous suspension containing 1 mg/mL of TiO$_2$ particles in ultrapure water was prepared. Just before performing the photo-generation of ROS, DMPO (100 mM) was added to Fenton's reagents or aqueous suspensions containing TiO$_2$. Subsequently, 2 mL aliquots of the prepared samples were transferred into small Pyrex beakers (5 mL volume, 20 mm outer diameter and 30 mm height) and exposed to simulated solar light under constant agitation. Subsequently, the solutions of either the Fenton's reagents or the water suspensions of TiO$_2$ particles were drawn into thin glass capillaries (0.7 mm ID/0.87 mm OD, from VitroCom, NJ, USA), which were then sealed on both ends using the Cha-Seal™ tube-sealing compound (Medex International, Inc, USA). ESR measurements were carried out at room temperature using a Model EleXsys 500 Bruker X-band spectrometer (Bruker BioSpin, Karlsruhe, Germany) equipped with a high-Q cylindrical TE$_{011}$ microwave cavity, Model ER4123SHQE. The instrumental settings were: frequency of 9.4 GHz; microwave power of 0.63 mW; scan width of 120 G; magnetic field resolution of 2048 points; modulation frequency of 100 kHz; modulation amplitude of 1.0 G; receiver gain of 60 dB; conversion time of 40.96 ms; time constant of 20.48 ms and sweep time of 84 s.

The spin-adducts concentrations were measured using double-integration of the first-derivative ESR spectra. The resulting areas were compared with the ESR signal from 10 μmol/L of a stable nitroxide radical, 4-hydroxy-2,2,6,6-tetramethylpiperidine 1-oxyl (TEMPOL, Sigma–Aldrich, Switzerland). The data analysis was carried out using Origin Pro 9.0 software.

3.2.3 Bacterial strains and growth media

The bacterial strain used was *E. coli* K12 (MG1655), a non-pathogenic wild-type strain that can be handled with little genetic manipulation. Bacteria was inoculated from a stock in Luria–Bertani (LB) and incubated at 37 °C and 180 rpm in a shaker incubator. After 8 h, cells were diluted (1% v/v) in pre-heated LB broth and incubated at 37 °C for 15 h in the incubator until a stationary physiological phase was reached. Cells were separated during the stationary growth phase by centrifugation (15 min at 5000 rpm and 4 °C). The bacterial pellet was re-suspended and washed for 10 min in the centrifuge (twice). This

procedure resulted in a bacterial pellet of approximately 10^9 colony forming units per milliliter (CFU/mL).

3.2.4 Photo-inactivation experiments

At the beginning of each experiment, the Pyrex reactors (4 cm x 9 cm, 100 mL) containing the bacterial suspension in ultrapure water were placed in the dark at 25 °C and kept under magnetic for at least 30 min to let the bacteria adapt to the new matrix and to allow the die-off and equilibration of the most stress sensitive species. Then, Fenton's or TiO_2 reagents were added and exposed to irradiation. Aliquots were taken during set intervals within the inactivation time. The control experiment consisted of an *E. coli* suspension without reagents. Concentrations were set as follows: Fenton's reagents ($Fe^{2+/3+}$ 0.6 mg/L, H_2O_2 10 mg/L), and TiO_2 photocatalysis (1 mg/mL). These concentrations are in the optimal range reported in the literature for photo disinfection studies (Spuhler *et al.*, 2010).

Light was provided by a solar simulator CPS Suntest System (Heraeus Noblelight, Hanau, Germany). The Suntest bears a lamp that emits ~0.5% of the photons at wavelengths < 300 nm (UVC cut-off at 290 nm), ~7% between 300 and 400 nm and the rest follow the solar spectrum above that value until Infrared range (IR) (IR was cut-off by filtering). The radiance intensity was measured by a spectroradiometer, Model ILT-900-R (International Light Technologies) and corresponded to 1322 W/m^2 of light global intensity (32.6 W/m^2 on the UV).

Bacterial reactivation and/or growth of bacteria were determined for some experiments by leaving the last samples in the dark at room temperature (20–25 °C) for 24 h before the measurement of the CFU.

3.2.5 Determination of lipid peroxidation

Lipid peroxidation level was measured using the accumulation of malondialdehyde (MDA) and quantified through HPLC after both photo-oxidative treatment methods on *E. coli* and LPS (Karatas *et al.*, 2002). Briefly, chromatographic determinations were performed on an Agilent 1100 series HPLC equipped with a UV absorbance detector. Samples filtered were injected *via* autosample and eluted at a flow rate of 0.9 mL/min through a column (Nucleosil C18, Marcherey-Nagel) using as mobile phase a mixture of 3 mM de KH_2PO_4–MeOH

(65+35% v/v) at pH 4.0. Chromatograms were monitored at 268 nm and the retention time of MDA was 3.9 min. For calibration purposes, a solution of MDA was prepared through acid hydrolysis of 1,1,3,3-tetraethoxypropane, as in Tsaknis *et al.*, (1998).

3.2.6 Damage in cell envelope by photo-Fenton and TiO$_2$ photocatalysis

Ortho-nitrophenyl-β-D-galactoside (ONPG) is a synthetic chromogenic substrate for the intracellular β-D-galactosidase of *E. coli* that can be used to gauge the level of cellular damage during the photocatalytic process and assess to it any correlation of cell death. ONPG is hydrolyzed to *o*-nitrophenol (ONP) when it reacts with β-D-galactosidase, which results in a yellow color under alkaline conditions. The production of ONP over time was monitored using a spectrophotometer at 420 nm. This assay was carried out as described by Huang *et al.*, (2000), with minor modifications. In order to enhance the synthesis of β-D-galactosidase by *E. coli*, the following culturing method was employed. *E. coli* grown in LB Broth for 18 h at 37 °C was further spiked to a flask containing 1 mM of isopropyl β-D-thiogalactopyranoside and 100 mL of LB Broth. After incubation for 4 h at 32 °C in a shaking incubator, the suspension was centrifuged at 4500 rpm for 10 min at 4 °C and washed using ultrapure water.

The hydrolysis rate for intact and lysed cells was determined. An aliquot of 9 mL washed cells was mixed with 1 mL ONPG (5 mM in sterile ultrapure water) then, 0.9 mL samples were transferred to sterile Eppendorf tube. Each 3 min interval for 12 min, 0.1 mL of a 1 M sodium carbonate/bicarbonate buffer (pH 10) was added to both stop the enzyme-substrate reaction and to obtain maximal absorbance. The kinetics was determined by following the absorbance of the samples and the slope was determined by linear regression of absorbance *versus* time.

A sample from the photocatalytic experiments were taken at 15 min intervals for 120 min in duplicate. The ONPG hydrolysis reactions were initiated by transferring 4.5 mL of illuminated samples to the dark in duplicates in a tube, followed by an addition of an equal volume of ultrapure water and 1 mL of ONPG. TiO$_2$ and cells were removed by centrifugation at 4 °C and 4500 rpm for 10 min. Exceeding H$_2$O$_2$ was neutralized with catalase for photo-Fenton treatment. The pH of the supernatant was raised to 10 by the addition of a sodium carbonate/bicarbonate buffer. The absorbance of the mixture was measured at 420 nm and the hydrolysis rate was determined as described in section 2.6.

The effect of TiO₂ photocatalyst and photo-Fenton treatment on cell-free β-D-galactosidase was examined using cell lysate. An aliquot of 2 mL washed cell was transferred in a beaker and followed by the addition of 50 µL chloroform and vigorous stirring for 15 min. This solution was then diluted 1:10 in ultrapure water and subjected to TiO₂ photocatalytic and photo-Fenton treatment as described before in this section. The illuminated cell lysates were transferred to the dark at 15 min intervals for 120 min followed by the ONPG assay as described above.

3.3   Results and discussion

3.3.1   Comparative bacterial inactivation mechanisms under near-neutral photo-Fenton and TiO₂ photocatalysis

To determine cell wall damage in *E. coli*, lipid peroxidation was monitored through accumulation of MDA, one of the most abundant aldehyde forms originating from the peroxidation of bacterial lipid membranes (Esterbauer and Cheeseman, 1990; Candan, 2008). As Figure 3-1 (a) (traces ((▲) and ♦)) shows, even though MDA accumulation was low for both TiO₂ photocatalysis and near-neutral photo-Fenton treatment before 120 min, this effect was nevertheless sufficient to induce a significant bacterial inactivation, a ~5 $\log_{10}$ reduction (99.99%) of the initial *E. coli* concentration as shown in Figure 3-1 (b) (traces (▲) and (♦)).

Thus, *E. coli* inactivation, monitored by the cultivability measurements in petri dishes, does not correlate in time with the appearance of MDA. This low MDA accumulation before 120 min can be explained by (i) limited peroxidation (not noticeable by significant MDA accumulation), which is enough to induce cultivability losses, and (ii) the contribution of other parallel processes that lead to physiological perturbations related to the attack of cell wall components. At a more advanced stage of treatment (up to 120 min, Figure 3-1 (a), trace (▲)), TiO₂ photocatalysis leads to important MDA accumulation compared with the photo-Fenton process that seems to be produced from inactivated and dead bacteria for both processes.

(a)

(b)
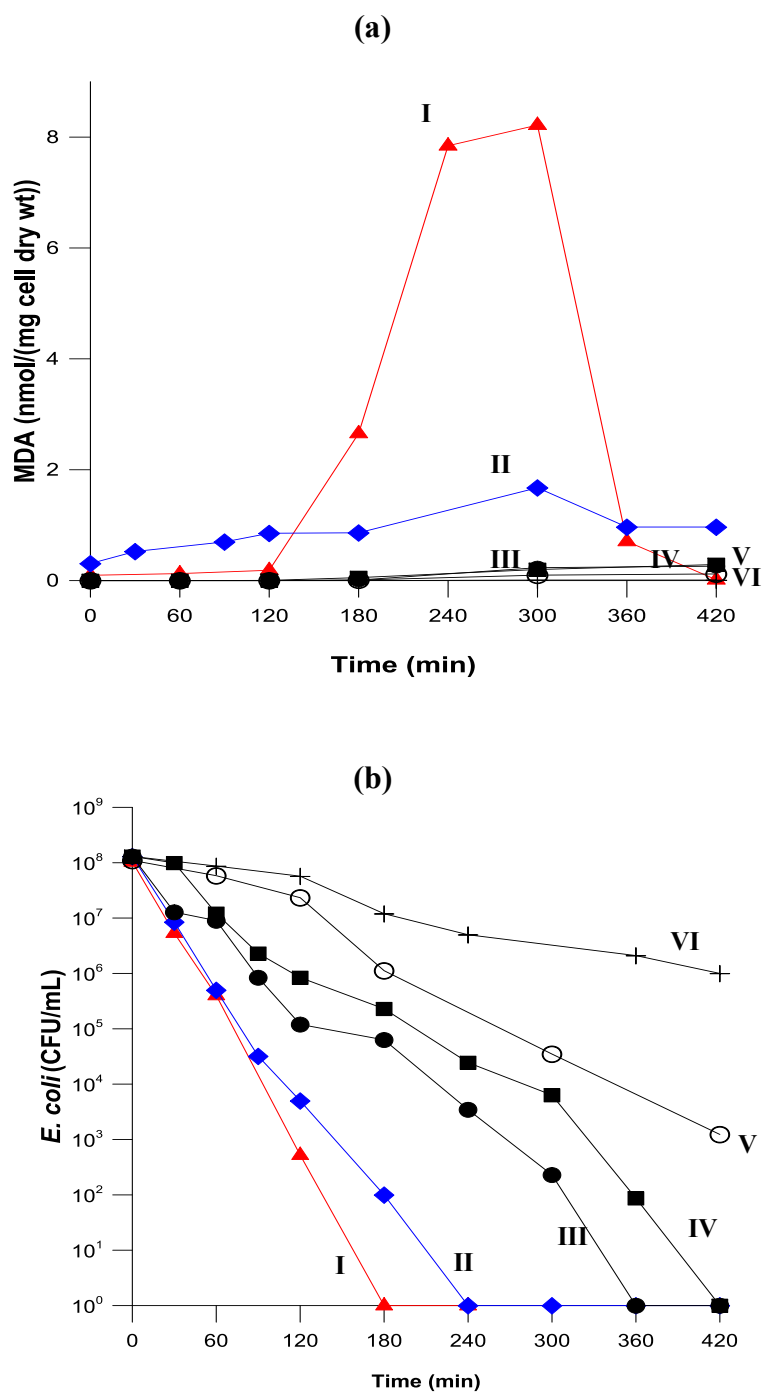
Figure 3-1: (a) Lipid peroxidation based on MDA accumulation and (b) *E. coli* inactivation during: (I) (▲) TiO$_2$ photocatalysis (1 mg/mL); (II) (♦) photo-Fenton (III) (●) FeSO$_4$ under light; (IV) (■) H$_2$O$_2$, under light; (V) (○) light alone; (VI) (+) Fenton. Experimental conditions: [Fe^{2+}]: 0.6 mg/L, [H$_2$O$_2$]: 10 mg/L. Irradiated with simulated solar light. Experiments were conducted in triplicate and standard error was found to be approximately 5%.

The *E. coli* inactivation under photo-Fenton treatment resulted in accumulation of MDA at time zero with a maximum concentration at 300 min (Figure 3-1 (a), trace (♦)). The low accumulated concentration of MDA found in photo-Fenton processes compared with TiO_2 photocatalysis are similar to levels found when using chemical disinfectants such as ozone, chlorine dioxide, free chlorine, and UV irradiation to inactivate *E. coli*. Cell wall damage was reported to be more pronounced with a strong oxidant (such as ozone), causing delayed diffusion as the oxidant reacts with various cell components. In contrast, damage in the inner cell components was more apparent with weaker oxidants (such as free chlorine) that have limited reactions with cell walls and that reach the cell plasma (Cho *et al.*, 2010). This situation may occur for near-neutral photo-Fenton treatment resulting in efficient bacterial inactivation, but that reveals rather limited lipid peroxidation (Figure 3-1 (a), trace (♦)). Control experiments Fe^{2+}/hv; H_2O_2/hv; *hv* alone and Fenton does not significantly contributed to lipid peroxidation (Figure 3-1 (a)). However, the complete bacterial inactivation was achieved for Fe^{2+}/hv and H_2O_2/hv system controls and 5 log and 2 log reduction of bacteria under light alone and Fenton systems were reached at 420 min of treatment (Figure 3-1 (b)). Thus, extensive membrane damage may not be the only pathway in the inactivation of bacteria by photo-Fenton treatment. The intensification of internal (photo)Fenton processes by the synergistic action of UV-A light and external Fenton's reactants seem important to bacterial inactivation by photo-Fenton process at near-neutral pH.

Although the initial Fe^{2+} added to the solution was 0.6 mg/L, the concentration of total dissolved iron measured at time 0 min was 0.3 mg/L, 0.2 mg/L at 60 min, and negligible beyond 60 min of treatment (Table 3-2). This loss of dissolved iron may be provoked by (i) the iron precipitation as ferric (hydr)oxide attributable to near-neutral pH (Table 3-.1) (Cornell and Schewetmann, 2003), (ii) adsorption on the bacterial wall, and (iii) Fe^{2+} intake by bacteria. Thus, after 60 min of treatment (Figure 3-1 (b), trace (♦)), *E. coli* inactivation could be mediated by heterogeneous photocatalytic action of solid iron species as iron (hydr)oxide, mostly goethite (α-FeO(OH)) and/or lepidocrocite (γ-FeO(OH)) that could be formed by oxidation of Fe^{2+} in solution at near-neutral pH (Cornell and Schewetmann, 2003). This result corresponds to previous findings by Nieto-Juarez *et al.*, (2010) who showed that inactivation of MS2 coliphage in a Fenton-like system at pH 6.8 was mediated by iron colloids rather than dissolved iron.

To detect the ROS generated on the surface of the catalyst under illumination with simulated solar light, the ESR spin trap technique with DMPO was used. In particular, DMPO

scavenges both HO$^\bullet$ and O$_2^{\bullet-}$ radicals, thus leading to the formation of spin-adducts, DMPO–OH and DMPO–OOH, respectively. Both resulting paramagnetic products reveal distinct and easily recognizable ESR spectra. However, the DMPO–OOH spin adduct is well known to be highly unstable and rapidly decomposes into the DMPO–OH spin adduct (Buettner and Mason, 1990). Therefore, as a result, a characteristic ESR spectrum of the DMPO–OH spin adduct consisting of four well resolved peaks (1:2:2:1 quartet, $a_N = a_H = 14.9$ G) is usually observed (insert in Figure 3-2). In fact, such ESR spectra were observed for all of the studied photo-catalytic systems after exposure to simulated solar light, highlighting their ability to generate both HO$^\bullet$ and O$_2^{\bullet-}$ radicals.

The Figure 3-2 summarizes the ESR spin-trapping experiments for TiO$_2$ photocatalysis and photo-Fenton systems. The intensity plots of the ESR signal of DMPO–OH as a function of illumination time represent the photocatalytic efficiency of the studied systems. The steepest slope of the DMPO–OH intensity plots was observed for TiO$_2$ (Figure 3-2, trace (▲)). The corresponding time-evolution of acquired ESR signals is shown in the insert to Figure 3-2. Note that no ESR signals of DMPO–OH were detected before illumination in this experiment. These results suggest that exposure to the simulated solar light was essential for generation of reactive oxygen species, including HO$^\bullet$, on the surface of the TiO$_2$ photocatalyst. This phenomenon also points to a classical mechanism of the light-induced promotion of valence band electrons to the conduction band, which yields valance band holes (h$_{vb}^+$) and produces HO$^\bullet$ radicals at the particle surface. The high efficiency of the photo-generation of ROS in the presence of the TiO$_2$ photocatalyst corroborates with the observed high rate of lipid peroxidation in *E. coli* cells exposed to the photo-catalytic action of this catalyst (Figure 3-1 (a), trace (▲)). Thus, HO$^\bullet$ radicals, along with other ROS, such as O$_2^{\bullet-}$, and H$_2$O$_2$ generated on the illuminated TiO$_2$ surface, can attack polyunsaturated phospholipids in *E. coli* cell membranes, leading to their breakdown and cell death (Maness *et al.*, 1999). Additionally, h$_{vb}^+$ of the catalyst can disturb cell membranes, leading to oxidative stress and, eventually, cell death (Figure 3-1 (b), trace (▲)). These findings show that the TiO$_2$ photocatalyst was highly efficient in the inactivation of *E. coli* under simulated solar light even if TiO$_2$ utilizes only 4% of the solar spectrum and cannot efficiently utilize visible light which is approximately 43% of the solar spectrum for photocatalytic disinfection.

The oxidative species were also generated by FeSO$_4$–based photo-Fenton system, as shown in Figure 3-2 trace (♦). Interestingly, for the FeSO$_4$–based photo-Fenton system, a small ESR signal of DMPO-OH resulting from the Fenton process in the dark was already observed

before illumination. This ESR signal markedly increased on illumination with simulated solar light (Figure 3-2, trace (♦)). The observed difference in the extent of lipid peroxidation found between the photo-catalytic action of TiO_2 and the $FeSO_4$ based photo-Fenton system (Figure 3-1 (a) traces (▲) and (♦) is attributed to the cellular charge effect that may facilitate the adsorption of bacteria cells to TiO_2 particles, leading to the production of $HO^{\bullet}$ close to bacteria affecting the cell wall lipopolysaccharides (Saito *et al.*, 1992). The adsorption of bacteria on TiO_2 and the photocatalytic reactivity of TiO_2 are affected by the pH of the suspension. In the experiments involving the TiO_2 photocatalyst, the pH decreased from 6.5 to 5.0 (Table 3-1). This concomitant decrease in pH is the result of (i) generation of aliphatic acids during photocatalytic oxidation of bacteria and (ii) production of protons (Guillard *et al.*, 2008).

Because the isoelectric point (IEP) of titania is between 6.5 and 7.0 and the pH decreased during the treatment, the density of $TiOH_2^+$ groups increased in the solution and the TiO_2 surface becomes positively charged. Gumy *et al.*, (2006a) investigated the electrostatic attraction between the *E. coli* and commercial TiO_2 powders. They observed that the isoelectric point is correlated with the catalytic activity of TiO_2 powders in *E. coli* inactivation. When the TiO_2 surface is positive, the *E. coli* inactivation process was observed to be more efficient. More recently, studies reported by Pigeot-Rémy *et al.*, (2011) showed the importance of the cell wall envelope as the primary target of TiO_2 treatment. Even in the dark, the contact between TiO_2 and bacteria damages the cell wall. In contrast, contact between *E. coli* and SiO_2 did not induce changes in bacterial permeability which was explained by the different electrostatic charges on the two types of surfaces at the pH of the reaction.
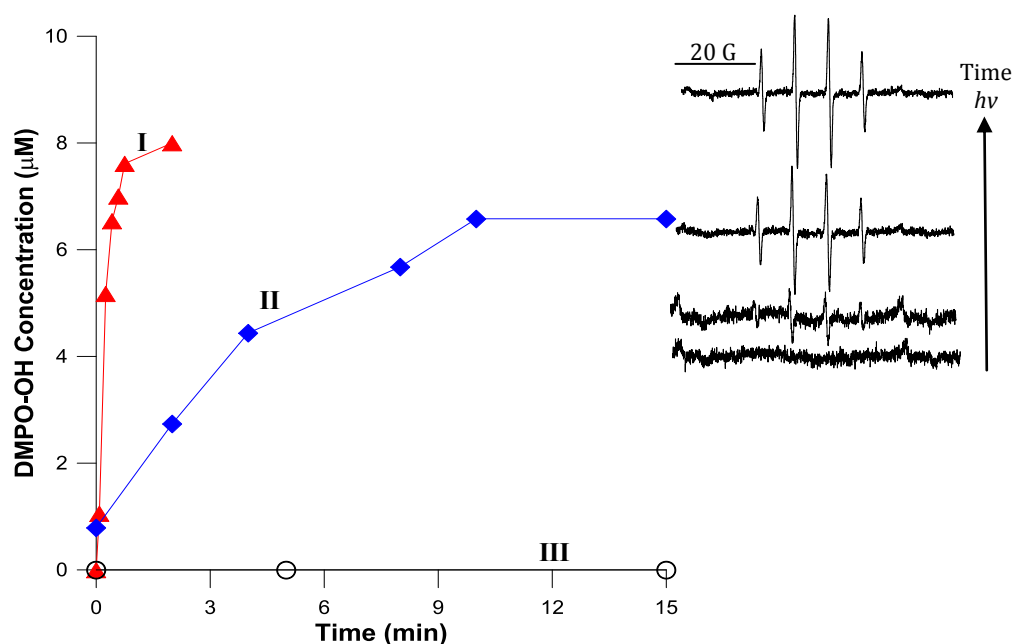
Figure 3-2: The ESR-measured formation of hydroxyl radical (HO•): (i) (▲) TiO$_2$ photocatalysis (1 mg/ml); (ii) (♦) photo-Fenton (FeSO$_4$ ([Fe^{2+}]: 0.6 mg/l), H$_2$O$_2$ (10 mg/l), under light), (III) (○) light alone. *Insert*: typical time evolution of the ESR traces of the paramagnetic spin adducts, DMPO-OH, during the photocatalytic process mediated by nanoTiO$_2$.

Table 3-1: Initial (i) and final (f) values of pH and H$_2$O$_2$ for various systems

Systems under simulated solar light	pH$_i$	pH$_f$	H$_2$O$_{2i}$	H$_2$O$_{2f}$
Figure 3-1 (a), (b)				
Photo-Fenton: FeSO$_4$ (Fe^{2+} 0.6 mg/L), H$_2$O$_2$ (10 mg/L), *hv*	6.7	6.1	10.0	0.5
TiO$_2$ photocatalysis (1 mg/mL)	6.5	5.0	-	-
Figure 3-3				
TiO$_2$ photocatalytic (1 mg/mL)	6.8	5.2	-	-
Photo-Fenton: FeSO$_4$ (Fe^{2+} 0.6 mg/L), H$_2$O$_2$ (10 mg/L), *hv*	6.8	6.4	10.0	5.2
Figure 3-5 (a), (b)				
FeSO$_4$ (Fe^{2+} 12 mg/L), *hv*	5.7	5.3	-	-
FeCl$_3$ (Fe^{3+} 12 mg/L), *hv*	5.4	4.7	-	-
Figure 3-6 (a), (b)				
Photo-Fenton: FeSO$_4$ (Fe^{2+} 0.6 mg/L), H$_2$O$_2$ (10 mg/L), *hv*	6.5	5.6	10.0	0.4
TiO$_2$ photocatalysis (1 mg/mL)	6.2	5.1	-	-

Table 3-2: Evolution of total dissolved iron (Fe_{tot} mg/L) for various systems.

Systems	Time of reaction (min)				
	0	60	120	180	300
Figure 3-1 (a), (b)					
Photo-Fenton: $FeSO_4$ (Fe^{2+} 0.6 mg/L), H_2O_2 (10 mg/L), hv	0.3	0.2	0.0	0.0	0.0
Figure 3-3					
$FeSO_4$ (Fe^{2+} 0.6 mg/L), H_2O_2 (10 mg/L), hv) pH 7.0	0.4	0.4	0.3	0.1	0.0
Figure 3-6 (a), (b)					
Photo-Fenton: $FeSO_4$ (Fe^{2+} 0.6 mg/L), H_2O_2 (10 mg/L), hv	0.3	0.1	0.0	0.0	0.0

3.3.2   Lipid peroxidation using lipopolysaccharide (LPS)

To test whether MDA was indeed a product of bacterial lipid peroxidation, pure LPS, a component of bacterial wall (Nadtochenko *et al.*, 2006), was used as a model target and was exposed to both photo-Fenton and TiO_2 photoctalysis. Figure 3-3 (trace (▲)) shows that MDA levels started to increase to a maximum value of 50 nmol/mg LPS at 30 min, indicating that important peroxidation of membrane lipid was occurring with TiO_2 treatment. For near-neutral photo-Fenton treatment under simulated solar light, low MDA accumulation (maximal concentration of 2.5 nmol/mg before 300 min of treatment) was detected compared with TiO_2 treatment (Figure 3-3, trace (♦)). Dissolved iron was observed until 180 min of treatment (Table 3-2), probably resulting from the LPS chelating effect that favors the maintenance of iron in solution, even a near-neutral pH (Table 3-1). Modest lipid peroxidation, even on relatively high concentrations of pure LPS, support the hypothesis that this pathway is not the only one in bacterial inactivation and death by photo-Fenton treatment at near-neutral pH. In each experiment, a residual peroxide concentration was detected at the end of the experiments, ensuring that a photo-Fenton reaction occurred during entire treatment period (Table 3-1).
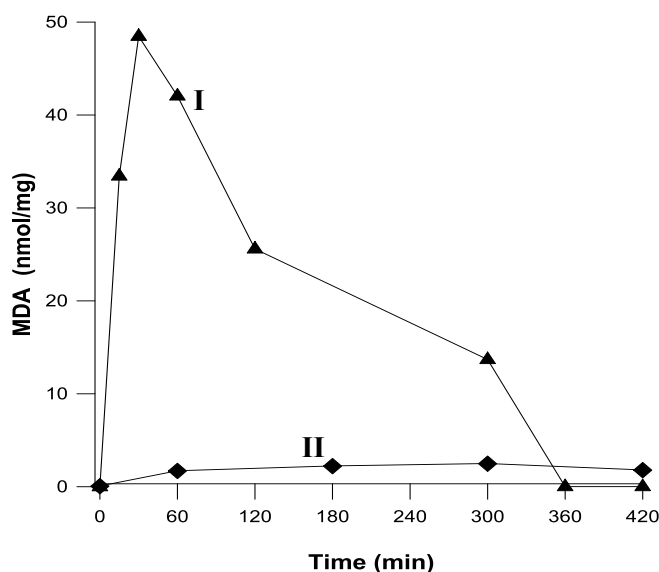
Figure 3-3: Lipid peroxidation based on MDA accumulation on LPS (0.4 mg/L) during: (I) (▲) TiO$_2$ photocatalysis (1 mg/mL); (II) (♦) photo-Fenton (FeSO$_4$ ([Fe^{2+}]: 0.6 mg/L), H$_2$O$_2$ (10 mg/L), under light). Experiments were conducted in triplicate and standard error was found to be approximately 5%.

3.3.3 MDA degradation

Lipid product MDA is known as a target of oxidative degradation. Thus, to assess the extent of the oxidative degradation of MDA under both photocatalytic treatments, different MDA solutions (2.0 nmol/mL) were treated for 30 min with both TiO$_2$ photocatalysis and photo-Fenton process. The residual amount of MDA was determined using the same analytic method of HPLC. Figure 3-4, trace (▲)) shows that MDA was oxidatively destroyed within 10 min by TiO$_2$ photocatalysis, whereas the degradation kinetic for photo-Fenton treatment was slower (longer than 20 min) (Figure 3-4, trace (♦)). These results indicate that MDA under photo-catalytic conditions is a relatively unstable product that undergoes further metabolic transformations. MDA has two aldehyde groups, and the degradation products are expected to be ring cleavage products, such as malonic semialdehyde, malonate, monoaldehydes (formaldehyde, acetaldehyde), monoketons (acetone), and carboxylic acids (formic and/or acetic acid), or complete mineralization products such as CO$_2$, and H$_2$O (Janero, 1990). Therefore, the MDA values in each peroxidation lipidic experiment are the net result of its production and photocatalytic degradation in oxidative conditions. Thus, eventually, the rate of MDA degradation exceeds the rate of MDA production, as observed after 300 min of reaction in the TiO$_2$ photocatalysis, and photo-Fenton treatment on bacteria

(Figure 3-1 (a), trace (▲)) and 30 and 300 min on LPS (Figure 3-3 (traces (▲) and (♦)). Although the TiO_2 photocatalysis treatment degrades MDA at higher rates, its accumulation during lipid peroxidation was also higher when compared with the photo-Fenton treatment with a similar disinfection efficiency (Figure 3-1 (a), traces (▲) and (♦)).
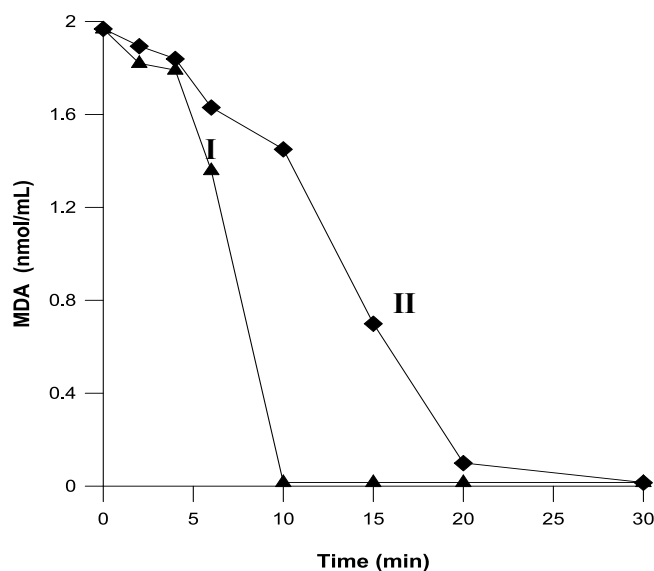
Figure 3-4: MDA degradation during: (I) (▲) TiO_2 photocatalysis (1 mg/mL); (II) (♦) photo-Fenton ($FeSO_4$ ([Fe^{2+}]: 0.6 mg/L), H_2O_2 (10 mg/L), under light). Experiments were conducted in triplicate and standard error was found to be approximately 5%.

3.3.4 Bacterial inactivation mechanism depending on the use of Fe^{2+} or Fe^{3+}

Several studies reported that extracellular Fe^{2+} can penetrate into the cell or react with oxygen, leading to the formation of ROS under light (Catastini *et al.*, 2002; Lau *et al.*, 2013). At near-neutral pH values, Fe^{3+}-organo complexes are able to play an important role in the photogeneration of $HO^{\bullet}$ radicals that attack cellular membranes, causing lipid peroxidation. Because we used ultrapure water, these Fe-organo complexes are formed by by-products generated from bacteria degradation and lysis. Therefore, we evaluated the effect of Fe^{2+} and Fe^{3+} under simulated solar light on lipid peroxidation during bacterial inactivation. As Figure 3-5 (a) (traces (■) and (●)) shows, higher MDA accumulation was observed for the treatment initiated with Fe^{3+}/*hv* compared with Fe^{2+}/*hv* system. Nevertheless, the inactivation rates for both photo-treatment methods were similar with a 7 $\log_{10}$ reduction in *E. coli* concentration reached after 5 h (Figure 3-5 (b), traces (■) and (●)). The significant MDA accumulation

observed with Fe^{3+} under simulated solar light is probably the result of Fe^{3+} binding to proteins of the bacterial membrane and their carboxylic endgroups forming Fe^{3+}-bacteria complexes. The photo-reduction of these complexes under UV-A and visible radiation, leads to a reduction of Fe^{3+} to Fe^{2+} and oxidation of the chelating ligand *via* LMCT (Feng and Nansheng, 2000). Both, Fe^{2+} and ligand radicals react with O_2, forming ROS ($O_2^{\bullet-}$, $HO^{\bullet}$, H_2O_2) close to the target bacteria and leading to lipid peroxidation chains (Cabiscol *et al.*, 2000) and bacterial inactivation (Figure 3-5 (b), trace (■)), for example, because of increased permeability and/or the disruption of trans membrane ion gradients (Braun, 2001; Cieśla *et al.*, 2004; Spuhler *et al.*, 2010).

To manage the transport of Fe^{3+} into the cell, *E. coli* elaborate and secrete high affinity extracellular ferric chelators called siderophores to solubilize iron prior to transport (Köster, 2001). The first step in the internalization process (for Gram-negative bacteria) requires outer membrane (OM) receptor proteins that bind cognate ferri-siderophores with high specificity to transfer iron into the cytoplasm. Once internalized, this process is thought to involve reduction of the siderophore-associated iron resulting in oxidized siderophore dissociation attributable to the relatively low affinity of siderophores for Fe^{2+}. Thus, into the cell, Fe^{2+} can react with metabolic H_2O_2 to generate internal $HO^{\bullet}$ radicals. However, the internal photo-Fenton reaction promoted by the siderophores penetration of Fe^{3+} and its subsequent delivery as Fe^{2+} is considerably less rapid than that originating from the direct penetration of Fe^{2+} forms. Hence, the *E. coli* inactivation observed for Fe^{3+} under light in Figure 3-5 (b) (trace (■)) could be mediated principally by the ROS generated by the photosensitization of Fe^{3+}-bacteria complexes and Fe^{3+}-siderophore complexes (Borer *et al.*, 2005). The formation of these complexes with bacteria can be corroborated through the detection of dissolved ferric species using the Ferrozine method even at pH 5.4 (Figure 3-5 (c), trace (▧)) in which the ferric species are complexed and, thus, solubilized by internal bacteria components (A. Safarzadeh-Amiri *et al.*, 1996). However, the dissolved ferric species decrease further in the treatment. The quasi-stationary concentrations observed for dissolved Fe^{2+} and Fe^{3+} in photocatalytic redox cycle after 120 min to 300 min in Figure 3-5 (c), trace (▧) result from Fe^{2+} generation by photo-reduction of Fe^{3+}-bacteria, Fe^{3+}-siderophore, and Fe^{3+} by-product complexes from one side and the oxidation of Fe^{2+} by O_2 on the other side. However, part of the Fe^{3+} precipitates as insoluble Fe-(hydr)oxides at the experimental pH (Table 3-1) because an average of 54% of total dissolved iron was lost.

The photo-inactivation rate observed in the treatment initiated with Fe^{2+} under light (pH 5.7) (Figure 3-5 (b), (trace (●)) is the result of intracellular Fenton's reactions because added Fe^{2+} can diffuse freely into cells given a lower charge density compared with Fe^{3+}, and it is enhanced by favorable osmotic forces present in ultrapure water (Cartron *et al.*, 2006; Spuhler *et al.*, 2010). Additionally, Fe^{2+} can be transported into the cytoplasmic membrane through specific proteins, essential for Fe^{2+} uptake in bacteria (Lau *et al.*, 2013). Once internalized, Fe^{2+} leads to the generation of $HO^{•}$ radicals when reacting with metabolic H_2O_2 accumulated once catalase is inactivated by UV-A radiation (Braun, 2001). Even though MDA accumulation was not detected in the presence of Fe^{2+} before 180 min of treatment (Figure 3-5 (a), trace (●)), 5 $\log_{10}$ of the initial *E. coli* concentration was inactivated at this time (Figure 3-5 (b), trace (●)). This result indicates that, under light treatment, and in contrast to Fe^{3+}, Fe^{2+} does not significantly contribute to lipid peroxidation to inactivate bacteria. MDA accumulation begun to be detected only after 180 min of treatment (Figure 3-5 (a), trace (●)) because Fe^{2+} goes in, becomes Fe^{3+}, and targets the cell membrane. Further in the treatment, a significant concentration of dissolved ferrous species was observed during the treatment (Figure 3-5 (d), trace (▦)), favored by (i) the formation of complexes with by-products generated from bacterial inactivation that may help Fe^{2+} solubilisation, and (ii) the pH because at near-neural pH, soluble iron species such as $[Fe]^{2+}$, $[Fe(OH)]^{+}$ and $[Fe(OH)_2]$ are formed in the aqueous system, and the $[Fe(OH)_2]$ species dominates before undergoing subsequent oxidation by O_2 (Morgan and Lahav, 2007). In our cases, the oxidation rate could be reduced through the high concentration of Fe^{2+} in the solution because the amount of dissolved oxygen is inversely proportional to the iron content of the water (Dendy, 1968).

The control experiment under simulated light irradiation (Figure 3-5 (b), trace (○)) shows a 5 $\log_{10}$ reduction of initial *E. coli* concentration before 420 min of irradiation. Thermal inactivation can be excluded because temperatures did not exceed 38 °C (Berney *et al.*, 2006); therefore, inactivation was predominantly the result of optical effects. A part of the observed photo-inactivation in ultrapure water could be the result of the endogenously generated ROS. The excited endogenous photosensitizer may react directly with cellular biomolecules, including the attack of proteins and cell membrane components (Gourmelon *et al.*, 1994a), leading to lipid peroxidation chains as was observed after 180 min of treatment (Figure 3-5 (a), trace (○)) and cell inactivation.
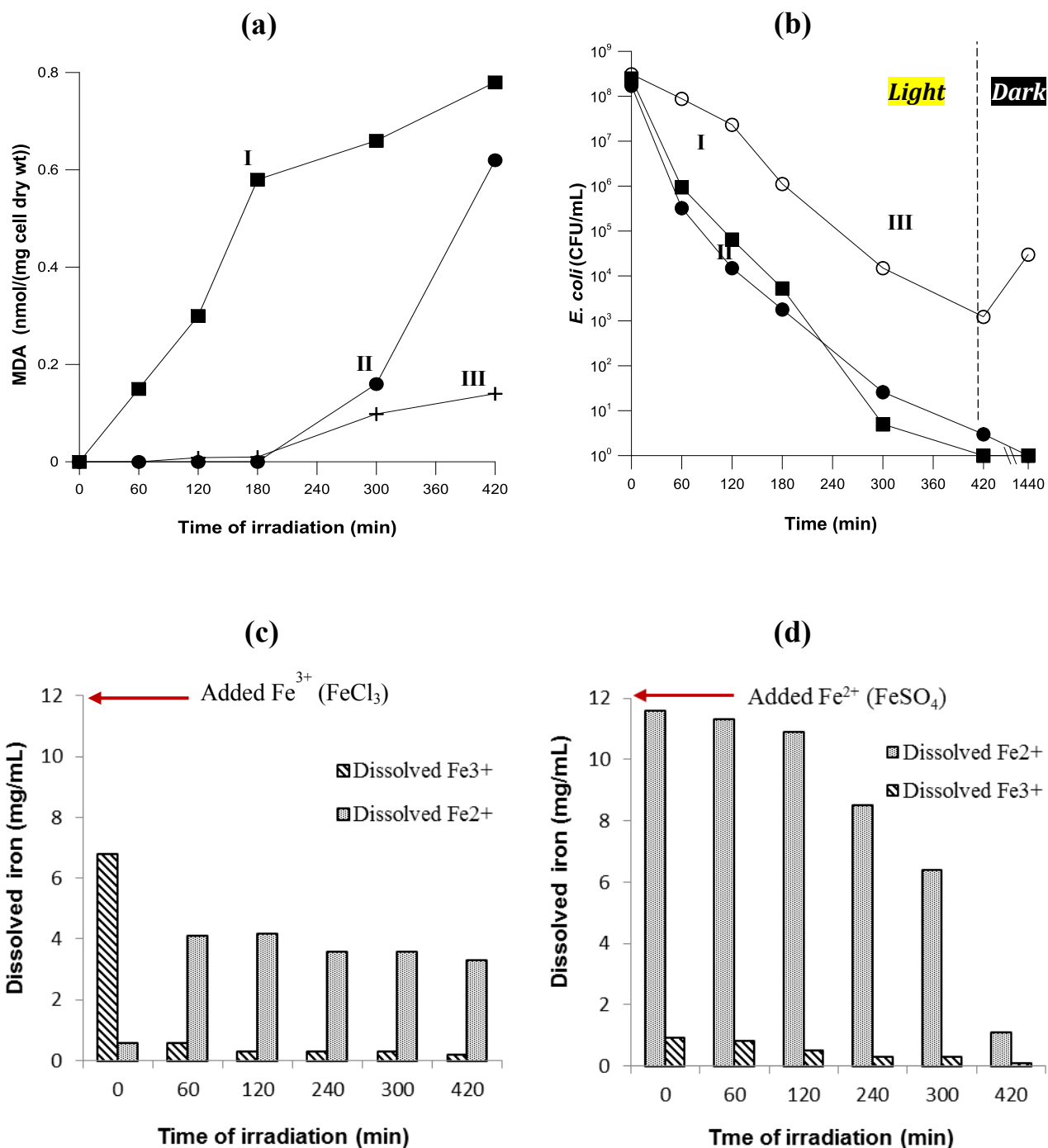
Figure 3-5: (a) Lipid peroxidation based on MDA accumulation. (b) *E. coli* inactivation, during: (I) (■) $FeCl_3$ ([Fe^{3+}]: 12 mg/L), under sole light; (II) (●) $FeSO_4$ ([Fe^{2+}]: 12 mg/L), under sole light; (III) (+) hv light. (c) Evolution of dissolved iron (Fe^{2+}, Fe^{3+}) after filtration during photo inactivation of *E. coli* suspended in a solution of $FeCl_3$ ([Fe^{3+}]: 12 mg/L). (d) Evolution of dissolved iron (Fe^{2+}, Fe^{3+}) after filtration during photo inactivation of *E. coli* suspended in a solution of $FeSO_4$ ([Fe^{2+}]: 12 mg/L). H_2O_2 was not added. Experiments were conducted in triplicate and standard error was found to be approximately 5%.

To further evaluate the bactericidal effect of simulated solar light in the presence or absence of Fe^{2+} after stopping illumination, post-irradiation events were monitored during 24 h of subsequent dark storage. As shown in Figure 3-5 (b) (trace (○)) in the dark, reactivation and/or growth of bacteria occur for bacteria treated with simulated solar light. After 24 h, 1 log_{10} in bacterial counts were obtained. For the photo-assisted Fe^{2+} treatment (Figure 3-5 (b) trace (●)), no reactivation and/or growth of bacteria were observed and a delayed disinfection effect was observed to continue in the dark period. These results are interesting because no addition of hydrogen peroxide is needed and iron naturally present or added in water can act as a low-cost "photocatalyst" for solar water disinfection.

The literature described the efficiency of the Fe^{2+} and Fe^{3+} for *E. coli* inactivation using simulated solar light. Previous work demonstrated that in the presence of 0.6 mg/L of Fe^{2+} or Fe^{3+} under light, total bacterial inactivation was reached from 10^6 CFU/mL in 120 and 180 min for Fe^{2+} and Fe^{3+}, respectively (Spuhler *et al.*, 2010). In contrast, no significant differences were observed in our results as a function of the oxidation state of iron. García-Fernández *et al.*, (2012) also reported complete *E. coli* inactivation after 15 min (1.2 kJ/L) of solar exposure in the presence of 10 mg/L of Fe^{3+} with total dissolved iron of 1.4 mg/L.

3.3.5 Disruption of bacteria cell wall by photo-Fenton and TiO₂ photocatalytic action

The ortho-nitrophenyl-*β*-D-galactoside (ONPG) hydrolysis rate was measured to determine the damage in cell walls during near-neutral photo-Fenton and TiO_2 photocatalysis. Interestingly, in contrast to cellular permeability, the bacterial inactivation experiments mediated by both TiO_2 photocatalysis and photo-Fenton proceeded with similar inactivation kinetics (Figure 3-6 (b), traces (▲) and (♦)). Indeed, the extent of cell damage measured using ONPG concentration was very different for both photo-oxidative treatments (Figure 3-6 (a), traces (▲) and (♦)). The experiment with TiO_2 photocatalysis resulted in an immediate increase in the hydrolytic rate of ONPG with a maximum concentration at 90 min. Suggesting that TiO_2 treatment disrupted the cell wall and/or cytoplasmic membrane, leading to an increase in cell envelope permeability by either an increase in small molecules toward the cell, such as ONPG, and/or the leakage of large intracellular molecules out of the cell. These results were also consistent with the results of Saito *et al.*, (1992), Maness *et al.*, (1999), Pigeot-Rémy *et al.*, (2011), and Swetha *et al.*, (2012), who confirmed that the cell envelope of

E. coli is indeed the initial target of TiO_2 photocatalytic reactions and a primary cause of cell death. Under photo-Fenton treatment, a rise in the ONPG hydrolysis rate was observed after 15 min (Figure 3-6 (a), trace (♦)) with a maximum concentration at 75 min of treatment. The corresponding damage of the *E. coli* cell envelope was lower compared with TiO_2 photocatalytic treatment. Thus, although photo-Fenton treatment induced only limited damage to the cell envelope, its overall deleterious effect could be sufficient to disrupt the external structure of bacteria and allow external H_2O_2 and/or iron ions to diffuse into the cell. In the latter case, the internal Fenton's reactions are enhanced to produce powerful oxidative radicals that subsequently degrade intracellular components. These results are indicative of the difference in the extent of cell damage by photo-Fenton and TiO_2 photocatalysis and possibly different mechanisms of bacterial inactivation.

Figure 3-6 (a) shows that the ONPG hydrolysis rate declines beyond 75 and 90 min during the photo-Fenton or TiO_2 photocatalysis treatment, respectively suggesting a loss of enzyme activity. Therefore, the effect of both photo-oxidative treatment methods on direct inactivation of cell-free β-D-galactosidase was evaluated using cell lysate. TiO_2 photocatalysis showed a major loss of enzyme activity (90%) compared to photo-Fenton treatment (50%) beyond 45 min of treatment (Figure 3-7). However, Figure 3-6 (a) shows that whole cells can maintain some level of enzymatic activity indicating that damage to the intracellular content can be precluded at the initial stages by the cell wall and cytoplasmic membrane. This observation confirms the role of the cell envelope as the primary target of TiO_2 attack.

(a)

(b)
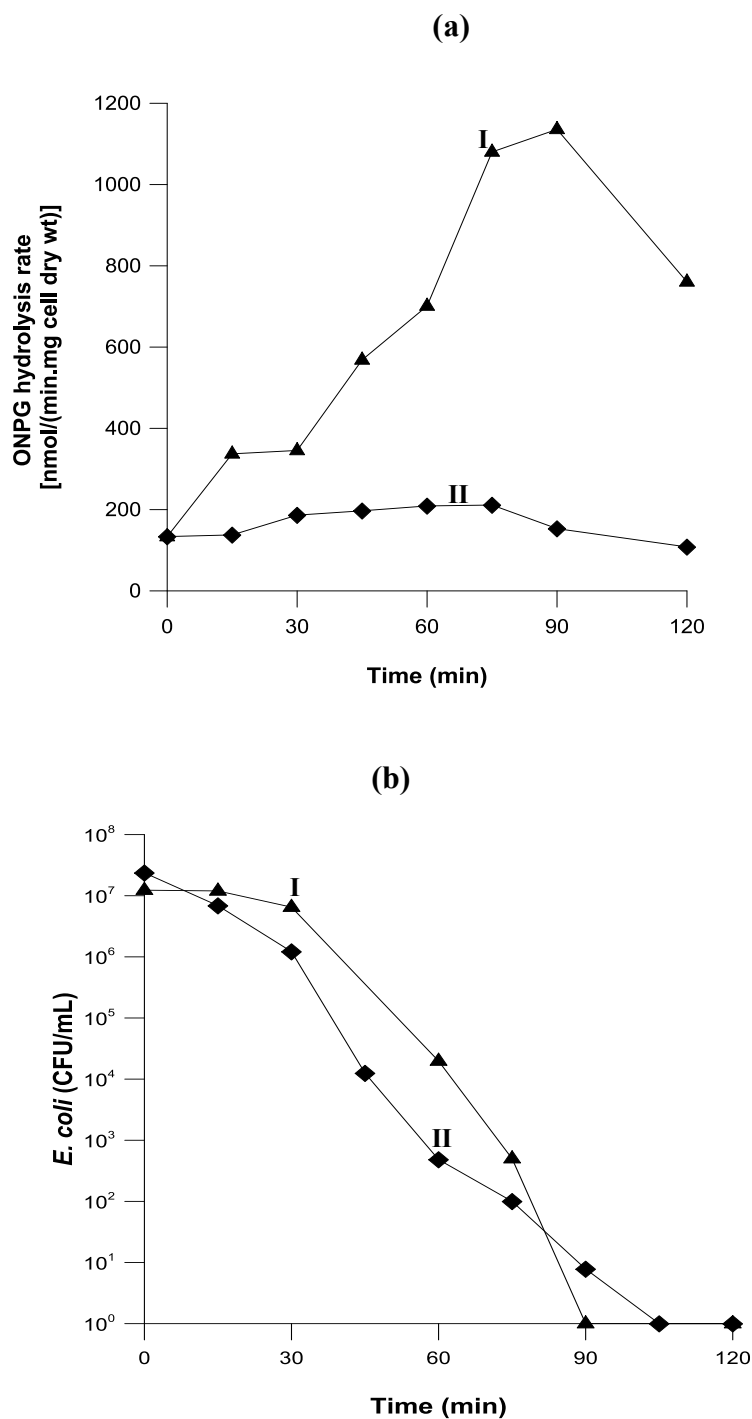
Figure 3-6: (a) Cell permeability change based on ONPG hydrolysis rate (b) *E. coli* inactivation during: (I) (▲) TiO$_2$ photocatalysis (1 mg/mL); (II) (♦) photo-Fenton (FeSO$_4$ ([Fe^{2+}]: 0.6 mg/L), H$_2$O$_2$ (10 mg/L), under light). Experiments were conducted in triplicate and standard error was found to be approximately 5%.
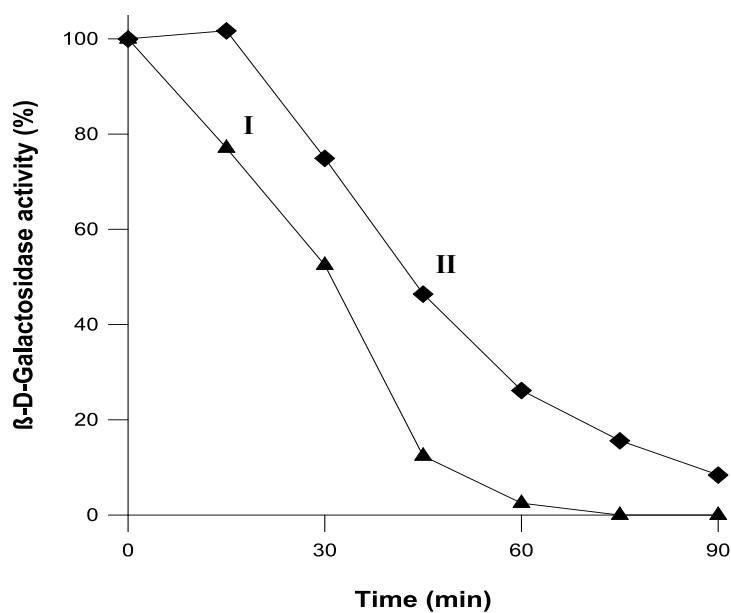
Figure 3-7: Effect of the photocatalytic treatments on cell-free β-D-galactosidase activity using cell lysate: (I) ($\blacktriangle$) TiO$_2$ photocatalysis (1 mg/mL); (II) ($\blacklozenge$) photo-Fenton (FeSO$_4$ ([Fe^{2+}] 0.6 mg/L), H$_2$O$_2$ (10 mg/L), under light). Experiments were conducted in triplicate and standard error was found to be approximately 5%.

3.4   Conclusions

The results of lipid peroxidation and permeability change in the cell envelope suggest a mechanism of bacterial inactivation difference for near-neutral photo-Fenton and TiO$_2$ photocatalysis. The bacterial inactivation mechanism by photo-Fenton process at near-neutral pH is mediated by both internal and external processes that occur in bacteria. In contrast, for TiO$_2$ photocatalysis, the cell envelope damage is a significant target. However, further investigations are required to elucidate this aspect.

We propose that the mechanism of bacterial inactivation by photo-Fenton treatment at near-neutral pH is mediated by both internal and external processes. Internal (photo)Fenton processes are mediated by the synergistic action of UV-A and external Fenton reactants. For external events, homogeneous and heterogeneous photocatalytic actions contributed to efficient bacterial inactivation.

E. coli inactivation rates photo-assisted by the bare presence of Fe^{2+} and Fe^{3+} in the absence of H$_2$O$_2$ are similar. However, the specific action mode of each ionic form was not the same. For Fe^{3+}/hv, the cell membrane damage was more important compared with Fe^{2+}/hv. Fe^{3+} binds to the cellular membrane and siderophores and generates localized ROS that attack

cellular membranes, causing lipid peroxidation. Conversely, Fe^{2+} can diffuse into the cell through the FeO system and participate in intracellular Fenton's reactions, leading to the generation of $HO^\bullet$ radicals when reacting with metabolic H_2O_2 inside the cells. Because iron is naturally present or added in water as Fe^{3+}, the findings of this study are relevant to water disinfection *via* low-cost photocatalysts.

4. Iron oxides semiconductors are efficient for solar water disinfection: a comparison with photo-Fenton processes at near-neutral pH.

Iron oxides photo-assisted bacterial inactivation in water
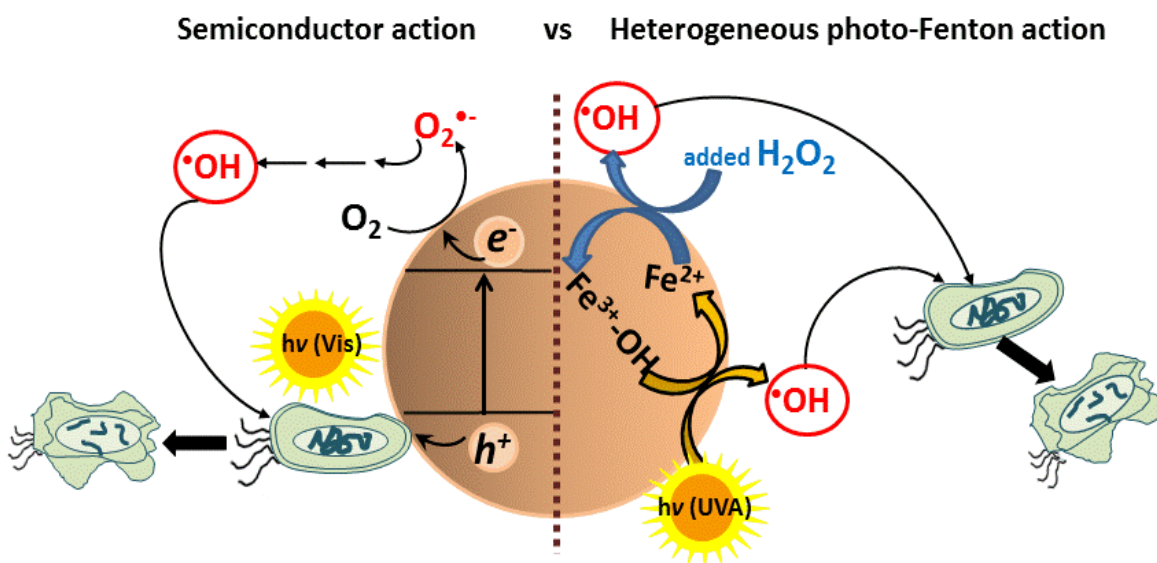
4.1   Introduction

Drinking water scarcity is one of the most serious global challenges of our time (Aldhous, 2003; Brame *et al.*, 2011). The necessity for advanced water purification in terms of eliminating contaminants and killing bacteria will continue to increase, especially in developing countries where water treatment is often inadequate or non-existent. The photo-assisted Fenton oxidation is one of the most popular and widely studied advanced oxidation processes (AOPs). In particular, photo-Fenton reactions play a key role in sunlight-assisted AOPs due to the fact that they take advantage of UV, near-UV and visible light up to 600 nm, thus comprising 35% of the total energy coming from the solar spectrum. Until now, the pH of the process was generally perceived as the limiting factor for photo-Fenton systems, because $Fe(OH)^{2+}$, *i.e.* the most photo-active Fe^{3+}-hydroxy complex under UV-A and visible solar light, is predominant at low pH (~2.8) (A. Safarzadeh-Amiri *et al.*, 1996; Pignatello *et al.*, 2006). However, recently, the photo-inactivation of *E. coli* by photo-Fenton system at near-neutral pH has been reported (Rincón and Pulgarin, 2006; Spuhler *et al.*, 2010; Ruales-Lonfat *et al.*, 2013; Rodríguez-Chueca *et al.*, 2014a; Rodríguez-Chueca *et al.*, 2014b; Ruales-Lonfat *et al.*, 2014). A near-neutral pH, a spontaneous chemical oxidation of ferrous ions to ferric by dissolved oxygen in water occurs, involving a variety of partially oxidized meta-stable ferrous–ferric intermediate species (*e.g.* green rusts). These iron intermediates ultimately transform into a variety of stable iron oxide end-products such as hematite, magnetite, goethite and lepidocrocite (Jolivet *et al.*, 2004; Morgan and Lahav, 2007).

Recent researches haves focused on the idea of replacing dissolved iron with solid catalysts in so-called heterogeneous Fenton reactions. In particular, quite a number of iron-containing systems have been developed for organic pollutants degradation, including iron oxides (He *et al.*, 2002; Matta *et al.*, 2007; Xue *et al.*, 2009), iron-immobilized materials (Lv *et al.*, 2005; Shin *et al.*, 2008; Mazille *et al.*, 2010), clays and carbon materials (Tabet *et al.*, 2006; Chueca *et al.*, 2012), *etc*.

Iron oxides are among the most chemically reactive components of suspended matter in aquatic systems and can be easily prepared in laboratory conditions (Cornell and Schewetmann, 2003). Additionally, they are considered non-toxic and environmentally friendly compounds, similarly to free iron ions (Xu *et al.*, 2012). Most of them reveal

semiconductor properties and then may also act as photocatalysts, even though their overall efficacy can be impaired by a very efficient hole–electron recombination (Zhangl *et al.*, 1993).

Possible semiconducting mechanisms involved in iron oxide can be summarized as follows. In the first step, a photon with energy equal to or greater than the material's band gap, which separates the conductance band (CB) and valence band (VB), is absorbed by a semiconducting particle of iron oxide. This gives rise to the generation of the electron/hole pair (Eq. (4.1)). Although the excited electron/hole pair can recombine and release the energy as heat, some of the excited electrons and holes can contribute to redox reactions on the surface of a semiconducting particle of iron oxide. The most relevant redox processes, which take place after the photo-generation of electrons (e^-_{cb}) and holes (h^+_{vb}) in semiconducting particles of iron oxide suspended in aqueous medium, containing also an organic substance (RX), are summarized in Eqs. (4.1)–(4.5) (Cornell and Schewetmann, 2003). (> Fe^{2+} and > Fe^{3+} represent the Fe^{2+}/Fe^{3+} species in solid or solution phase).

$$Fe_2O_3 + hv \rightarrow Fe_2O_3\ (e^- + h^+) \tag{4.1}$$
$$e^-_{(cb)} + O_2 \rightarrow O_2^{\bullet-} \tag{4.2}$$
$$h^+_{(vb)} + O_2^{\bullet-} \rightarrow {}^1O_2 \tag{4.3}$$
$$e^-_{(cb)} + > Fe^{3+} \rightarrow > Fe^{2+} \tag{4.4}$$
$$h^+_{(vb)} + RX_{ad} \rightarrow RX_{ad}^{\bullet+} \tag{4.5}$$

Irradiation may also enhance the heterogeneous Fenton process on iron-bearing particles, by promoting the photo-reduction of > $Fe^{3+}OH$ to > Fe^{2+} (Eq. (4.6)), which subsequently reacts with H_2O_2 generating $HO^\bullet$ radicals at the particle surface (Eq. (4.7)).

$$> Fe^{3+}OH + hv \rightarrow > Fe^{2+} + HO^\bullet \tag{4.6}$$
$$> Fe^{2+} + H_2O_2 \rightarrow > Fe^{3+} + OH^- + HO^\bullet \tag{4.7}$$
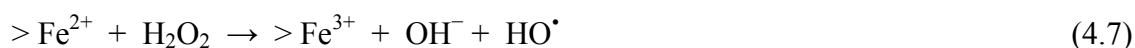
A large number of studies have demonstrated that iron oxide minerals such as magnetite, hematite, goethite or ferrihydrite are effective for oxidation of organic pollutants and compounds that affect water quality (Huang *et al.*, 2001; He *et al.*, 2002; Andreozzi *et al.*, 2003; Matta *et al.*, 2007; Yuan *et al.*, 2013). However, since little research has been conducted on these compounds towards inactivation of microorganisms present in aqueous

solutions (Mazille *et al.*, 2010; Pecson *et al.*, 2012; Asadishad *et al.*, 2013; Nieto-Juarez and Kohn, 2013; Ruales-Lonfat *et al.*, 2014), their role in bacterial inactivation is not well known. In our previous paper (Ruales-Lonfat *et al.*, 2014), it was shown that goethite was efficiently inactivating bacteria, acting as semiconductor *via* a photocatalytic process and as an heterogeneous iron source in Fenton process around neutral pH.

In this work, bacterial inactivation by addition of $FeSO_4$ in illuminated water at initial pH of 6.5 and 7.5 were studied in the absence or presence of H_2O_2. Also, the ferric precipitates formed during the treatments were identified. The main purpose of this work was to investigate the disinfection ability of four iron (hydr)oxides in aqueous media under solar light illumination, at near-neutral pH of 6.5, in the absence or presence of H_2O_2, to better distinguish their action mode, either as semiconductors or catalysts of the heterogeneous photo-Fenton process. The iron (hydr)oxide (hematite, goethite, wüstite and magnetite) used in this study are the most common constituents of the sub-surface environment. Furthermore, ROS generated by iron (hydr)oxides during these processes were identified and quantified. Finally, the influence of NOM on the activity of hematite during bacterial inactivation was evaluated.

4.2   Materials and methods

4.2.1   Chemicals

Ferrous sulphate heptahydrate ($FeSO_4 \cdot 7H_2O$) (Riedel-de Haën 99-103.4%), hydrogen peroxide (H_2O_2) 30% w/v (Riedel de Haën). Sodium hydroxide (NaOH, 98%) and hydrochloric acid (HCl, 36.5%), were purchased from Sigma-Aldrich. The spin-trap, 5,5-dimethyl-1-pyrroline-N-oxide (DMPO), was purchased from Enzo Life Sciences (ELS) AG (Lausen, Switzerland). The spin probes, 4-hydroxy-2,2,6,6-tetramethylpiperidine-1-oxyl (TEMPOL) and 4-oxo-2,2,6,6-tetramethylpiperidine-1-oxyl (TEMPONE), as well as their respective precursors, *i.e.* 2,2,6,6-tetramethyl-4-piperidinol (TMP-OH) and 2,2,6,6-tetramethyl-4-piperidone (TEMPONE precursor), were purchased from Sigma Aldrich (Buchs, Switzerland). The commercially available iron (hydr)oxides particles, *i.e.* goethite, hematite, wüstite, and magnetite, were purchased from Sigma-Aldrich. The particles size were

(<50 mesh and <5 μm). The most relevant physicochemical properties of these iron (hydr)oxides particles are shown in Table 4-1.

All solutions were prepared immediately prior to irradiation with the use of ultrapure water. Two different types of water were used to suspend bacteria *i.e.* ultrapure water and the natural water from Lake Geneva. Table 4-2 shows the physicochemical characteristics of these waters.

Table 4-1: Physicochemical properties of the particles studied.

Iron minerals	Formula	Iron oxidation state	Surface area $(m^2/g)^a$	IEP[b]	Band-gap energy[b] (eV)
Goethite	α-FeOOH	+3	37.0	7.5-8.5	2.1
Hematite	α-Fe$_2$O$_3$	+3	-	8.5	2.2
Wüstite	FeO	+2	10.0	8.0	2.4
Magnetite	Fe$_3$O$_4$	+2, +3	2.0	6.0-6.5	0.1

[a] Surface area reported by the manufacturer and from references (Matta *et al.*, 2007; Han *et al.*, 2011)
[b] Isoelectric point and band gap energy, from references (Xu and Schoonen, 2000; Cornell and Schewetmann, 2003)

Table 4-2: Physicochemical characteristics of the waters used in the experiments.

Parameter	Ultrapure water	Lake Geneva water
Conductivity at 20 °C (μS/cm)	<0.055	252
Transmittance at 254 nm (%)	100	96
pH	6.5	8.4
Total organic carbon (TOC) (mg C/L)	<0.005	0.8-1
Iron (mg/L)	-	0.019
Phosphates (mg PO$_4^{-3}$/L)	-	0.012
Hydrogen carbonate (mg HCO$_3^-$/L)	-	108
Chloride (mg Cl$^-$/L)	-	8.0
Sulfate (mg SO$_4^{-2}$/L)	-	48
Nitrate (mg NO$_3^-$/L)	-	2.7

4.2.2 Bacterial strains and growth media

The bacterial strain used was *E. coli* K12 (MG1655), a non-pathogenic wild-type strain, which can be handled with little genetic manipulation. Bacteria was inoculated from a stock in a rich medium, Luria-Bertani (LB) broth, and incubated in a shaker incubator at 37 °C and 180 rpm. After 8 h, cells were diluted (1% v/v) in the pre-heated LB broth and incubated at 37 °C for 15 h in the incubator until a stationary physiological phase was

reached. Cells were separated during the stationary growth phase by centrifugation (15 min at 5000 rpm, at 4 °C). The bacterial pellet was re-suspended and washed for 10 min in the centrifuge (twice). This procedure resulted in a bacterial pellet of approximately 10^9 colony forming units per millilitre (CFU/mL).

4.2.3 Photocatalytic semiconductor and (photo)-Fenten-mediated inactivation experiments

All bacterial inactivation experiments were performed in Pyrex reactors (4 cm x 9 cm, 100 mL). The Pyrex reactors containing the bacterial suspension in water (approximately 10^6 CFU/mL) were placed in the dark at 25 °C and kept under magnetic stirring for at least 30 min to let the bacteria adapt to the new matrix and to allow the die-off and equilibration of the most stress-sensitive species. In the experiments with cationic iron, $FeSO_4$ (0.6 mg/L relative to the Fe^{2+} content) were added to a solution of *E. coli*. Then, the pH was adjusted to 6.5 or 7.5 depending of the experiment and the samples were exposed to H_2O_2 (10 mg/L) and/or simulated solar light over 2 h hours, under continuous stirring. Aliquots were taken during set intervals within the inactivation time. These concentrations were determined experimentally as being optimal (results not shown) and corresponded to the limit, where bacterial inactivation could not be further enhanced, when more of Fe^{2+} was added (Spuhler *et al.*, 2010).

In the experiments with iron (hydr)oxide particles at a concentrations of 0.6 mg/L relative to the Fe content were added to a solution of *E. coli*. Then, the pH was adjusted to 6.5 and *E. coli* inactivation was studied for each particle type to test four different inactivation mechanisms: in the dark in ultrapure water only (control), in the dark with H_2O_2 (dark Fenton), under sunlight (photocatalysis) and under sunlight, in the presence of H_2O_2 (photo-Fenton). H_2O_2 was added to the reactor as the last component at a concentration of 10 mg/L.

Photo-Fenton and photocatalysis experiments were carried out using a solar simulator CPS Suntest System (Heraeus Noblelight, Hanau, Germany). The Suntest bears a lamp that emits ~0.5% of the photons at wavelengths < 300 nm (UVC cut-off at 290 nm), ~7% between 300 and 400 nm and the rest follow the solar spectrum above that value until IR range (IR was cut-off by filtering). The radiance intensity was measured by a spectroradiometer, Model ILT-

900-R (International Light Technologies) and corresponded to 820 W/m^2 of light global intensity (20.2 W/m^2 on the UV).

During the experiments, the temperature in the reactors did not exceed 38 °C. After each experiment, the reactors were rinsed with nitric acid (10%), followed by washing with distilled water and, finally, autoclaved. All the experiments were conducted triplicate, with good reproducibility (<10% difference between replicates).

Bacterial reactivation and/or growth were determined for some experiments by leaving the last samples in the dark at room temperature (20-25 °C) for 24 h before the measurement of the CFU.

4.2.4 Analytical methods

Dissolved Fe^{2+} was measured using the Ferrozine method as described previously (Spuhler *et al.*, 2010) and total dissolved iron was measured using an Inductively Coupled Plasma Mass Spectrometer (ICP-MS), Model ICPE-9000 (Shimadzu, Japan). Samples were filtered (0.25 µm) and kept in acid solution prior to the determination. The detection limit ranges of spectrometry used for this experiment were (0.2–0.9 µg/L). The concentration of H_2O_2 was monitored using a titanium (IV) oxysulfate solution *via* a spectrophotometric method at 410 nm (modified method DIN 38 402 H15). The titanium (IV) oxysulfate method has a 0.1 mg/L detection limit. The bonding structure in particle samples was analyzed by Fourier transform infrared spectroscopy (FT-IR) (Nicolet 6700), using the KBr self-supported pellet technique in the frequency range of 400–4000 cm^{-1}. The pH was measured with a pH-metre Metrohm 827 pH-lab using a glass electrode.

4.2.4.1 Electron spin resonance spectroscopy (ESR)

ESR in combination with spin-trapping were used to monitor the formation of ROS, namely HO$^\bullet$ and O$_2^{\bullet-}$ radicals, generated by photocatalytic semiconductor and heterogeneous photo-Fenton processes in the presence of iron (hydr)oxide particles. A stock solution of DMPO (0.5 M) was prepared in ultrapure water and was stored at -20 °C. Just before performing the photo-generation of ROS, DMPO (final concentration of 100 mM) was added to aqueous suspensions containing reagents. Subsequently, 2 mL aliquots of the prepared samples were transferred into small Pyrex beakers (5 mL volume, 20 mm outer diameter and 30 mm height)

and exposed to simulated solar light under constant agitation. Subsequently, the sample of the Fenton's reagents was drawn into thin glass capillaries (0.7 mm ID/0.87 mm OD, from VitroCom, NJ, USA), which were then sealed on both ends using the Cha-Seal™ tube-sealing compound (Medex International, Inc. USA). ESR measurements were carried out at room temperature using a Bruker X-band spectrometer, Model EleXsys 500 (Bruker BioSpin, Karlsruhe, Germany) equipped with a high-Q cylindrical TE_{011} microwave cavity, Model ER4123SHQE. The typical instrumental settings were: frequency of 9.4 GHz; microwave power of 0.63 mW; scan width of 120 G; magnetic field resolution of 2048 points; modulation frequency of 100 kHz; modulation amplitude of 1.0 G; receiver gain of 60 dB; conversion time of 40.96 ms; time constant of 20.48 ms and sweep time of 84 s.

The spin-adducts concentrations were estimated using the double integration of the first-derivative ESR spectra. The actual concentrations of spin-adducts were derived by comparison with a calibrated ESR signal, which was acquired for a stable nitroxide radical, TEMPOL (10 µmol/L). The data analysis was carried out using Origin Pro 9.0 software.

4.3   Results and discussion

4.3.1   Photo-inactivation of bacteria by addition of $FeSO_4$ at pH 6.5 and 7.5 in the absence or presence of H_2O_2. Evolution of soluble forms of iron during the treatment.

The Figure 4-1 shows the complete *E. coli* inactivation before 90 min during the $FeSO_4$-based photo-Fenton treatment at initial pH 6.5 and 7.5 (Figure 4-1, traces (▲) and (♦)). In particular, the photo-Fenton treatment at pH 6.5 showed faster bacterial inactivation rate (under 60 min), as compared with the same system at pH 7.5. This is due to the presence of dissolved ferrous iron ions in the system at pH 6.5 (Table 4-3). They contribute to the homogeneous photo-catalytic cycle, thus accelerating the decomposition of H_2O_2, which, in turn, results in enhancement of $HO^•$ production. This observation was corroborated by the hydrogen peroxide consumption that was greater for the photo-Fenton treatment at pH 6.5 than at pH 7.5 (Table 4-3).

The inactivation of *E. coli* by homogeneous photo-Fenton process may be explained by several mechanisms. One possibility is an internal process, where endogenous photo-sensitizers and internal iron sources synergistically coupled with external UV and Fenton reactants lead to oxidative stress through the intracellular Fenton's reaction. As a result, highly toxic $HO^{\bullet}$ radicals are generated, which can directly attack DNA and other internal cell components, thus leading to bacterial growth inhibition. The other scenario might be due to the contribution of external pathways, where exogenous ROS, such as $^1O_2$, H_2O_2 and $HO^{\bullet}$, are formed outside of the cell and can direct attack to the external cell membrane, thus initiating chain reactions of lipid peroxidation. This results in an increase of cell membrane permeability, impairs cellular functioning and severely affects cell viability (Cabiscol *et al.*, 2000). In our opinion, the internal (photo)Fenton mechanism represents a key contribution to the overall inactivation process. This is based on our previous findings pointing to only very weak lipid peroxidation and slight cell permeability changes under photo-Fenton treatment at near-neutral pH (Ruales-Lonfat *et al.*, 2014).

In contrast to the same treatment at pH 6.5, dissolved iron was not detected in the filtrate samples during the reaction at pH 7.5 (Table 4-3). In the latter case, *E. coli* inactivation was achieved before 90 min of treatment (Figure 4-1, trace (♦)), and was principally mediated by heterogeneous photo-Fenton reactions. Goethite (α-FeO(OH)) and/or lepidocrocite (γ-FeO(OH)) which have been reported to be formed by oxidation of Fe^{2+} in solution at neutral pH (Cornell, 2000), are probably involved in this process.

In control experiments conducted in the absence of H_2O_2, for the Fe^{2+}/light system at pH 6.5, ~3.5 $\log_{10}$ reduction of the number of live bacteria was reached before 120 min of treatment (Figure 4-1, trace (△)). As can be seen in Table 4-3, dissolved iron was present throughout treatment. The bactericidal effect of the photo-assisted Fe^{2+} is the result of the combined action of the Fe^{2+} and light into the bacterial cell. Indeed, added Fe^{2+} can easily diffuse into the cell (Cartron *et al.*, 2006; Ruales-Lonfat *et al.*, 2014) and catalase, which regulates H_2O_2 concentration into the bacteria, is degraded by UV-A radiation, leading to intracellular Fenton reactions enhancement. On the contrary, in the experiments conducted at pH 7.5, Fe^{2+} was effectively oxidized and transformed in solid iron forms by O_2, in the absence of H_2O_2 (Table 4-3). This system was not efficient neither as heterogeneous photocatalyst nor as semiconductor, as it lead only to ~2 $\log_{10}$ reduction of the bacterial concentration before 120 min of treatment, values similar to the bacterial inactivation reached under a light-alone

system (Figure 4-1, traces (◊) and (✿)). The solid iron formed at pH 7.5 does not enhance significantly the photo-inactivation of bacteria, probably because this pH is close to the isoelectric point of goethite (IEP = 7.5-8.5) and lepidocrocite (IEP = 7.3-7.5) which are iron oxides formed by oxidation of Fe^{2+} at this pH (Cornell and Schewetmann, 2003). Thus, the contact/attraction of > FeOH groups with average negative membrane of *E. coli* is not favourable because hydroxyl groups at the iron oxide surface are uncharged.
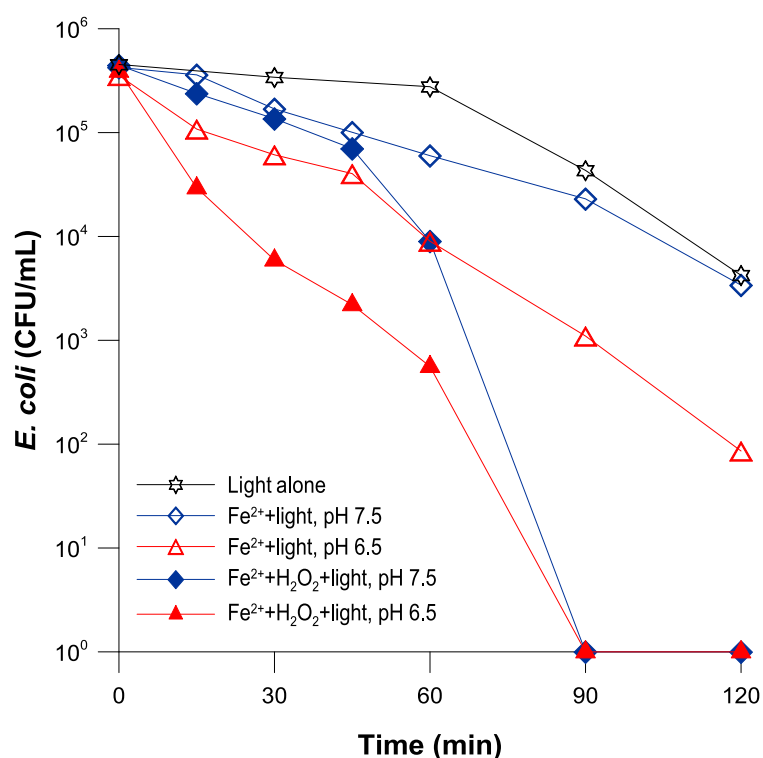
Figure 4-1: *E. coli* inactivation by: (▲) photo-Fenton at pH 6.5; (♦) photo-Fenton at pH 7.5; (△) Fe^{2+}, under light at pH 6.5; (◊) Fe^{2+}, under light at pH 7.5; (✿) light alone. FeSO$_4$: 0.6 mg/L relative to the Fe^{2+} content, H$_2$O$_2$: 10 mg/L. Experiments were conducted under simulated solar light and performed in triplicate (the standard error was found to be approximately 5%).

The effect of the presence of bacteria in the solubilisation of iron during photo-Fenton process was evaluated at pH 6.5 and 7.5. Table 4-4 shows that soluble iron species were not detected during the FeSO$_4$-based photo-Fenton system at pH 6.5 and 7.5 in the absence of bacteria. It was the result of the formation of the aquo hydroxo zero-charge complexes, which are the precursors of the solid-phase iron (Jolivet *et al.*, 2004), formed in the absence of complexing ligands. On the contrary, in the presence of bacteria, complexing substances are liberated from the beginning or generated as by-products during bacterial inactivation. This explains

why soluble iron was detected at pH 6.5 when bacteria are present. It could be mediated by secreted siderophores (*e.g.*, ferritins and aerobactin from *E. coli*) (Andrews *et al.*, 2003) that can chelate iron, allowing its solubilisation. The photo-reduction of Fe^{3+}-siderophore complexes under UV-A and visible radiation, produces $HO^{\bullet}$ and regenerates Fe^{2+} *via* LMCT (Köster, 2001; Upritchard *et al.*, 2007). In contrast to pH 6.5, at pH 7.5 no dissolved iron was observed in the presence of bacteria during entire treatment period even if detection limit ranges of ICP-MS spectrometry used for this experiment were 0.2–0.9 µg/L. This could be due to non-soluble crystalline forms of iron species formed at high pH (7.5), which are more stables to be photo-reduced by siderophores (Sulzberger and Laubscher, 1995). These results are in good agreement with those reported by Waite and Morel (Waite and Morel, 1984), who detected photo-reduced iron from amorphous Fe-hydroxides at pH 6.5, but not at pH 8.0. They proposed that a hydroxylated ferric surface species is the primary chromophore (light absorbing compound), analogous to the photoreduction of $Fe(OH)^{2+}$, and that at pH 8 the Fe^{3+} surface complex was more strongly hydrolyzed and less prone to photoreduction.

Table 4-3: Values of pH, total dissolved iron (Fe_{tot} mg/L) and H_2O_2 during bacterial inactivation for different systems. Iron sulfate or iron (hydr)oxide: 0.6 mg/L relative to the Fe content, H_2O_2: 10 mg/L, irradiated with simulated solar light.

Iron(hydr)-oxide particles	pH		Fe (mg/L)			H_2O_2 (mg/L)		
	0 min	120 min	0 min	60 min	120 min	0 min	60 min	120 min
Figure 4-1								
Iron sulfate+H_2O_2+light	6.5	6.0	0.3	0.2	N.D	10.0	5.2	5.0
Iron sulfate+light	6.5	6.2	0.4	0.3	0.1	-	-	-
Iron sulfate+H_2O_2+light	7.5	6.8	N.D	N.D	N.D	10.0	8.0	7.4
Iron sulfate+light	7.5	7.1	N.D	N.D	N.D	-	-	-
Figure 4-4 (a-d)								
Wustite+H_2O_2+ light	6.5	6.3	N.D	N.D	N.D	10.0	9.4	8.6
Wustite+light	6.5	6.2	N.D	N.D	N.D	-	-	-
Hematite+H_2O_2+ light	6.5	6.3	N.D	N.D	N.D	10.0	9.6	8.9
Hematite+Light	6.5	5.9	N.D	N.D	N.D	-	-	-
Magnetite+H_2O_2+ light	6.5	6.4	N.D	N.D	N.D	10.0	9.3	9.3
Magnetite+light	6.5	6.3	N.D	N.D	N.D	-	-	-
Goethite+ H_2O_2+light	6.5	6.2	N.D	N.D	N.D	10.0	9.6	8.8
Goethite +light	6.5	6.3	N.D	N.D	N.D	-	-	-

Experiments were conducted in triplicate and standard error was found to be approximately 5%. N.D.: not detectable

Table 4-4: Values of total dissolved iron (Fe_{tot} mg/L) from $FeSO_4$-based photo-Fenton processes in the presence and absence of bacteria. $FeSO_4$: 0.6 mg/L relative to the Fe^{2+} content, H_2O_2: 10 mg/L, irradiated with simulated solar light.

Initial pH	Time	Dissolved iron (mg/L) in the absence of *E. coli*	Dissolved iron (mg/L) in the presence of *E. coli*
	0	N.D	0.4
	15	N.D	0.4
6.5	30	N.D	0.4
	60	N.D	0.2
	120	N.D	N.D
	0	N.D	N.D
	15	N.D	N.D
7.5	30	N.D	N.D
	60	N.D	N.D
	120	N.D	N.D

Experiments were conducted in triplicate and standard error was found to be approximately 5%. N.D.: not detectable

4.3.1.1 Identification of generated solid species in the $FeSO_4$-based photo-Fenton process in the absence of bacteria at pH 6.5 and 7.5

Figure 4-2 shows the decrease in dissolved Fe^{2+} concentration in a stirred water solution, initiated with 0.6 mg/L of $FeSO_4$, relative to the Fe^{2+} content at pH 6.5 and 7.5. It was conducted in the absence of bacteria and in the absence or presence of H_2O_2 (10 mg/L). In the absence of H_2O_2, a remarkable difference in Fe^{2+} oxidation rates and subsequent precipitation of generated iron oxides were observed at pH 6.5 and 7.5 (Figure 4-2, traces (—△—) and (—◇—)). The loss of ferrous ions in the solution in the absence of H_2O_2 is due to the oxidation by dissolved oxygen. Morgan and Lahav, (2007) reported that at neutral pH and $[Fe^{2+}] < 1$ mg/L, soluble iron species like $[Fe]^{2+}$, $[Fe(OH)]^+$ and $[Fe(OH)_2]$ are initially formed in the aqueous system, according to Eqs. (4.8)-(4.10) before undergoing subsequent oxidation by O_2 (Eqs. (4.11)-(4.13)). However, "hydrolysed" ferrous iron species are more readily oxidized than non-hydrolysed ones in the following order: $[Fe(OH)_2] \gg [Fe(OH)]^+ \gg [Fe]^{2+}$. The oxidation of soluble ferrous species $[Fe(OH)_2]$ by O_2 (Eq. (4.13)), producing partially oxidized ferro-compounds like meta-stable ferrous–ferric species as $[Fe_4(OH)_8(H_2O)_8]$ (Eq. (4.14)). These compounds are subsequently transformed into end-products such as hematite, magnetite, goethite, and lepidocrocite, which are insoluble ferric species (Eq. (4.15)) (Jolivet *et al.*, 2004).

$$Fe^{2+} + 6H_2O \rightarrow [Fe(H_2O)_6]^{2+}_{(aq)} \tag{4.8}$$

$$[Fe(H_2O)_6]^{2+}_{(aq)} + OH^- \rightarrow [Fe(OH)(H_2O)_5]^+_{(aq)} \tag{4.9}$$

$$[Fe(OH)(H_2O)_5]^+_{(aq)} + OH^- \rightarrow [Fe(OH)_2(H_2O)_4]_{(aq)} \tag{4.10}$$

$$[Fe(H_2O)_6]^{2+} + O_2 \rightarrow [Fe(H_2O)_6]^{3+} + O_2^{\bullet-} \tag{4.11}$$

$$[Fe(OH)(H_2O)_5]^+ + O_2 \rightarrow [Fe(OH)(H_2O)_5]^{2+} + O_2^{\bullet-} \tag{4.12}$$

$$[Fe(OH)_2(H_2O)_4] + O_2 \rightarrow [Fe(OH)_2(H_2O)_4]^+ + O_2^{\bullet-} \tag{4.13}$$

$$4[Fe(OH)_2(H_2O)_4] \rightarrow [Fe_4(OH)_8(H_2O)_8]_{(S)} + 8\ H_2O \tag{4.14}$$

$$[Fe_4(OH)_8(H_2O)_8]_{(S)} + O_2 \rightarrow 4FeOOH_{(S)} + 10H_2O \tag{4.15}$$
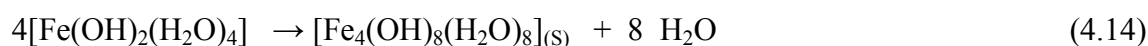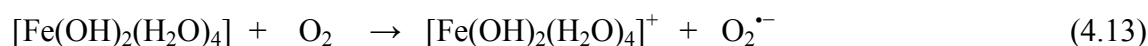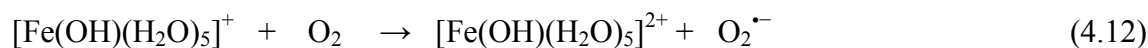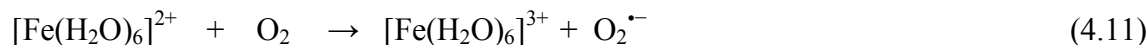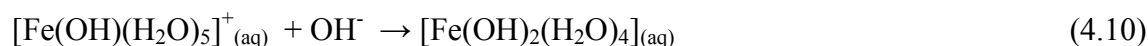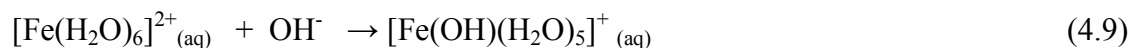
The fact that dissolved Fe^{2+} was not found shortly after the addition of H_2O_2, confirms the loss of ferrous ions in the solution at both pH levels (Figure 4-2, traces (--▲--) and (--◆--). Thus, the addition of H_2O_2 increases oxidation rates, indicating that both O_2 and H_2O_2 contribute to the fast oxidation of ferrous iron species at near-neutral pH and, in concert, lead to spontaneous oxidation and subsequent formation of insoluble ferric species. Therefore, in the absence of complexing ligands (secreted by bacteria from the beginning or generated as by-products during bacterial inactivation), soluble iron species are negligible in a photo-Fenton process at neutral pH.

To identify the solid iron species formed during the photo-Fenton treatment at pH 6.5 and 7.5 in the absence of bacteria, the precipitated iron were recovered for FT-IR analysis. Although the sample colour was yellow for insoluble iron species obtained at pH 6.5 and brown for these obtained at pH 7.5, the IR spectrum was similar for both compounds. This could be due to the variation of parameters affecting the surface area and morphologies of the precipitate as follows: the final pH of the solution, which specially influences the Fe:OH ratio, the precipitation rate (slow/fast), temperature (usually 40-90 °C) and the time of hydrolysis and oxidation process (minutes to weeks) (Jolivet *et al.*, 2004). In our case, the last three parameters were well controlled and, consequently, only the Fe:OH ratio, related to the final pH of the solution, affected the colour of the samples.
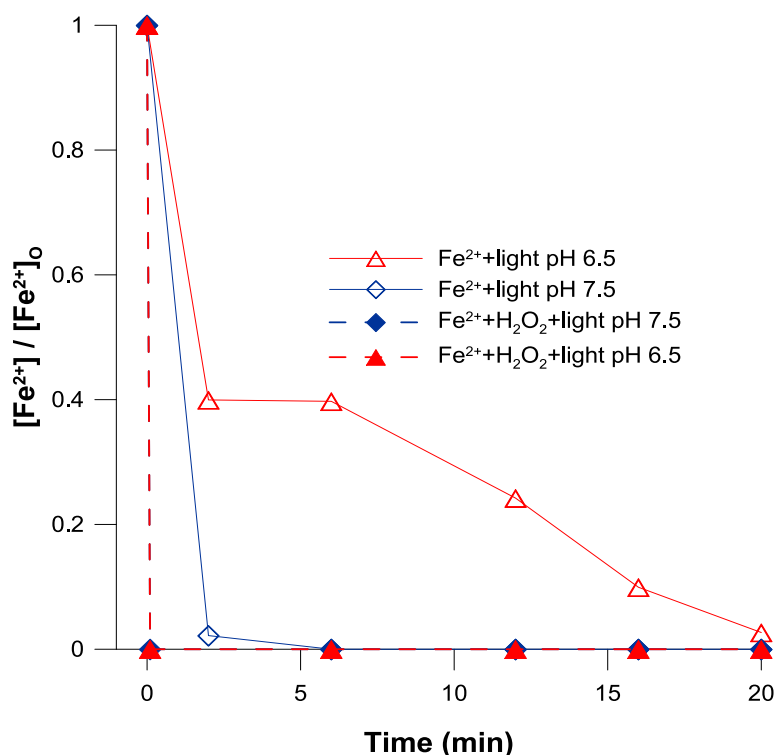
Figure 4-2: The time evolution of the ferrous iron ions concentration remaining in solution at pH 6.5 ($\Diamond$) and 7.5 (Δ), in the presence (---) or absence (–) of 10 mg/L H_2O_2. $FeSO_4$ concentration: 0.6 mg/L relative to the Fe^{2+} content. Experiment performed in the absence of bacteria. Experiments were conducted under simulated solar light and performed in triplicate (the standard error was found to be approximately 5%).

Figure 4-3 shows the infrared spectra of insoluble ferric species obtained at pH 7.5. The three absorption band observed at approximately 740, 553 and 462 cm^{-1} correspond to those of α-FeOOH, which can be attributed to the stretching vibration of Fe–O and Fe–O–H (Durães *et al.*, 2005). The band at 553 cm^{-1} is assigned to the hexagonal environmental characteristic of hematite or goethite (Santilli *et al.*, 1990). The band at 491 cm^{-1} confirms the octahedral positions of the H_2O and OH groups in the ferric complexes (Durães *et al.*, 2005; Kwon *et al.*, 2006). The absorption band above 3000 cm^{-1} is originated by the H-bonded OH groups, since the isolated OH groups absorb above 3600 cm^{-1}. This broad peak is due to the combined contributions of iron (hydr)oxide, and the adsorbed water in the samples. Iron hydroxide, if present, may also contribute to this broad peak. Absorption bands at 3396 and 1633 cm^{-1} are characteristic bending vibration of O–H of crystal water, indicated the presence of water in the coordination sphere of the metal. Furthermore, the absorption band at 1020 cm^{-1} is produced by HO–Fe interaction in the (0 1 0) plane bending of lepidocrocite (γ-FeOOH) (Cambier, 1986). Considering all these features, the observation of the infrared spectra in Figure 4-3

leads to the conclusion that the insoluble iron species formed under photo-Fenton process at pH 6.5 and 7.5 are mainly iron (hydr)oxide alone or mixed as goethite (α-FeOOH) and lepidocrocite (γ-FeOOH).
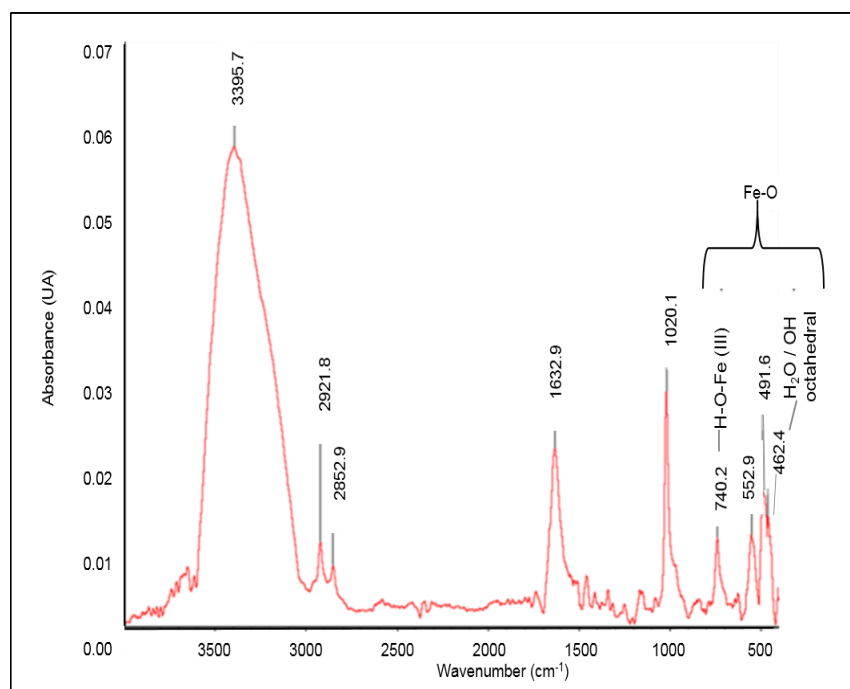
Figure 4-3: FT-IR spectra of ferric precipitates formed during the photo-Fenton reactions at pH 7.5.

4.3.2   Contribution of photocatalytic semiconductor vs heterogeneous photo-Fenton processes to bacterial inactivation at near-neutral pH

In our previous work (Ruales-Lonfat *et al.*, 2014), we have demonstrated that goethite was beneficial for bacterial inactivation at near-neutral pH, both as a photocatalytic semiconductor and as heterogeneous photo-Fenton catalyst. To determine whether iron (hydr)oxide enhanced inactivation, and to determine whether such an enhancement is due to photocatalytic semiconducting mechanism or heterogeneous photo-Fenton reactions, bacterial inactivation studies were conducted in the presence of different commercial iron (hydr)oxides, as well as H_2O_2 and/or simulated solar light. The iron (hydr)oxide compounds selected were: goethite and hematite because these are the most reactive and abundant solid iron oxides present in nature (sources of iron Fe^{3+}) (Cornell and Schewetmann, 2003), magnetite (source of iron Fe^{2+}/Fe^{3+}), and wüstite (source of iron Fe^{2+}) which exists also in nature (Wang *et al.*, 2012).

Figure 4-4 (a)-(d) shows that in the dark, the studied iron (hydr)oxides did not yield inactivation in the absence or presence of H_2O_2, indicating that heterogeneous Fenton processes (iron (hydr)oxides and H_2O_2) did not contributed to bacterial inactivation under our experimental conditions. Some studies reported that magnetite is a promising Fenton catalyst for oxidative processes for dye removal, and phenol and aromatic hydrocarbon degradation (Lee *et al.*, 2006; Matta *et al.*, 2007). They explained that magnetite has a combination of +2 iron and +3 iron atomic states that aids to increase decomposition of hydrogen peroxide and the production of $HO^{\bullet}$ that enhance decomposition of organic contaminants. This was not observed in our experiments on bacterial inactivation (Figure 4-4 (d)) possibly due to:

(i) The uncharged magnetite surfaces in our experimental pH of 6.5 (IEP: 6.0–6.5 (Table 4-1)) offer unfavourable sites for the adsorption of negatively charged bacteria. It was reported that adsorption onto magnetite particles was a prerequisite for achieving significant virus inactivation (Nieto-Juarez and Kohn, 2013),

(ii) The formation of the particle agglomeration that was favoured in our experimental conditions (pH 6.5, Table 4-3) since agglomeration is enhanced when pH values of the suspension is near to isoelectric point of the material (Sun *et al.*, 1998; Vikesland *et al.*, 2007). Agglomeration of magnetite particles affects the available reactive surface area (site blockage) as the active sites can become less accessible for bacteria and for H_2O_2 (kinetic effect) (Buzmakov and Pshenichnikov, 1996). This can explain the lower consumption of H_2O_2 during magnetite-based photo-Fenton systems compared to the other iron (hydr)oxides that contain only Fe^{3+} in the structure, as goethite and hematite (data not shown),
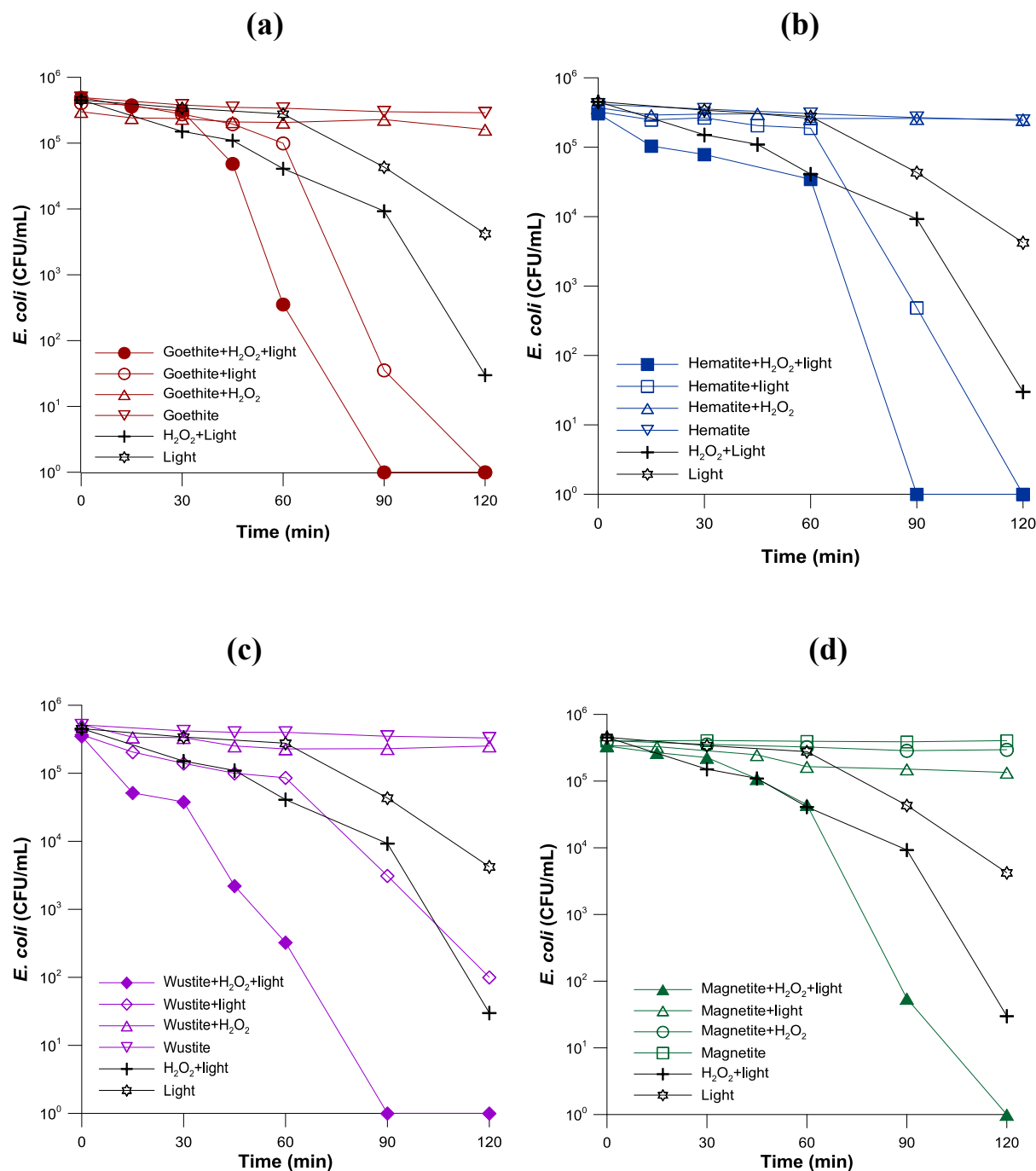
Figure 4-4: *E. coli* inactivation by iron (hydr)oxide particles in the presence or absence of sunlight and H_2O_2 for (a) goethite, (b) hematite, (c) wüstite and (d) magnetite. Experimental conditions: pH 6.5; iron (hydr)oxides concentrations: 0.6 mg/L relative to the Fe content; H_2O_2: 10 mg/L. Experiments were conducted under simulated solar light and performed in triplicate (the standard error was found to be approximately 5%).

(iii) The oxidation of structural Fe^{2+} to Fe^{3+} by O_2 and H_2O_2. This oxidation produces an outer Fe^{3+} oxide layer which reduces electron transfer activity on the surface and inhibits the catalytic efficiency towards Fenton catalysis (Costa *et al.*, 2006; Pinto *et al.*,

2012). Kong *et al.*, (1998) compared to surface of unused magnetite, that of used magnetite treated with H_2O_2. Used magnetite exhibited self-precipitate as revealed by scanning electron microscopy (SEM) analysis. This precipitate seemed to cause lower treatment efficiency in magnetite system.

Wüstite (FeO) also contains Fe^{2+} in the structure but its efficiency in Fenton processes for bacterial inactivation was also very low probably because of the same reason (the oxidation of structural Fe^{2+} to Fe^{3+} by O_2 and H_2O_2) that that proposed for magnetite. The use of wüstite as heterogeneous Fenton catalysts is not documented in the literature.

The combination of iron (hydr)oxides and light show semiconductor properties with a band gap of 2.2 eV for hematite, 2.1 eV for goethite, and 2.4 for wüstite (Table 4-1). Photo-inactivation curves with goethite and hematite showed a shoulder (Figure 4-4 (a) and (b)). This initial period of latency indicates that a contact between bacteria and oxide was necessary and that self-defence mechanisms of bacteria have to be overpassed to effectively photo-inactivate bacteria with these oxides. After that, the bacterial inactivation rate increased considerably. Thus, goethite, hematite and wüstite were photoactive under simulated solar light irradiation to efficiently inactivate bacteria, using only oxygen (from air) as electron acceptors. Similarly, in our previous work, we have demonstrated the photocatalytic semiconducting activity of goethite towards bacterial inactivation (Ruales-Lonfat *et al.*, 2014). In contrast, magnetite was not capable of inactivating bacteria under light (Figure 4-4 (d), trace (Δ) and its negative screen effect was observed with regard to the control experiment under light alone (Figure 4-4 (d), trace (✿)). This is the result of the narrower band gap of the magnetite (0.1 eV) compared to those of goethite, hematite and wüstite (2.2–2.4 eV) (Figure 4-1) and the existence of both Fe^{2+} and Fe^{3+} in its lattice, leading to a continuous electron hopping between the two, which increases the electron–hole recombination and the lowering of its photoactivity (Beydoun *et al.*, 2000; Beydoun *et al.*, 2002; Cornell and Schewetmann, 2003; Chou *et al.*, 2013). Furthermore, the extent of recombination depends to some extent on the pH of the solution and its effect on the proportion of > FeOH groups at the surface (Zhangl *et al.*, 1993). Thus, as was mentioned before, the contact/attraction of > FeOH groups with *E. coli* is not favourable because hydroxyl groups at the surface are uncharged, leading to an increase in the electron-hole recombination rate (Zhangl *et al.*, 1993) and a decrease in the efficiency of the reactions of the valance-band hole with bacteria. In addition, the photo-generated holes in the valence–band of magnetite have weak oxidation

potential which is not enough to generated $HO^{\bullet}$. Goethite and hematite present an IEP between 7.5 and 8.5 (Figure 4-1) (Cornell and Schewetmann, 2003), indicating that hydroxyl groups at the surface are partially protonated ($> Fe-OH_2^+$). The surface interaction of $> Fe-OH_2^+$ with *E. coli* is favoured by electrostatic attraction forces because the *E. coli* surface is negative charged between pH 3 and pH 9 due to the phospholipids and lipopolysaccharides on its cell surface (Maness *et al.*, 1999).

The iron hydr(oxides) particles studied under the simultaneous presence of light and H_2O_2 caused considerable bacterial inactivation enhancement when compared with the other systems and with control experiments (Figure 4-4 (a)–(d)). *E. coli* inactivation was reached before 90 min of treatment for goethite, hematite and wüstite (Figure 4-4 (a)-(c)) and at 120 min for magnetite (Figure 4-4 (d)). The total dissolved iron was determined by ICP-MS spectrometry during the reaction process. Photo-dissolution of iron hydr(oxides) was not significant in the reactions since the concentration of total iron was below detection limit. Thus, *E. coli* inactivation with iron hydr(oxides) was in this case mediated principally by a heterogeneous (photo)-Fenton process. Such systems combine photocatalytic semiconductor character and photo-assisted heterogeneous Fenton oxidation in a single material.

The relative little difference of required time to inactivate bacteria by photo-assisted hematite and goethite in the presence (90 min) or absence (120 min) of H_2O_2 suggest that from the application point of view, small concentrations (0.6 mg/L relative to the Fe content) of these iron (hydr)oxides can be applied as semiconductor to efficiently disinfect water. These results are interesting because the omission of H_2O_2, significantly reduces the cost of the treatment. Therefore, the iron (hydr)oxide particles, including those already present in environmental waters, have great potential for low-cost "photocatalyst" in solar water disinfection, as it has already been demonstrated in our previous work in Africa (Ndounla *et al.*, 2013).

No bacterial reactivation and/or growth were observed after 24 h and 48 h of dark storage for the iron (hydr)oxide-based photo-Fenton treatment. The same antimicrobial activity was obtained for the photocatalytic semiconducting action of hematite and goethite. Additionally, a delayed disinfection effect was observed to continue in the dark period for the photo-assisted wüstite-based treatment.

4.3.3 ROS generated by photocatalytic semiconductor and heterogeneous photo-Fenton processes in the presence of iron (hydr)oxide

In general, the ability of iron oxide particles to produce ROS under light defines their potential to inactivate microorganisms or degrade biomolecules by oxidation. Therefore, by employing the ESR spin-trapping technique, we quantified ROS, *i.e.* $HO^{\bullet}$, $O_2^{\bullet-}$ and $^1O_2$, produced photo-assisted iron (hydr)oxide in the absence or presence of H_2O_2. DMPO was used as a spin trap to identify both $HO^{\bullet}$ and $O_2^{\bullet-}$ radicals, thus leading to the formation of spin-adducts, DMPO–OH or DMPO–OOH, respectively. Both resulting paramagnetic products reveal distinct and easily recognizable ESR spectra. However, the DMPO–OOH spin adduct is well known to be highly unstable and rapidly decomposes into the DMPO–OH spin adduct (Buettner and Mason, 1990). Therefore, as a result, a characteristic ESR spectrum of the DMPO–OH spin adduct consisting of four well resolved peaks (1:2:2:1 quartet, $a_N = a_H = 14.9$ G) was observed (insert in Figure 4-5).

Figure 4-5 (a) and (b)) shows that ESR signals of DMPO–OH were not detected before illumination in the experiments. These results suggest that exposure to the simulated solar light was essential for generation of ROS for the iron (hydr)oxide in the absence or presence of H_2O_2. The growth of the ESR signal intensity of DMPO–OH confirmed the generation of $HO^{\bullet}$ and $O_2^{\bullet-}$ radicals, contributing in the photocatalytic semiconducting process of iron (hydr)oxide (Figure 4-5 (a)). A higher ESR signal intensity for photo-assisted hematite system was observed compared with goethite, even if the bacterial inactivation rate was similar (120 min) (Figure 4-4 (a) and (b), traces (○), (□)). It could be result of the different physico-chemical properties of the iron (hydr)oxides used as IEP, particle size, specific surface area of particle, *etc*. that influences in the ROS generation (Stefaniak *et al.*, 2010; Xu *et al.*, 2013). This result is in agreement with previous findings by Xu *et al.*, (2013), who reported that among the oxides, hematite is the most active in $HO^{\bullet}$ generation under neutral pH. Photo-assisted magnetite generated the lowest $HO^{\bullet}$ radicals production (Figure 4-5 (a)), that is in correlation with the negligible bacterial inactivation rate observed in Figure 4-4 (d), trace (Δ). Possibly due to the aggregation of magnetite particles, and the weak oxidative potential of the photo-generated holes in the valence-band as were explained before.

The mechanism of ROS generation by iron (hydr)oxides illuminated under simulated solar light involves semiconductor photocatalysis (Mazellier and Bolte, 2000; Cornell and

Schewetmann, 2003; Xu *et al.*, 2013). Thus, the photo-induced reactive species (electron–hole pairs) are formed on iron oxides under illumination (Eq. (4.1)). Conduction band electrons could react with O_2 to form superoxide radicals ($O_2^{\bullet-}$) (Mazellier and Bolte, 2000) (Eq. (4.2)), followed by reaction between hole and superoxide radical to form singlet oxygen as given by Eq. (4.3). Also electrons could participate in the regeneration of Fe^{2+} species (Eq. (4.4)). It was reported that the valence band (VB) of the iron (hydr)oxides is above the $OH^-/HO^{\bullet}$ potential (Xu *et al.*, 2013). Therefore, the oxidation of OH^- by holes in the iron (hydr)oxides VB is thermodynamically unfavouruable, leaving O_2 reduction as the most viable pathway for ROS production. On the contrary, holes in the excited surface of iron (hydr)oxides can directly react with bacteria (Eq. (4.5)). It is thermodynamically favourable because hole possess a positive oxidation potential of ~+1.7 at pH = 7 (Xu and Schoonen, 2000; Xu *et al.*, 2013), that is below to the redox potential of microorganism and cell (redox potential of bacteria +0.45 to +0.72 V vs. SCE, pH = 7) (Widdel *et al.*, 1993; Brasca *et al.*, 2007; TitanPE Technologies, 2011).

Alternatively, Xu *et al.*, (2013) proposed that the formation of H_2O_2 and $HO^{\bullet}$ (Eqs. (4.16) and (4.17)) in photo-assisted hematite suspensions involved reduction of O_2 of electrons (Eq. (4.2)), which was inhibited under anaerobic conditions.

$$e^-_{(cb)} \; + \; O_2^{\bullet-} + 2H^+ \; \rightarrow \quad H_2O_2 \tag{4.16}$$
$$e^-_{(cb)} \; + \; H_2O_2 \; \rightarrow \; OH^- + \; HO^{\bullet} \tag{4.17}$$

Nevertheless, some controversy exists in the literature about the photocatalytic properties of goethite and iron oxides particles. Kiwi and Gratzel, (1987) argued that the semiconductor mechanism is not likely to be important except in very small (colloidal) iron oxide particles because of the short diffusion length of electrons and holes in iron oxide semiconductors.

The reactive ROS formed during these processes at the iron (hydr)oxide surface and the direct oxidation of bacteria by surface holes contributed to achieving complete bacterial inactivation for the goethite, hematite and ~3 log_{10} reduction of the bacterial concentration for the wüstite after 120 min of treatment under simulated solar light (Figure 4-4 (a)-(c)).

(a)

(b)
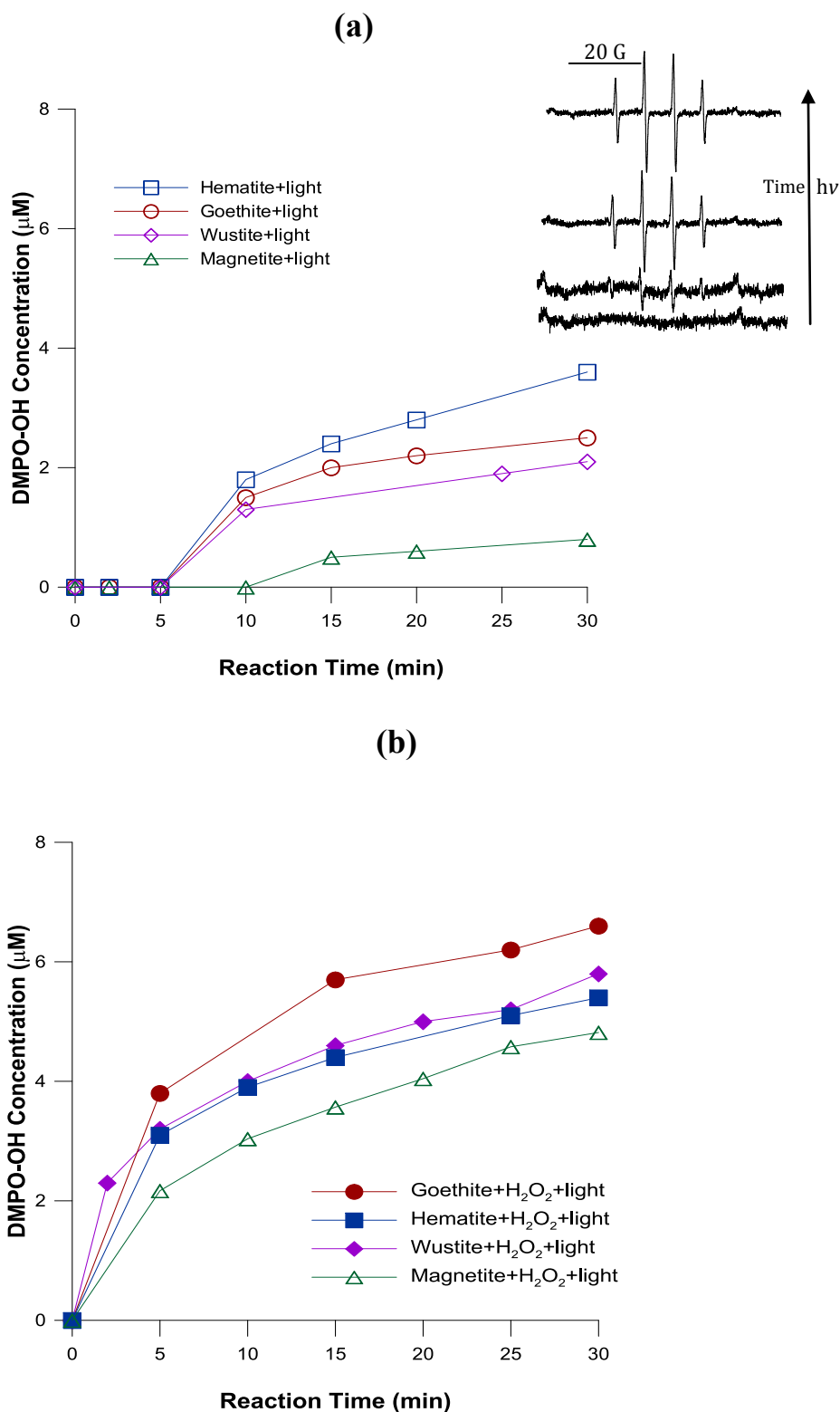
Figure 4-5: The ESR-measured formation of hydroxyl radical in aqueous suspensions of iron (hydr)oxide particles under simulated solar light: (a) in the absence of H_2O_2 and (b) in the presence of 10 mg/L of H_2O_2. *Insert*: typical time evolution of the ESR traces of the paramagnetic spin adducts, DMPO-OH. Iron (hydr)oxide concentrations: 0.6 mg/L relative to the Fe content, pH 6.5.

The presence of H_2O_2 in the photo-assisted iron (hydr)oxide suspension promoted a rapid generation of $HO^\bullet$ (Figure 4-5 (b)), that contributed to a more efficient bacterial inactivation observed in Figure 4-4 (a)-(d). The beneficial effect of the added H_2O_2 under light is due its electron acceptor properties. Thus, electrons generated on illuminated iron oxides from Eq. (4.1) are trapped by the H_2O_2 forming $HO^\bullet$ (Eq. (4.17)). Also H_2O_2 initiates chain reactions by heterogeneous Fenton reactions (Eqs. (4.18) and (4.19)), leading to the formation of hydroperoxyl radical ($HO_2^\bullet$) by contact with Fe^{3+} sites available on the surface of iron particles dispersed in aqueous solution. Concomitantly, Fe^{3+} is reduced to Fe^{2+} (Eq. (4.18)). New Fe^{2+} reaction sites are then formed and allow H_2O_2 to generate $HO^\bullet$ radicals when the Fe^{3+} sites are recovered through oxidation of Fe^{2+} in the cyclic mechanism (Eq. (4.19)). The Fe^{2+} regeneration (which is the rate determinant step of Fenton reaction) could occur *via* the photo-reduction of Fe^{3+} species (Eq. (4.6)) as well, through the photo-Fenton reaction (Eq. (4.20)). Another positive effect of the presence of H_2O_2 is the reduction of the electron–hole recombination rate and consequently the hole will be more active to react with bacteria. Photo-dissolution of iron hydr(oxides) was not significant in the reactions since the concentration of total iron was below detection limit of ICP-ES used (0.2 µg/L). Thus, *E. coli* inactivation with iron hydr(oxides) was mediated by a heterogeneous (photo)-Fenton process. Such systems combine photocatalytic semiconductor character and photo-assisted heterogeneous Fenton oxidation in a single material. (> Fe^{2+} and > Fe^{3+} represent the Fe^{2+}/Fe^{3+} species in solid or solution phase

$$> Fe^{3+} + H_2O_2 \rightarrow \; > Fe^{2+} + H^+ + HO_2^\bullet \qquad (4.18)$$
$$> Fe^{2+} + H_2O_2 \rightarrow \; > Fe^{3+} + OH^- + HO^\bullet \qquad (4.19)$$
$$> Fe^{3+} + H_2O_2 + h\nu \rightarrow \; > Fe^{2+} + H^+ + HO^\bullet \qquad (4.20)$$

He *et al.*, (2002) suggested a different reaction mechanism for the heterogeneous photo-Fenton reaction under UV-light irradiation in the presence of hematite and goethite, based on the experimental observations of degradation of a model azo dye, Mordant Yellow 10 (MY10):

$$> Fe^{3+}OH + H_2O_2 \rightarrow \; > Fe^{3+}OOH + H_2O \qquad (4.21)$$
$$> Fe^{3+}OOH + h\nu \rightarrow \; > Fe^{4+}=O + HO^\bullet \qquad (4.22)$$
$$> Fe^{4+}=O + H_2O \rightarrow \; > Fe^{3+}OH + HO^\bullet \qquad (4.23)$$
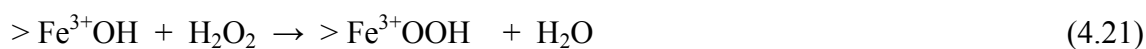
The reactions are initiated by the formation of a precursor surface complex of H_2O_2 with the oxide surface metal centres. Under UV irradiation, the excited $> Fe^{3+}OOH$ bond is broken to produce $> Fe^{4+}=O$ species and $HO^\bullet$ radical. The $> Fe^{4+}=O$ is highly unstable and reacts immediately with H_2O forming another active hydroxyl radical. Therefore, the radicals photogenerated from Eqs. (4.17)–(4.23) increase the signal of DMPO-OH in Figure 4-5 (b) and contribute to enhance bacterial inactivation (Figure 4-4 (a)-(d)).

Previous studies have reported that in aqueous suspensions containing goethite under room light (wavelength between 400 and 700 nm) at pH 7.5 in the absence and presence of the H_2O_2, not $HO^\bullet$ radicals but singlet oxygen and superoxide ions acts as a keys reactive species of the ROS (Paciolla *et al.*, 1999; Mazellier and Bolte, 2000; Han *et al.*, 2011). Nevertheless, in our experimental conditions (UV containing light), the DMPO-OH signal was generated in a significant extend (Figure 4-5 (a) and (b), traces (○) and (●)), which were completely inhibited in the presence of $HO^\bullet$ scavenger, isopropyl. We also performed ESR reactive trapping experiments using TMP-OH as singlet oxygen scavenger. The formation of singlet oxygen was confirmed by observation of a characteristic 1:1:1 triplet signal of TEMPOL (Figure 4-6 (a)). However, no convincing 'isotope' effect was observed, when the standard ultrapure water was replaced by heavy water (D_2O). This isotope effect, if present, could be associated with $^1O_2$ generation by photo-assisted goethite and hematite suspensions. Although a weak ESR signal of TEMPOL was detected, thus indicating that production $^1O_2$ for photo-assisted goethite and hematite in the absence or presence of H_2O_2 under simulated solar light is negligible. This result was confirmed using another precursor, TEMPONE, which monitors predominantly the formation of $^1O_2$ in the polar phase (Figure 4-6 (b)). Therefore, the principal radicals produced in our experimental conditions for the photo-assisted iron (hydr)oxide tested in the absence or presence of H_2O_2 were $HO^\bullet$ and $O_2^{\bullet-}$ radicals.

(a)

(b)

H₂O

D₂O
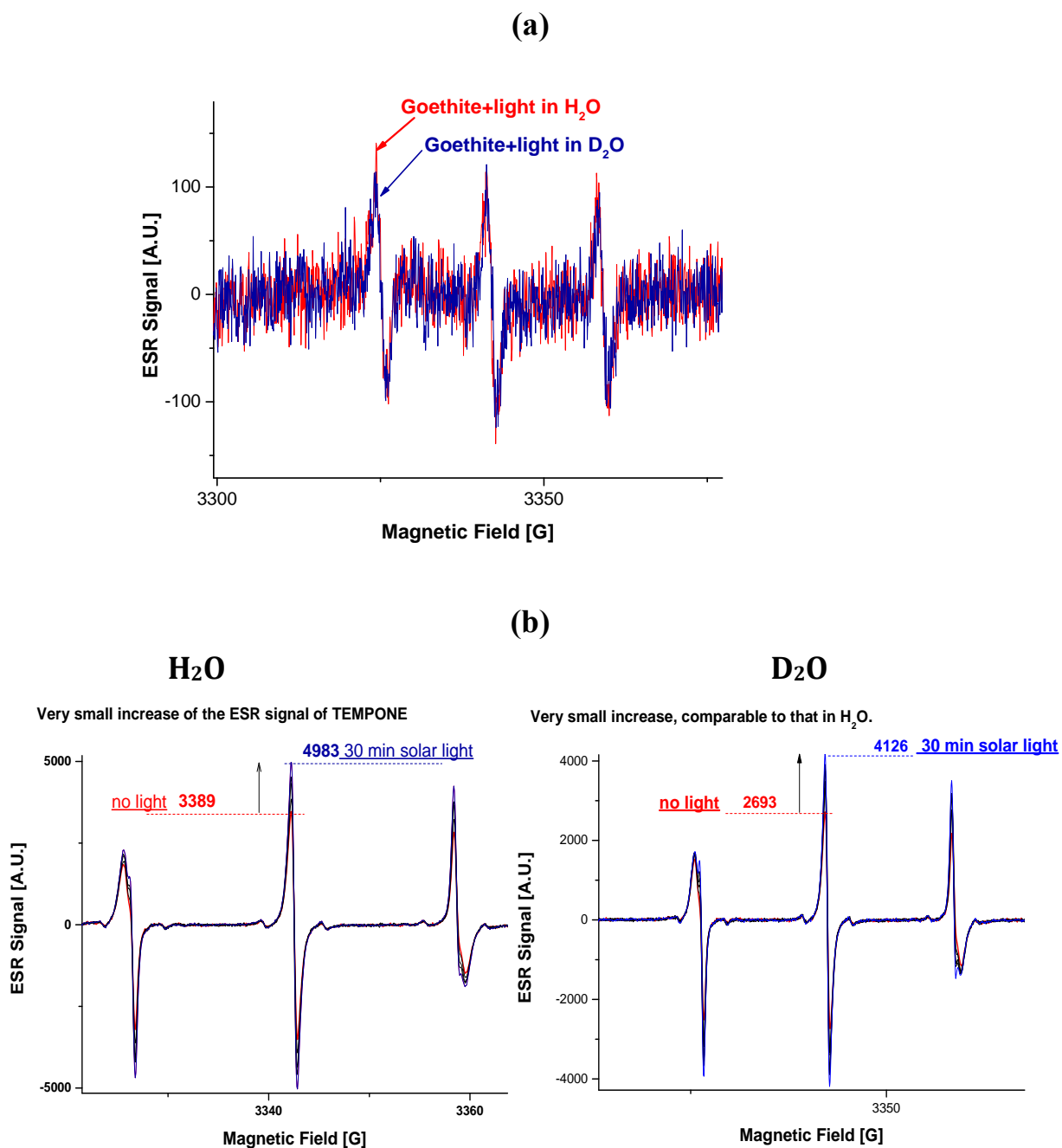
Figure 4-6: (a) ESR spectra of TEMPOL photo-generated in the aqueous suspensions of goethite in the presence of singlet oxygen scavenger, TMP-OH, observed after 30 min of illumination by simulated solar light in H₂O (red trace) and D₂O (blue trace). Experimental conditions: TMP-OH: 15 mM, goethite: 0.6 mg/L relative to the Fe content. (b) The time evolution of ESR spectra of TEMPONE photo-generated in the aqueous suspensions of goethite the presence of singlet oxygen scavenger, TEMPONE precursor (50 mM). Left: ESR traces recorded in H₂O. Right: ESR traces recorded in D₂O. Goethite concentration: 15 mg/mL relative to the Fe content.

4.3.4 Bacterial inactivation in natural water by photocatalytic semiconducting and photo-Fenton action of hematite

In order to evaluate the effect of dissolved organic and mineral matter present in natural water sources on the activity of hematite during bacterial inactivation, water samples originating from Lake Geneva were used and compared with ultrapure water. As can be seen in Figure 4-7 (traces (□) and (□)), for the hematite/light system, a complete *E. coli* inactivation was achieved before 120 min of treatment in both natural and ultrapure water, respectively. Thus, the components of natural water (Table 4-2), did not inhibit the photocatalytic semiconducting action of hematite against bacterial inactivation in a significant extent. It was reported that under UV radiation, dissolved organic matter (DOM) can be involved in positive mechanics to contribute to inactivation of bacterial by the action of photo-sensitizer species (Wenk *et al.*, 2011). Here the excited triple state (^{3}DOM*) promoted by UV light absorption by DOM has not shown a significant contribution. However, the chemical components of the natural water enhance bacterial inactivation by photo-Fenton reaction. As showed in Figure 4-7 (trace (■)), at 60 min of treatment, 3 $\log_{10}$ of bacteria were inactivated in lake water compared with less than 1 $\log_{10}$ in ultrapure water (Figure 4-7, trace (■)) respectively. This is related with the presence of NOM which has a positive effect on the complexation and solubilisation of iron, that concomitantly participates in homogeneous photo-Fenton reaction generating additional HO$^•$, thus enhancing bacterial inactivation. According to Spuhler *et al.*, (2010), the presence of resorcinol during a photo-Fenton reaction for *E. coli* inactivation enhanced the disinfection rate when compared with that founded without organic matter. They suggested the presence of photo-active Fe^{3+} or Fe^{2+}-resorcinol complexes which may favor the process. In general, the NOM is composed of organic ligands such as fulvic acids and smaller carboxylic and dicarboxylic acids able to form Fe^{3+} complexes which, under light, reduce Fe^{3+} and generate complex with Fe^{2+} and ligand radicals as shown in the next equation (Eq. (4.24) (Pignatello *et al.*, 2006; Spuhler *et al.*, 2010):

$$Fe^{3+}-(L)_n + h\nu \rightarrow Fe^{2+}-(L)_{n-1} + L_{ox}^{•} \tag{4.24}$$

Both Fe^{2+} and ligand radicals can react with O_2 leading to the formation of ROS, and the concomitant reaction of Fe^{2+} with H_2O_2 leads to the regeneration of Fe^{3+} and the production of

HO$^\bullet$ (Eq. (4.19)). Thus, Fe^{3+} organo-complexes play an important role for the efficiency of the photo-Fenton systems.

Finally, no bacterial reactivation and/or growth were observed for the photocatalytic semiconducting and heterogeneous photo-Fenton action of hematite in natural water.
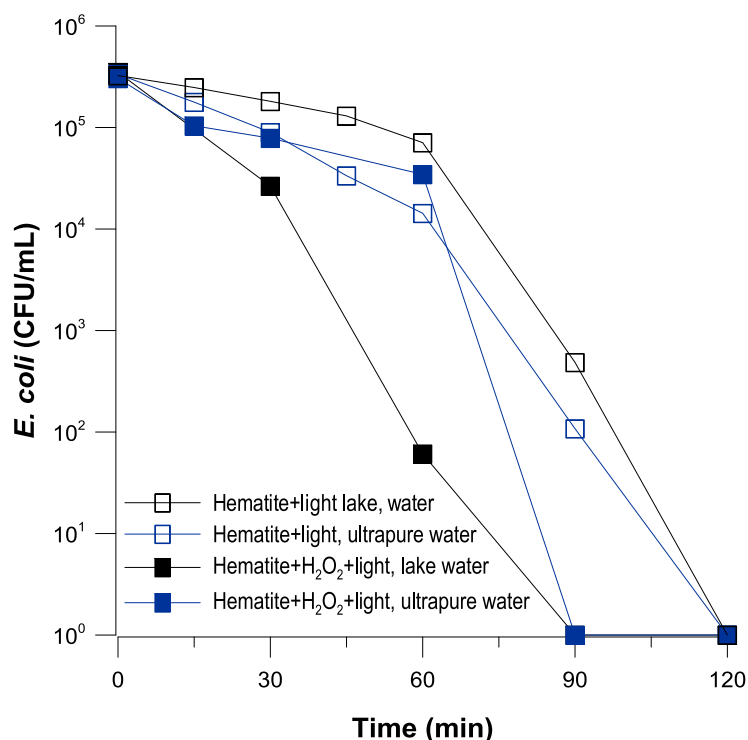
Figure 4-7: *E. coli* inactivation by photo-assisted hematite in the presence and absence of H$_2$O$_2$. *E. coli* were suspended in ultrapure water and natural water having the characteristics described in Table 4-2. Hematite concentration: 0.6 mg/L relative to the Fe content, H$_2$O$_2$: 10 mg/L. Experiments were conducted under simulated solar light and performed in triplicate (the standard error was found approximately 5%).

4.3.5 Influence of iron concentration on bacterial inactivation by hematite-based heterogeneous photo-Fenton

Bacterial inactivation by hematite-based photo-Fenton was evaluated employing three iron concentrations of hematite (0.6, 2.3, and 3.8 mg/L relative to the Fe content). Figure 4-8 shows that the complete bacterial inactivation was achieved in all cases before 90 min of treatment. Considering the loss of bacteria cultivability at 60 min of treatment, it is evident that bacterial inactivation was dependent of the semiconductor concentration and a liner relationship between hematite concentration and loss of cultivability was observed in this

range of concentrations (Figure 4-8). Bacterial inactivation kinetics increased with the catalyst dosage, due to the more active iron sites on the catalyst surface, accelerating the decomposition of H_2O_2 and leading to an increase in the number of $HO^{\bullet}$ radicals that obtain bacterial inactivation. The consumption of H_2O_2 in 120 min of treatment, for 0.6, 2.3, and 3.8 mg/L of Fe^{3+} were 1.0, 1.4, and 2.1 mg/L respectively. These results indicate that low ranges of concentration of hematite (0.6–3.8 mg/L relative to the Fe content) in heterogeneous photo-Fenton system are adequate to efficiently inactivate *E. coli* without reactivation and/or growth of bacteria under specific experimental conditions. It is interesting to underline that this range of concentrations is close to the concentration found in some lakes, rivers, and ground waters and is low compared with the concentration of iron oxides used for the transformation of organic molecules in aquatic systems (100–500 mg/L of iron oxides) (He *et al.*, 2002; Andreozzi *et al.*, 2003; He *et al.*, 2005)
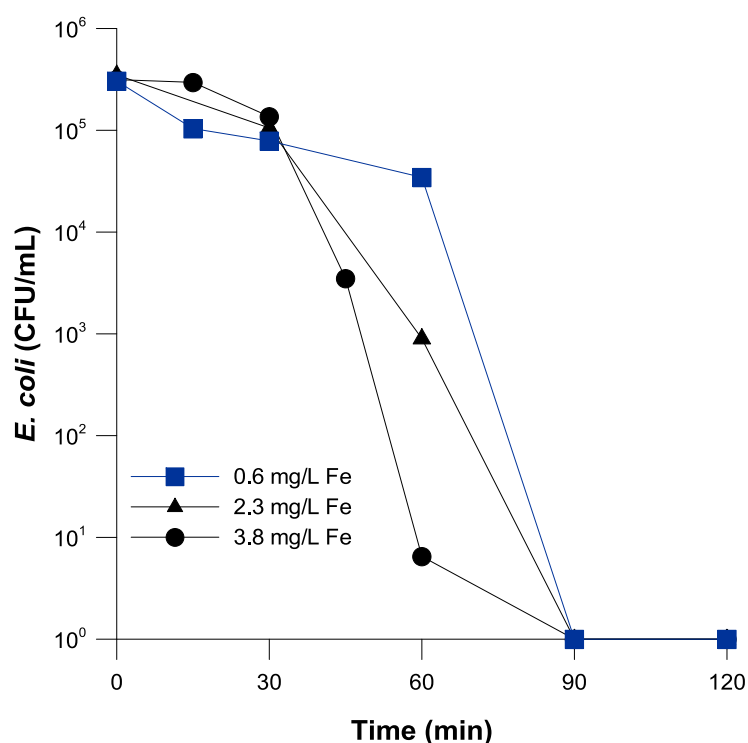
Figure 4-8: *E. coli* inactivation under hematite-based photo-Fenton process with different concentrations of Hematite: 0.6 mg/L, 2.6 mg/L, and 3.8 mg/L relative to the Fe content. H_2O_2: 10 mg/L. Experiments were conducted under simulated solar light and performed in triplicate (the standard error was found approximately 5%).

4.4   Conclusions

Our study demonstrated that heterogeneous photo-Fenton process catalyzed by low concentration of iron (hydr)oxide particles under sunlight may serve as a disinfection method for waterborne bacteria. In particular, we found that, with the exception of magnetite, all the other iron (hydr)oxides tested were photoactive under sunlight in the absence of H_2O_2, these involves semiconductor photocatalysis.

The relative low difference of time necessary to inactivate bacteria for photo-assisted hematite and goethite in the absence or presence of H_2O_2 suggest that, from the application point of view, these iron (hydr)oxides can be applied alone as semiconductors to efficiently disinfect water. These results are interesting because the avoidance of H_2O_2 significantly reduces the cost of the treatment. Therefore, the iron (hydr)oxide particles, even those already present in environmental waters, represent low-cost photocatalysts for solar water disinfection. Furthermore, no bacterial reactivation and/or growth were observed for the photocatalytic semiconducting and heterogeneous photo-Fenton action of hematite and goethite, whereas a delayed disinfection effect was observed to continue in the dark period for the photo-assisted wüstite treatment.

ESR spin trap technique confirmed that the principal ROS photo-generated for iron (hydr)oxide in the absence or presence of H_2O_2 were $HO^{\bullet}$ and $O_2^{\bullet -}$ radicals. The presence of H_2O_2 in iron (hydr)oxide suspensions promoted a more rapid photo-generation of $HO^{\bullet}$, thus contributing to a more efficient bacterial inactivation.

The components of natural water (*i.e.* NOM and inorganic substances) did not interfere with the photocatalytic semiconducting action of hematite to bacterial inactivation. However, these components enhanced bacterial inactivation by heterogeneous photo-Fenton action of hematite. In particular, NOM enhances the complexation and solubilisation of iron, which, in turn, may favour the process. No reactivation and/or growth of bacteria were observed for the photocatalytic semiconducting and heterogeneous photo-Fenton action of hematite in natural water.

Conclusively, our results demonstrated, for the first time, that low concentration of iron (hydr)oxides (0.6 mg/L relative to the Fe content) acting both as photocatalytic semiconductors or catalysts of the heterogeneous photo-Fenton process at near-neutral pH,

may provide a useful strategy for efficiently inactivate *E. coli* without reactivation and/or growth. This is important for the economic viability of the treatments because the levels of iron encountered in environmental waters are close to this iron concentration.

5. Bacterial inactivation with iron citrate complex: a new source of dissolved iron in solar photo–Fenton process at near-neutral and alkaline pH.

Bacterial inactivation during Fe–citrate–based photo-Fenton process
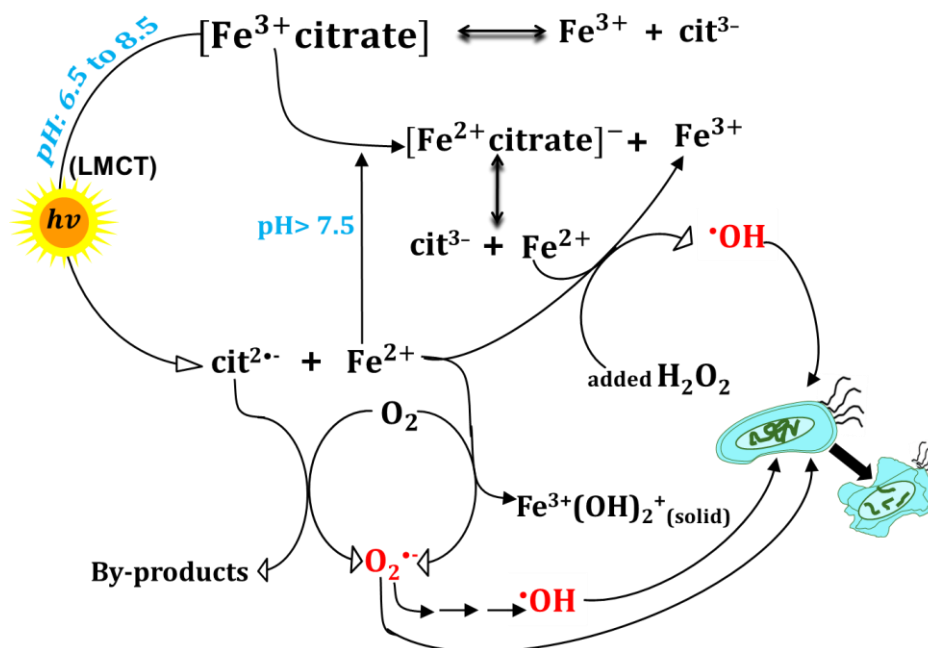
5.1   Introduction

The photo-assisted Fenton system is one of the most popular and widely studied advanced oxidation processes (AOPs). Its oxidative action is a result of the formation of reactive oxygen species (ROS), especially hydroxyl radicals, $HO^\bullet$, following the oxidation of ferrous iron by hydrogen peroxide (Eq. (5.1)). Ferrous iron, in the absence of any other complexing agents, has the tendency to rapidly get oxidized and form different aqua-Fe^{3+} species, depending on the pH levels of the medium. At low pH (~2.8), it tends to form $[Fe(H_2O)_5(OH)]^{2+}$, which exhibits significant photoactivity in the UV-visible part of the solar spectrum and allows for the regeneration of Fe^{2+}, when illuminated by solar radiation (Eq. (5.2)) (A. Safarzadeh-Amiri *et al.*, 1996; Pignatello *et al.*, 2006). The regenerated Fe^{2+} reacts again with H_2O_2, thus continuing the formation of $HO^\bullet$ radicals in the process known as photo-Fenton.

$$Fe^{2+} + H_2O_2 \; \rightarrow \; Fe^{3+} + HO^\bullet + OH^- \qquad\qquad (5.1)$$

$$[Fe(H_2O)_5(OH)]^{2+} + hv \; \rightarrow \; Fe^{2+} + HO^\bullet \qquad\qquad (5.2)$$

Despite its dual advantages of being economic and environmental friendly, the photo-Fenton reaction has not been widely used in microbial disinfection, due to the theoretical requirement of acidic conditions. However, from the seminal paper of Rincón and Pulgarín, (2006) interest has grown over the past few years, in the application of near-neutral photo-Fenton treatment for water and waswater disinfection (Rincón and Pulgarin, 2007a; Rodriguez-Chueca *et al.*, 2013; Ruales-Lonfat *et al.*, 2013; Ortega-Gómez *et al.*, 2014a; Ortega-Gómez *et al.*, 2014b; Rodríguez-Chueca *et al.*, 2014b; Ruales-Lonfat *et al.*, 2014; Ruales-Lonfat *et al.*, 2015). In the absence of iron ligands, at near-neutral pH, a spontaneous chemical oxidation of Fe^{2+} to Fe^{3+} by dissolved oxygen in water occurs, involving formation of ferric (hydr)oxides, like $Fe_2O_3 \cdot nH_2O$ (Morgan and Lahav, 2007), which do not re-dissolve in water, thus inhibiting the recycling in solution of Fe^{3+} back to Fe^{2+}. However, soluble iron in the mg/L range was detected at pH 6.5 in the presence of bacteria, due to siderophores secreted by bacteria and by-products generated from the degradation of bacterial components (Ruales-Lonfat *et al.*, 2015). So for the use of iron-chelating agents are exclusively being considered for organic pollutants degradation. The resulting iron complexes maintain Fe^{3+}/Fe^{2+} solubility at a wide pH range and exhibit high absorbance in the UV-Vis region, which allows for using a

considerable portion of the solar spectrum, thus reducing the operating costs. Iron complexes are photochemically reactive *via* participation LMCT transitions (Eq. (5.3)) (Zepp *et al.*, 1992; Silva *et al.*, 2007; Papoutsakis *et al.*, 2015a). Therefore, soluble Fe^{2+} can participate in homogeneous Fenton reaction and thus enhance the production of hydroxyl radicals (Eq. (5.1)).

$$[Fe^{3+}L] + hv \; \rightarrow \; [Fe^{3+}L]^* \; \rightarrow Fe^{2+} + L^{\bullet} \qquad\qquad (5.3)$$
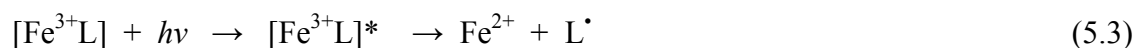
(L: complexing agent or polycarboxylic acid)

Several Fe^{3+} chelates have been evaluated for oxidation of hydrogen peroxide at circumneutral pH (Sun and Pignatello, 1992). However, the harmful effects of some chelating agents, such as ethylenediaminetetraacetic acid (EDTA) and nitrilotriacetic acid, have recently been acknowledged, and their use in environmental applications and especially in drinking water disinfection has been avoided. Many other low molecular weight organic compounds (*e.g.* oxalate, citrate, malonate) were used as model organic ligands in numerous studies, showing that photochemical reactions of their complexes with Fe^{3+} were potentially important sources of Fe^{2+}, $O_2^{\bullet-}/HO_2^{\bullet}$, H_2O_2 and $HO^{\bullet}$ in illuminated surface waters (Faust and Zepp, 1993; Balmer and Sulzberger, 1999; Cho *et al.*, 2004b; Papoutsakis *et al.*, 2015a). Ferric citrate complex is a good alternative for iron solubilization in the photo-Fenton processes. Although its photolysis shows a lower quantum yield for Fe^{2+} generation than that observed for ferrioxalate, citrate is less toxic (Sillanpaa and Pirkanniemi, 2001; Liang *et al.*, 2004; Silva *et al.*, 2007), has higher cumulative stabilization constants (log β = 14.29) (Feng *et al.*, 2012), is readily available and can be used at higher pH values than oxalate (up to pH 9.0) (Abrahamson *et al.*, 1994). Ferric citrate complexes have been successfully implemented for the photo-Fenton treatment at near-neutral pH conditions and with using artificial or solar light towards degradation of organic compounds in polluted waters (Zepp *et al.*, 1992; Sun and Pignatello, 1993; Katsumata *et al.*, 2006; Silva *et al.*, 2007; Trovó and Nogueira, 2011). However, there has been no report on the application of this system as a disinfection technology.

In this work, the influence of the pH (6.5, 7.5 and 8.5) on the photo-degradation of Fe–citrate complex and on the generation of ROS during Fe–citrate–based photo-Fenton process was assessed. The aim of this research was to study the disinfection ability of the Fe-citrate complex in photo-Fenton treatment under simulated solar light illumination, at near-neutral

and alkaline pH in water. The effects of the solution pH and Fe-citrate complex concentration on *E. coli* inactivation during the photo-Fenton reaction were investigated. Furthermore, bacterial inactivation by photo-Fenton process mediated by Fe-citrate complex, $FeSO_4$ and goethite at near-neutral pH were comparatively studied to evaluate homogeneous and heterogeneous contributions to the *E. coli* inactivation mechanism and the disinfecting ability of these systems were evaluated quantitatively.

Finally, the efficiency of the Fe–citrate–based photo-Fenton process was also demonstrated in real-world condition, *i.e.* in natural water samples from Lake Geneva (Switzerland) at pH 8.5 and containing 108 mg/L of HCO_3^-. The results of this research demonstrate promise of the first applications of Fe–citrate–based photo-Fenton chemistry applied to microbial inactivation under near-neutral and alkaline pH conditions.

5.2   Materials and Methods

5.2.1   Chemicals

Ferrous sulphate heptahydrate ($FeSO_4 \cdot 7H_2O$) (Riedel-de Haën 99-103.4%); Goethite (α-FeO(OH)), 30–50 mesh (Sigma–Aldrich South Africa); Ferric chloride ($FeCl_3$) (98% carlo erba), Trisodium citrate dihydrate ($Na_3C_6H_5O_7 \cdot 2H_2O$) (99% Merck); Sodium hydrogen carbonate ($NaHCO_3$) (analytical grade, Merck); Hydrogen peroxide (H_2O_2) 30% w/v (Riedel de Haën); Titanium (IV) oxysulfate ($TiOSO_4$) (Fluka); Sodium hydroxide (NaOH, 98%) and hydrochloric acid (HCl, 36.5%), were purchased from Sigma-Aldrich. The spin-trap, 5,5-dimethyl-1-pyrroline-N-oxide (DMPO), was purchased from Enzo Life Sciences (ELS) AG (Lausen, Switzerland).

All solutions were prepared immediately prior to irradiation with the use of ultrapure water. Two different types of water were used to suspend bacteria, *i.e.* ultrapure water and the natural water from Lake Geneva. Table 4-2 (Chapter 4) shows the physicochemical characteristics of these waters.

5.2.2   Fe–citrate complex preparation

Fe–citrate complex was prepared according to the modified European patent (Antonini and Vidic, 1994). Ferric chloride (4.0 g) and sodium hydrogen carbonate (3.0 g) were dispersed in 50 mL of distilled water and dissolved therein by stirring. This solution was degassed under vacuum for 2 h. Then, with constant stirring, Trisodium citrate dihydrate (4.0 g) were added. The colour of the solution turned to a pale brown. The solution was stored in the dark for 24 h. Then, 40 mL of methanol was added to the brown solution under constant stirring at 25 °C and a brown precipitate was formed. The resulting suspension was centrifuged (5 min at 5000 rpm) to remove the precipitate, and the clear supernatant solution was separated by filtration. The precipitate was washed with methanol at least three times and dried under vacuum at room temperature.

5.2.3   Bacterial strains and growth media

The bacterial strain used was *E. coli* K-12 (MG1655), a non-pathogenic wild-type strain, which can be handled with little genetic manipulation. Bacteria were inoculated from a stock in a nutrient-rich medium, Luria-Bertani (LB) broth, and incubated in a shaker incubator at 37 °C and 180 rpm. After 8 h, cells were diluted (1% v/v) in the pre-heated LB broth and incubated at 37 °C for 15 h in the incubator until a stationary physiological phase was reached. Cells were separated during the stationary growth phase by centrifugation (15 min at 5000 rpm, at 4 °C). The bacterial pellet was re-suspended and washed three times with a saline solution in the centrifuge. This procedure resulted in a bacterial pellet of approximately 10^9 colony forming units per millilitre (CFU/mL).

5.2.4   Experimental

5.2.4.1   Photo-degradation of Fe–citrate complex at various pH values

The photo-degradation of Fe–citrate complex in the presence of H_2O_2 at controlled pH levels of 6.5, 7.5 and 8.5 were determined by molecular absorption spectroscopy, using a UV-Vis spectrophotometer, Model 1700 (Shimadzu, Japan). Fe–citrate concentration: 3.8 mg/L relative to the Fe content. Hydrogen peroxide concentration: 10 mg/L.

5.2.4.2   Photo-inactivation experiments

All bacterial inactivation experiments were performed in Pyrex reactors (4 cm x 9 cm, 100 mL). The Pyrex reactors containing the bacterial suspension in water (approximately 10^6 CFU/mL) were placed in the dark at 25 °C and kept under magnetic stirring for at least 30 min to let the bacteria adapt to the new matrix and to allow the die-off and equilibration of the most stress-sensitive species.

The following systems were analysed for the inactivation effect on *E. coli*. (i) photo-Fenton process mediated by Fe–citrate (Fe–citrate concentration: 0.6 mg/L relative to the Fe content) at various pH values: 6.5, 7.5 and 8.5.; (ii) photo-Fenton process with different Fe–citrate concentrations: 0.1, 0.3, 0.6, 1.0 and 2.0 mg/L, relative to the Fe content; (iii) photo-Fenton process mediated by different iron sources Fe–citrate, $FeSO_4$, goethite and under control experiments: Fe–citrate/light, Fe–citrate/H_2O_2/dark, light alone and H_2O_2/light, (Fe–citrate concentration: 0.6 mg/L relative to the Fe content) and (iv) photo-Fenton process mediated by Fe–citrate suspended in natural water from lake Geneva (Switzerland). In the experiments, iron was added to a solution of *E. coli*. Then, the pH was adjusted to 6.5 or 7.5 or 8.5, depending on the experiment. Finally, H_2O_2 (10 mg/L) was added to the reactor as the last component. Aliquots were collected during set intervals within the inactivation time.

Solar exposure experiments were carried out using a solar simulator CPS Suntest System (Heraeus Noblelight, Hanau, Germany). The Suntest bears a lamp that emits ~0.5% of the photons at wavelengths < 300 nm (UVC cut-off at 290 nm), ~7% between 300 and 400 nm and the rest follow the solar spectrum above that value until IR range (IR was cut-off by filtering). The radiance intensity was measured by a spectroradiometer, Model ILT-900-R (International Light Technologies) and corresponded to 820 W/m^2 of light global intensity (20.2 W/m^2 on the UV).

During the experiments, the temperature in the reactors did not exceed 38°C. After each experiment, the reactors were rinsed with nitric acid (10%) followed by washing with distilled water and, finally, autoclaved. All the experiments were conducted triplicate, with good reproducibility (<10% difference between replicates).

5.2.4.3 Post-irradiation events

Bacterial reactivation and/or growth were determined for photo-Fenton experiments by keeping the final samples in the dark, at room temperature (20-25 °C) for 24 and 48 h before the measurement of the CFU.

5.2.5 Analytical methods

Total dissolved iron was measured using an Inductively Coupled Plasma Mass Spectrometer (ICP-MS), Model ICPE-9000 (Shimadzu, Japan). Samples were filtered (0.25 µm) and kept in acid solution prior to the determination. The detection limit ranges of spectrometry used for this experiment were (0.2–0.9 µg/L). The concentration of H_2O_2 was monitored using a titanium (IV) oxysulfate solution *via* a spectrophotometric method at 410 nm (modified method DIN 38 402 H15). The titanium (IV) oxysulfate method has a 0.1 mg/L detection limit. The pH was measured with a pH-metre Metrohm 827 pH-lab using a glass electrode.

5.2.5.1 Electron spin resonance spectroscopy (ESR)

ESR in combination with spin-trapping was used to monitor the formation of ROS, *i.e.* namely $HO^\bullet$ and $O_2^{\bullet-}$ radicals, generated by heterogeneous and homogeneous photo-Fenton processes mediated by Fe–citrate, $FeSO_4$ and goethite. A stock solution of DMPO (0.5 M) was prepared in ultrapure water and stored at –20 $^\circ$C.

The following systems were used to study the light-induced ROS formation in photo-Fenton process: (i) Fe–citrate concentration: 3.8 mg/L relative to the Fe content, H_2O_2:10 mg/L; (ii)

Fe–citrate or $FeSO_4$ or goethite concentration: 0.6 mg/L relative to the Fe content and 10 mg/L of H_2O_2. The solutions of system (i) were exposed to UV-A light (~365 nm) using a UV spot light source, Lightingcure™, model LC-8 (Hamamatsu Photonics, France). Systems (ii) were exposed to simulated solar light (global light intensity of 820 W/m^2 and 20.2 W/m^2 in the UV-A range) under constant agitation. Just before performing the photo-generation of ROS, DMPO (final concentration of 100 mM) was added to Fenton's reagents. Subsequently, 2 mL aliquots of the prepared samples were transferred into small Pyrex beakers (5 mL volume, 20 mm outer diameter and 30 mm height) and positioned in a solar light simulator, CPS Suntest System (Heraeus Noblelight, Hanau, Germany). Next, at the selected time intervals, the sample of the Fenton's reagents was drawn into thin glass capillaries (0.7 mm

ID/0.87 mm OD, from VitroCom, NJ, USA), which were then sealed on both ends using the Cha-Seal™ tube-sealing compound (Medex International, Inc. USA). ESR measurements were carried out at room temperature using a Bruker X-band spectrometer, Model EleXsys 500 (Bruker BioSpin, Karlsruhe, Germany) equipped with a high-Q cylindrical TE_{011} microwave cavity, Model ER4123SHQE. The typical instrumental settings were: frequency of 9.4 GHz; microwave power of 0.63 mW; scan width of 120 G; magnetic field resolution of 2048 points; modulation frequency of 100 kHz; modulation amplitude of 1.0 G; receiver gain of 60 dB; conversion time of 40.96 ms; time constant of 20.48 ms and sweep time of 84 s.

The spin-adducts concentrations were estimated using the double integration of the first-derivative ESR spectra. The actual concentrations of spin-adducts were derived by comparison with a calibrated ESR signal, which was acquired for a stable nitroxide radical, TEMPOL (10 μmol/L). The data analysis was carried out using Origin Pro 9.0 software.

5.2.6 Data treatment

The bacterial inactivation kinetics can be described by the first order kinetic model proposed by Chickse Watson (McGuigan *et al.*, 2012) (Eq. (5.4)):

$$N_t = N_0 e^{-kt} \tag{5.4}$$

where N_0 is the concentration of viable organisms before radiation exposure; N_t is the concentration of organisms surviving after irradiation time; t is the irradiation time (at constant light flux) and k is the first order inactivation rate.

To compare inactivation between the different treatments tested, the constants of inactivation rate were obtained, k_{obs}, from fitting of plots of log(CFU/mL) vs. time. The fitting was carried out by GInaFiT, a tool of Microsoft Excel for testing different types of microbial survival models on experimental data (Geeraerd *et al.*, 2005). The root mean square error of the fit to the experimental data was evaluated. The R^2 of the model was in most cases superior to 0.9.

The standard error was calculated by the sample standard deviation divided by the square root of the sample size, as follows: $SE = \frac{S}{\sqrt{n}}$, where S is the sample standard deviation, and n is the size (number of observations) of the sample. The standard deviation was calculated using a minimum of three measures. Standard error was found to be approximately 5%.

5.3 Results and discussion

5.3.1 Photo-degradation of Fe–citrate complex in the presence of H_2O_2 at different controlled pH levels

Before evaluating the photo-Fenton–mediated bacterial inactivation, control experiments were carried out in order to understand the behaviour of the iron-citrate complex during the photo-Fenton reaction in the absence of bacteria.

Figure 5-1(a) shows the UV–visible absorption spectra of the Fe–citrate complex in the presence of H_2O_2 at pH levels of 6.5, 7.5 and 8.5 determinated by NaOH addition. As can be seen, Fe–citrate complexes absorb in the UV–visible region (300–450 nm) and thus have the potential for utilizing sunlight as an irradiation source.

The curves of Fe–citrate disappearance kinetics at different controlled pH levels of 6.5, 7.5 and 8.5 upon irradiation with simulated solar light are presented in Figure 5-1(b). The total disappearance of Fe–citrate complex was observed at different pH values. However, it was markedly accelerated at pH 6.5 and 7.5 (Figure 5-1(b), traces (▲) and (■)). At these pH values, citrate forms stable complexes with ferric ions (Fe^{3+}) as can be observed in the conditional stability constants (Figure 5-2). The photochemical reactions of these complexes undergo *via* LMCT, thus by dissociating into Fe^{2+} and $Citrate^{2\bullet-}$ (Eq. (5.5)) (Chen *et al.*, 2011). Thus, the dissociation into citrate ligand is certainly responsible for the significant changes observed in the UV–visible absorption spectra (Vukosav *et al.*, 2010). It is interesting to notice that at pH 8.5, in contrast to pH 6.5 and 7.5, no significant degradation of the Fe-citrate was observed before 60 min of treatment (Figure 5-1(b), trace (●)) indicating that the Fe–citrate complex was more stable at this pH.

These results could be attributed to:

(i)   The possible structural changes of the Fe^{3+}–citrate complexes. In particular, Vukosav *et al.*, (2010), (2012) suggested a bond splitting between citrate hydroxyl oxygen and Fe^{3+} in the iron coordination sphere above pH 7.0. This change would enable the attachment of OH^- ions from the solution to the coordination sphere of Fe^{3+}-citrate complexes. In the reported experiments, the chemical changes in the complex were

evidenced only by voltammetric measurements, being, however, unlikely to be detected by UV–Visible spectrophotometry.

(ii)   The presence of Fe^{3+}/Fe^{2+} mixed–valence complexes which may occur at high pH (Königsberger *et al.*, 2000). The two mixed–valence complexes, $Fe^{3+}Fe^{2+}Cit^{2+}$ and $Fe^{3+}Fe^{2+}Cit_2H_2^{+}$, have been previously identified in aqueous citrate media from spectrophotometric absorption data (Binder, 1971).

(iii) Photo–generated ferrous iron–mediated ferric–ferrous ion exchange in the Fe^{3+}–citrate complex. According to the stability constants conditional of Fe–citrate ($\log K^{-1}$) (Figure 5-2), the Fe^{2+}–citrate complex becomes the predominant complex at pH above 7.5 (Rey *et al.*, 1998). Krishnamurti and Huang, (1991) have reported that citrate form a stable complex with Fe^{2+} that considerably retarded its oxidation at constant pH 6.0. A similar finding using fulvic acid have reported by Rey *et al.*, (1998). They observed that Fe^{2+}–fulvic acid complexes are formed at basic pH and increasing the pH results in a strong decrease in the rate constants for the dissociation of Fe^{2+}–fulvic acid complexes. Pham and Waite, (2008) have also supports the presence of Fe^{2+}–citrate species at near-neutral and alkaline solutions. Other studies indicate that Fe^{2+} in a complexed form (FeL^{2+}), is stable with respect to oxidation and such ligand stabilization has been suggested as an explanation for the apparent presence of Fe^{2+} in oxic solutions that contain relatively high levels of organic matter.

A good correlation between the photo–decomposition of the Fe–citrate complex with the precipitation of iron in the system at pH 6.5, 7.5 and 8.5 was found (Figure 5-1(b) and (c)). The iron precipitation at pH 6.5 and 7.5 before 20 min of reaction (Figure 5-1(c), traces (▲) and (■)) is due to the oxidative degradation of the citrate ligand (Eq. (5.6)) (Chen *et al.*, 2011). Thus, in the absence of citrate ligand and at near-neutral pH, a spontaneous chemical oxidation of Fe^{2+} ions to Fe^{3+} occurs by both dissolved oxygen in the aqueous solution and added H_2O_2. The subsequent hydrolysis leads to the formation of the ferric hydroxo–complex ($Fe(OH)_2^{+}$) (Eq. (5.7)). These iron intermediates ultimately transform into stable iron oxide end-products, such as goethite or lepidocrocite (Jolivet *et al.*, 2004). In contrast, in the experiments conducted at pH 8.5, dissolved iron was observed up to 60 min of reaction and began to precipitate when the Fe–citrate complex started to be degraded.

(a)

(b)   **(c)**
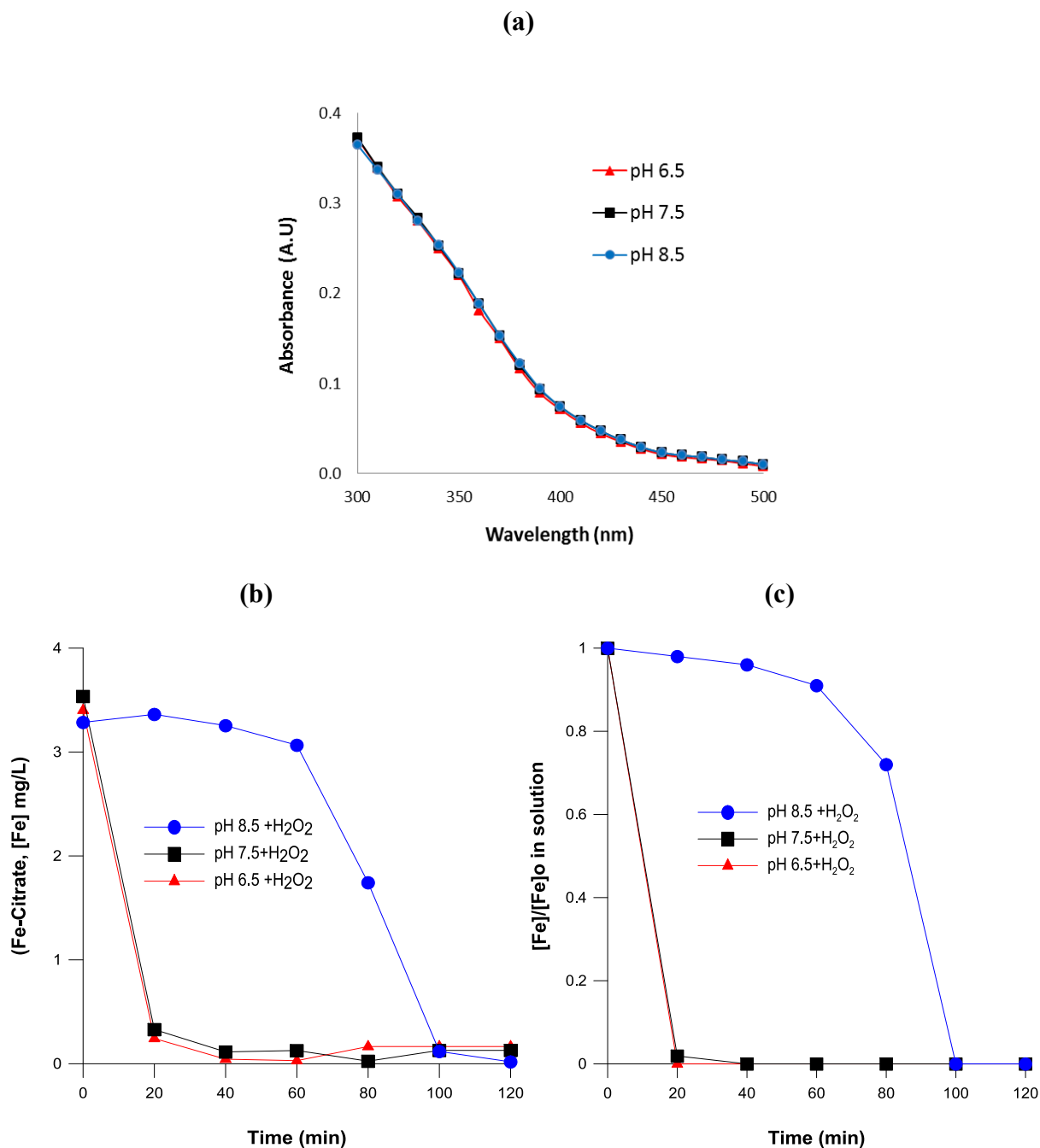
Figure 5-1: (a) UV–visible spectra of Fe–citrate; (b) Disappearance of Fe–citrate during photo-Fenton reaction; (c) Evolution of dissolved iron during photo-Fenton reaction at different controlled pH values: (▲) pH 6.5; (■) 7.5 and (●) 8.5. Fe-citrate concentration: 3.8 mg/L relative to the Fe content, $[H_2O_2]$: 10 mg/L. Irradiated with simulated solar light. Experiments were conducted in triplicate and standard error was found to be approximately 5%.
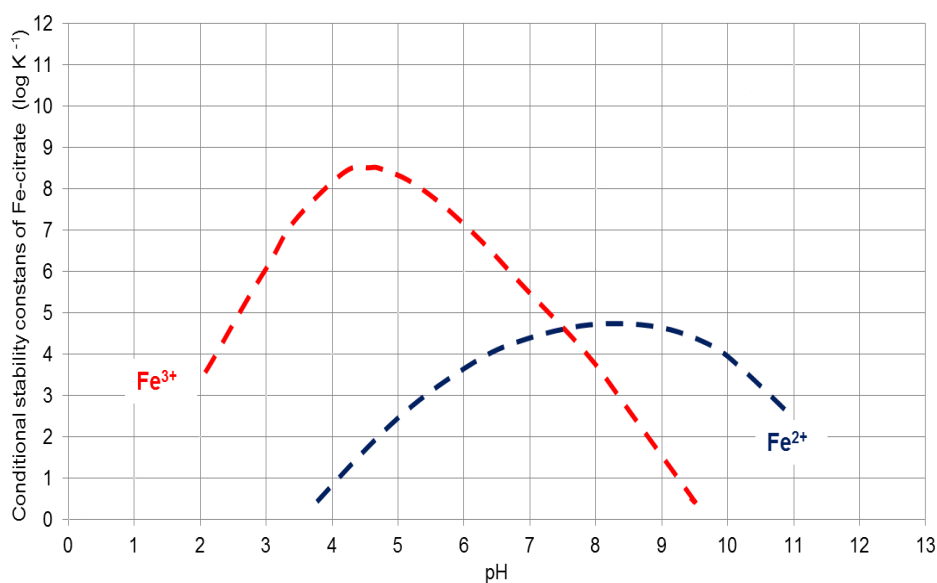
Figure 5-2: Conditional stability constants for iron with citric acid.

In our experiments, photo-products formed from the photo-dissociation of Fe–citrate did not contribute to solubilization of iron, contrary to the findings by Abida et al., (2012), who observed the stabilization of dissolved Fe^{2+} concentration at pH 6.0 after 120 min of irradiation.

$$[Fe^{3+}\text{–citrate}] \quad + \quad h\nu \quad \rightarrow \quad Fe^{2+} + citrate^{2\bullet-} \tag{5.5}$$

$$citrate^{2\bullet-} + O_2 \quad \rightarrow \quad product + CO_2 + O_2^{\bullet-} \tag{5.6}$$

$$Fe^{2+} + O_2 \rightarrow Fe^{3+} \rightarrow Fe(OH)^{2+} \rightarrow Fe(OH)_2^+ \tag{5.7}$$
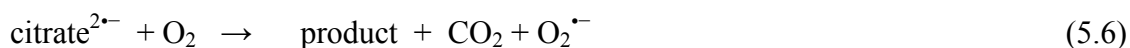
The results of Figure 5-1 (b) and (c)) show that the stability of Fe–citrate complex in the presence of H_2O_2 under simulated solar light is several times higher at pH 8.5 than at pH 6.5 and 7.5 and its photo-decay rates follow the order: $6.5 \approx 7.5 > 8.5$. In fact, previous work reported that oxalate was the best choice as ligand in acidic solutions and that citrate was preferable in neutral aqueous media for photo-Fenton studies (Zepp *et al.*, 1992). Therefore, citrate proved to be a good ligand for iron ions to be used at near-neutral and alkaline pH for photo-Fenton studies.

5.3.2 ROS generation during Fe–citrate–based photo–Fenton system at various pH values

The photo–generation of ROS, *i.e.* HO$^{\bullet}$ and O$_2^{\bullet-}$ in the aqueous solution was determined during the Fe–citrate–based photo-Fenton process at pH 6.5, 7.5 and 8.5. The ESR spin-trapping technique, with DMPO as a spin trap was employed to identify both HO$^{\bullet}$ and O$_2^{\bullet-}$ radicals, thus leading to the formation of spin-adducts, DMPO–OH or DMPO–OOH, respectively. Both resulting paramagnetic products reveal distinct and easily recognizable ESR spectra. However, the DMPO-OOH spin adduct is well known to be highly unstable and rapidly decomposing into the DMPO–OH spin adduct (Buettner and Mason, 1990).

Figure 5-3 shows that pH value has a great effect on the photo–generation of HO$^{\bullet}$ radicals. The photo-Fenton treatment at pH 8.5 (trace (●)) showed higher generation of HO$^{\bullet}$ radicals, as compared with the same system at pH 7.5 and 6.5 with 1.7, 1.0 and 0.9 mmol of HO$^{\bullet}$ radical, respectively (traces (■) and (▲)). It is due to the mayor stability of the Fe-citrate complex at pH 8.5 as was showed in Figure 5-1(b) and (c), trace (●), enhancing Fenton reaction and the HO$^{\bullet}$ production rate (Eq. (5.10)).

According to Chen *et al.*, (2011), the stability of Fe^{3+}/Fe^{2+}–citrate was a predominant factor for the pH–dependent generation of HO$^{\bullet}$ in the Fe–citrate solutions. The main Fe–citrate species with ferrous and ferric iron ions include [FeHcit], [Fecit]$^{-}$, [Fecit]$^{2-}$ and [FeHcit]$^{+}$, [Fecit], [FeOHcit]$^{-}$, respectively (Field *et al.*, 1974). However, there are some discrepancies in literature concerning the Fe^{3+}–citrate species dominant in solution at different pH values (Königsberger *et al.*, 2000; Zhang *et al.*, 2006).

The generation of HO$^{\bullet}$ radicals is induced by photoactive [FeOHcit]$^{-}$ complex, which is the main species formed at neutral pH (Zepp *et al.*, 1992; Chen *et al.*, 2011) and can presumably be interpreted according to the following reactions (Eqs.(5.8)–(5.14)).

$$[\text{FeOHcit}]^{-} + h\nu \xrightarrow{\text{LMCT}} \text{Fe}^{2+} + 3\text{–HGA}^{2\bullet-} \qquad k = 1.3 \times 10^{-2} \text{ M}^{-1} \text{ s}^{-1} \qquad (5.8)$$

$$\text{Fe}^{3+}\text{–siderophore} + h\nu \xrightarrow{\text{LMCT}} \text{Fe}^{2+} + \text{L}^{\bullet} \qquad (5.9)$$

$$[\text{Fe}^{2+}\text{cit}]^{-} + \text{H}_2\text{O}_2 \rightarrow \text{Fe}^{3+}\text{cit} + \text{OH}^{-} + \text{HO}^{\bullet} \qquad (5.10)$$

$$3\text{–HGA}^{2\bullet-} + \text{O}_2 \rightarrow 3\text{–HGA}^{2-} + \text{CO}_2 + \text{O}_2^{\bullet-} \qquad k = 1.0 \times 10^{6} \text{ M}^{-1} \text{ s}^{-1} \qquad (5.11)$$

$$\text{HO}_2^{\bullet} \rightleftarrows \text{O}_2^{\bullet-} + \text{H}^{+}, \ pK_a = 4.8 \qquad (5.12)$$

$$HO_2^{\bullet} + O_2^{\bullet-} + H_2O \quad \rightarrow \quad H_2O_2 + O_2 + OH^- \qquad\qquad (5.13)$$

$$HO_2^{\bullet} \;+\; HO_2^{\bullet} \quad \rightarrow \quad H_2O_2 + O_2 \qquad\qquad\qquad (5.14)$$
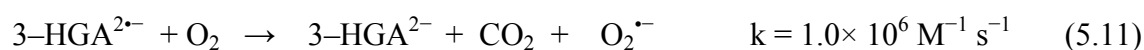
It has been well–established that the mechanism of photo–generation of $HO^{\bullet}$ radicals is generated through a LMCT transition and a subsequent Fenton reaction. Thus, the photoactive $[FeOHCit]^-$ complex and Fe^{3+}–siderophore complex (secreted by bacteria) undergoes a photolytic process whose primary step is a LMCT process with generate Fe^{2+} and ligand radical (Eqs. (5.8) and (5.9)) (Köster, 2001; Upritchard *et al.*, 2007). Fe^{2+} will undergo a Fenton reaction with added and formed hydrogen peroxide to produce $HO^{\bullet}$ (Eq. (5.10)). The citrate ligand oxidized $HGA^{2\bullet-}$ (3–hydroxyglutaric acid) in the presence of oxygen, result in superoxide radical anion $(O_2^{\bullet-})$ that is in acid–base equilibrium with the hydroperoxyl radical (Eqs. (5.11) and (5.12)). These radicals can disproportionate to hydrogen peroxide (Eqs. (5.13) and (5.14). It has been reported by speciation computations and kinetics experiments that Fe^{2+} and citrate complex react efficiently with H_2O_2 to produce $HO^{\bullet}$ in aqueous solutions with pH ranging from 3 to 8 (Zepp *et al.*, 1992).
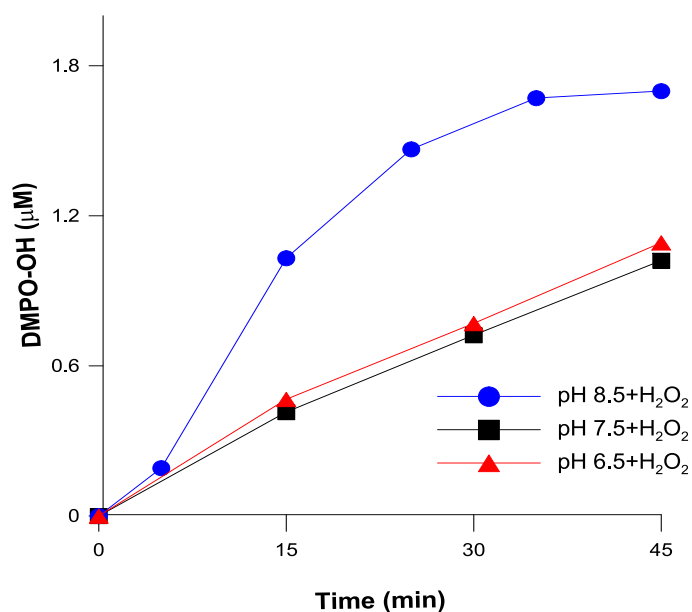
Figure 5-3: The ESR–measured formation of hydroxyl radical ($HO^{\bullet}$) during photo-Fenton process mediated by Fe–citrate at different pH values: (▲) pH 6.5; (■) 7.5 and (●) 8.5. Fe-citrate concentration: 3.8 mg/L relative to the Fe content, $[H_2O_2]$: 10 mg/L. Irradiated with UV−A radiation.

5.3.3 Effect of pH on bacterial inactivation rates during Fe–citrate–based photo-Fenton process

The influence of pH values of 6.5, 7.5 and 8.5 were evaluated on *E. coli* inactivation by photo-Fenton reagent in the presence of H_2O_2 and Fe–citrate complex as iron source. Interestingly, in this pH range, the efficiency of the Fe–citrate–based photo-Fenton process to bacterial inactivation is independent of pH. Figure 5-4 (traces (▲), (■) and (●)) shows that the complete bacterial inactivation was achieved in all cases before 30 min of treatment, with very close inactivation rate constants, at pH levels of 6.5, 7.5 and 8.5, respectively (Table 5-1). The bacterial inactivation rate was not correlated with the $HO^{\bullet}$ production rate for the tested pH values (Figure 5-3). Probably, in the full range of experimental conditions reported here, the $HO^{\bullet}$ production rate was high enough to reach the maximum bacterial inactivation rate. In other words, the process was not limited by the $HO^{\bullet}$ availability even at pH 6.5 and 7.5.
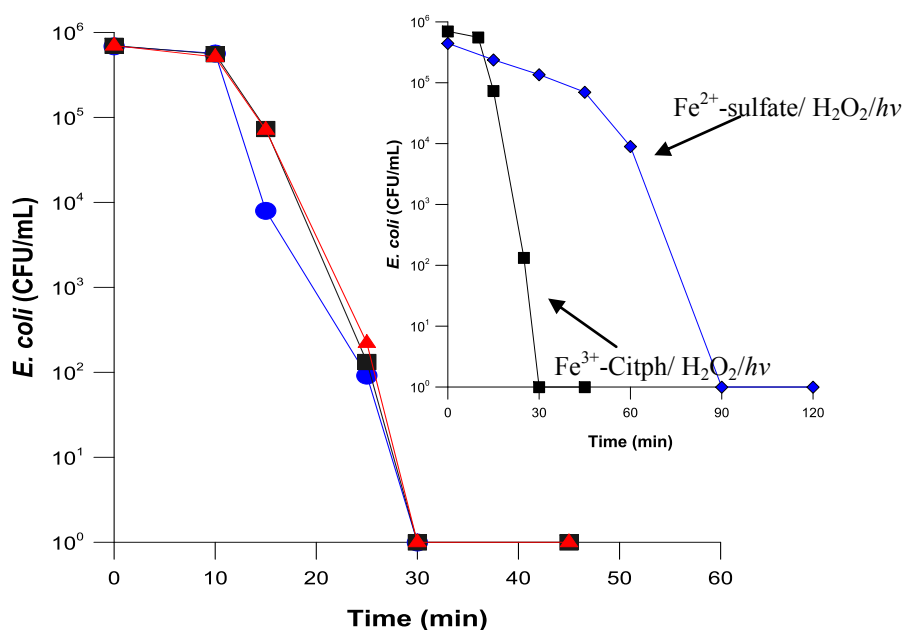
Figure 5-4: *E. coli* inactivation during photo-Fenton process mediated by Fe–citrate at different pH values: (▲) pH 6.5; (■) 7.5 and (●) 8.5. *Insert*: comparison of the photo-Fenton treatment using $FeSO_4$ and Fe–citrate at pH 7.5. Fe–citrate or $FeSO_4$ concentration: 0.6 mg/L relative to the Fe content, $[H_2O_2]$: 10 mg/L. Irradiated with simulated solar light. Experiments were conducted in triplicate and standard error was found to be approximately 5%.

Table 5-1: Summary of inactivation rate constants K_{obs} [min^{-1}] obtained from fitting of plots of log (CFU/mL) vs. time. Values of pH, dissolved Fe and H_2O_2 at the initial time (0 min) and final time (120 min) for all the experiments.

Systems	K_{obs} [min^{-1}]	pH		Fe (mg/L)			H_2O_2 (mg/L)	
		initial	final	0 min	60 min	120 min	initial	final
Figure 5-4: Effect of the pH								
Fe-citrate+H_2O_2+light	0.735±0.003	6.5	5.4	0.6	0.3	0.2	10.0	2.8
Fe-citrate+H_2O_2+light	0.754±0.014	7.5	6.2	0.6	0.2	0.2	10.0	2.2
Fe-citrate+H_2O_2+light	0.695±0.009	8.5	7.5	0.6	0.1	N. D	10.0	1.5
FeSO$_4$+H_2O_2+light	0.163±0.021	7.5	6.8	N. D	N. D	N. D	10.0	7.4
Figure 5-5: Effect of the Fe-citrate concentration								
	0.287±0.009	6.5	6.3	0.1	0.05	0.03	10.0	9.8
	0.485±0.015	6.4	6.1	0.3	0.04	0.02	10.0	5.9
Fe-citrate+H_2O_2+light	0.736±0.001	6.5	5.5	0.6	0.3	0.2	10.0	2.7
	0.737±0.003	6.5	5.7	1.0	0.5	0.2	10.0	2.8
	0.751±0.012	6.5	5.5	2.0	0.8	0.4	10.0	2.5
Figure 5-6: photo-Fenton process mediated by different iron sources								
Fe-citrate+H_2O_2+light	0.736±0.001	6.5	5.4	0.6	0.3	0.2	10.0	2.8
FeSO$_4$+H_2O_2+light	0.241±0.002	6.5	5.8	0.3	0.2	N. D	10.0	5.0
Goethite+H_2O_2+light	0.137±0.016	6.5	6.2	N. D	N. D	N. D	10.0	8.8
Fe-citrate+light	-	6.5	6.3	0.6	0.4	0.4	-	-
Fe-citrate+H_2O_2+dark	-	6.5	6.4	0.6	0.3	0.3	10.0	9.4
Figure 5-8: Photo-Fenton process in natural water (Lake Geneva)								
Fe-citrate+H_2O_2+light	0.263±0.012	8.3	8.2	0.6	0.4	0.2	10.0	2.0
Fe-citrate+light	-	8.3	8.3	0.6	0.4	0.4	-	-
Fe-citrate+H_2O_2+dark	-	8.3	8.3	0.6	0.5	0.5	10.0	9.2
H_2O_2+light	-	8.4	8.3	-	-	-	10.0	9.3
light	-	8.5	8.4	-	-	-	-	-

Dissolved iron was present during the entire Fe–citrate–mediated photo-Fenton reaction at pH 6.5 and 7.5 in the presence of bacteria (Table 5-1). In contrast, dissolved iron was not detected after 20 min of reaction at the same pH values in the absence of bacteria (Figure 5-1 (c), traces (▲) and (■)). This could be explained by the siderophores secreted by *E. coli* (*e.g.*, ferritins and aerobactin) (Andrews *et al.*, 2003) that can chelate iron, allowing for its solubilization. The photo-reduction of Fe^{3+} from Fe^{3+}–siderophore complexes under UV–A and visible radiation produces HO$^{\bullet}$ and regenerates Fe^{2+} *via* LMCT (Köster, 2001; Upritchard *et al.*, 2007). However, in the experiments conducted at pH 8.5, dissolved iron was negligible after 60 min of Fe–citrate–mediated photo-Fenton reaction in the presence of bacteria, even if the detection limit of the employed ICP-MS spectrometry was of 0.2–0.9 µg/L (Table 5-1).

This could be due to the non-soluble crystalline forms of iron species formed at high pH, which are more stable, to be complexed by siderophores (Sulzberger and Laubscher, 1995). These results are in good agreement with those reported by Waite and Morel (Waite and Morel, 1984), who detected photo-reduced iron from amorphous Fe-hydroxides at pH 6.5, but not at pH 8.0. They proposed that a hydroxylated ferric surface species is the primary chromophore (light absorbing compound), analogous to the photo-reduction of $Fe(OH)^{2+}$, they also said that at pH 8 the Fe^{3+} surface complex was more strongly hydrolyzed and less prone to photo-reduction. However, in this study, *E. coli* inactivation was reached before 30 min of treatment when dissolved iron was still detected. Therefore, the photo-Fenton reaction carried out at near-neutral and alkaline pH using citrate as source of iron was mainly conducted by a homogeneous reaction. Control experiments conducted in the absence of the Fenton reagents at different pH values of 6.5, 7.5 and 8.5 showed that the survival of bacteria was unaffected for the tested pH values under dark.

The insert in Figure 5-4 shows a comparison of *E. coli* inactivation during heterogeneous and homogeneous photo-Fenton reaction mediated by Fe–citrate and $FeSO_4$, respectively, at initial pH level of 7.5. In this latter condition, Fe^{2+} from $FeSO_4$ was instantaneously converted into solid iron oxides by O_2 and H_2O_2 (Table 5-1). In fact, goethite (α-FeO(OH)) and/or lepidocrocite (γ-FeO(OH)), which have been reported to be formed by oxidation of Fe^{2+} in solution at neutral pH (Cornell, 2000; Ruales-Lonfat *et al.*, 2015), are probably involved in the bacterial inactivation reached after 90 min of treatment (insert in Figure 5-4). In contrast, the Fe–citrate–mediated photo-Fenton reaction showed a faster bacterial inactivation rate compared to $FeSO_4$ system, with corresponding inactivation rate constants of 0.754 ± 0.014 min^{-1} and 0.163 ± 0.021 min^{-1}, respectively. This is due to the presence of dissolved iron ions in the Fe–citrate–based photo-Fenton treatment (Table 5-1). They contribute to the homogeneous catalytic cycle, thus accelerating the decomposition of H_2O_2, which, in turn, results in enhancement of $HO^{\bullet}$ production (Eq. (5.10)). This observation was corroborated by the hydrogen peroxide consumption that was greater for the Fe–citrate–mediated photo-Fenton reaction (78%) than $FeSO_4$–mediated photo-Fenton reaction (26%) (Table 5-1).

The pH of the solutions decreases roughly by 1 unit for all the studied systems (Table 5-1). This concomitant decrease in pH is the result of aliphatic acids generated during photocatalytic oxidation of both bacteria and citrate ligands by $HO^{\bullet}$ radical produced by photo-Fenton reaction. Previous studies have demonstrated that the pH value of Fe–citrate–

mediated photo-Fenton reaction had a great effect on the degradation extend of organic compounds. Silva *et al.*, (2007) showed a decrease of herbicide degradation efficiency as the pH increase during iron–citrate–based photo-Fenton process under solar irradiation. However, in this study, the application of this complex towards inactivation of microorganisms present in aqueous solution was not significantly affected by pH. This remarkable finding indicates that, when using Fe–citrate as source of iron during photo-Fenton treatment, the bacterial inactivation can be carried out at near-neutral and alkaline pH, which is advantageous for environmental applications.

5.3.4   Influence of Fe–citrate concentration on bacterial inactivation by photo-Fenton processes

To inspect the effect of Fe–citrate concentration on *E. coli* inactivation, the experiments was conducted in the presence of 0.1, 0.3, 0.6, 1.0 and 2.0 mg/L of iron, with 10 mg/L H_2O_2, at pH 6.5. Due to efficiency of the Fe–citrate–based photo-Fenton process to bacterial inactivation was independent of the pH in the range of 6.5 to 8.5 (section 5.3.3), a value of 6.5 was selected for the evaluation of the others parameters on the inactivation. The results shown in Figure 5-5 indicate that increasing the Fe–citrate concentration from 0.1 mg/L to 0.6 mg/L (concentrations relatives to the Fe content) has a positive effect on the rate of bacterial inactivation. The initial Fe–citrate concentration doses of 0.1 and 0.3 mg/L resulted in complete bacterial inactivation after 75 and 45 min of reaction, with inactivation rate constants of 0.287 ± 0.001 min^{-1} and 0.485 ± 0.015 min^{-1}, respectively (Figure 5-5, traces (●) and (▲)). When the Fe–citrate concentration was increased to 0.6 mg/L, the inactivation was improved with an inactivation rate constant of 0.736 ± 0.001 min^{-1} (Table 5-1). These results can be explained by an increase in the reaction kinetics due to the higher iron concentration (Herrera *et al.*, 1998; Pérez *et al.*, 2002), which was also observed in a faster consumption of H_2O_2. This certainly promotes a higher generation of hydroxyl radicals and consequently, induces an enhancement of bacterial inactivation rate. Correspondingly, after 120 min of treatment, 2%, 41% and 73% of H_2O_2 were consumed for 0.1, 0.3 and 0.6 mg/L of iron, respectively (Table 5-1). Nevertheless, at higher concentrations of Fe–citrate (1.0 and 2.0 mg/L), no significant differences were found in the inactivation rate constants, compared with a concentration of 0.6 mg/L, k_{obs} were 0.737 ± 0.003 min^{-1}, 0.751 ± 0.012 min^{-1} and 0.736 ± 0.001 min^{-1}, respectively. As shown in Eqs. (5.8) and (5.10), a higher level of HO⁺ radicals

generation was expected at a higher Fe–citrate concentration due to the enhanced absorption of light by Fe–complexes (Cho *et al.*, 2004b). However, photo–generated HO$^\bullet$ radicals could react with both bacteria and Fe–citrate complex. Thus, when the concentration of Fe–citrate increased, the role of the Fe–citrate as a competitor for the HO$^\bullet$ reaction could also be more important (Balmer and Sulzberger, 1999). These results indicate that low ranges of concentration of Fe–citrate (Fe–citrate concentration: 0.6 mg/L relative to the Fe content) in homogeneous photo-Fenton system at near-neutral pH are adequate to efficiently inactivate *E. coli* under specific experimental conditions.
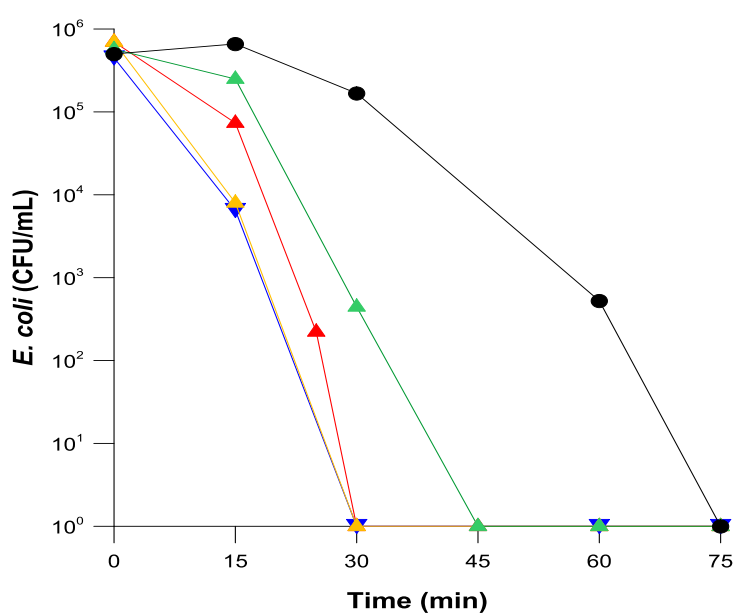
Figure 5-5: *E. coli* inactivation during photo-Fenton process with different Fe–citrate concentrations: (●) 0.1 mg/L; (▲) 0.3 mg/L; (▲) 0.6 mg/L; (▼) 1.0 mg/L and (▲) 2.0 mg/L. Concentrations relatives to the Fe content, [H$_2$O$_2$]: 10 mg/L, pH 6.5. Irradiated with simulated solar light. Experiments were conducted in triplicate and standard error was found to be approximately 5%.

5.3.5   Bacterial inactivation by photo-Fenton process using different iron sources

The positive effect of the Fe–citrate complex was compared, in terms of bacterial inactivation efficiency, with the other sources or iron: cationic iron (FeSO$_4$) and goethite at pH 6.5. The benefit of using the iron-citrate complex, as iron source in the photo-Fenton process for the bacterial inactivation was clear, reaching total bacterial inactivation before 30 min of treatment, while for FeSO$_4$ and goethite–based photo-Fenton systems bacterial inactivation

was reached before 90 min of treatment (Figure 5-6). The inactivation rate constants, presented in Table 5-1, confirmed the effects observed on the curves. The higher efficiency of bacterial inactivation observed with Fe–citrate complexes (k_{obs}: 0.736±0.001 min^{-1}) in relation to cationic iron (FeSO$_4$) (k_{obs}: 0.241±0.00 min^{-1}) or goethite (k_{obs}: 0.137±0.007 min^{-1}) can be attributed to several reasons. First of all, the citrate forms stable complexes with Fe^{3+} and leads to the higher solubility and stabilization of iron in aqueous solution at neutral pH, which leads to higher activity of iron in solution. Dissolved iron was observed during entire treatment period (Table 5-1). Secondly, the photoactivity of the Fe–citrate species, which generates Fe^{2+} with a relatively high quantum yield (Φ_{Fe2+}) that improve the photo-Fenton reaction [36, 37]. On the contrary, for the FeSO$_4$–based photo-Fenton systems, the dissolved iron passed from 0.3 mg/L to 0.2 mg/L after 60 min of reaction, suggesting a lesser contribution of a homogeneous photo-catalytic reaction than with Fe–citrate. Then, after 60 min of treatment, iron precipitates and a transition from a homogeneous to a heterogeneous process occurred (Table 5-1). Thus, after 60 min of treatment *E. coli* inactivation was mediated by the heterogeneous photocatalytic action of solid iron species that participated in the photo-Fenton reactions, although at slower rates than dissolved iron (Cornell and Schewetmann, 2003). In our previous paper (Ruales-Lonfat *et al.*, 2015), it was shown that iron (hydr)oxide alone or mixed as goethite (α-FeOOH) and lepidocrocite (γ-FeOOH) were formed by oxidation of Fe^{2+} in solution during photo-Fenton process at neutral pH. When goethite was used as source of iron in the photo-Fenton process, dissolved iron was not detected in the filtrate samples during the reaction (Table 5-1). Thus, *E. coli* inactivation was mediated by a heterogeneous photo-Fenton process from the beginning of the reaction.

The H$_2$O$_2$ consumption was related with the extent of dissolved iron for the three iron sources. 72%, 50% and 12% of H$_2$O$_2$ were consumed after 120 min of treatment in the presence of Fe–citrate, iron sulphate and goethite, respectively (Table 5-1). The higher H$_2$O$_2$ consumption in the presence of organic complexes is also related to the higher quantum yield of Fe^{2+} generation as compared to cationic iron (FeSO$_4$) or goethite. The quantum yield, in moles of Fe^{2+} produced per photon of incident UV radiation, increases in the following order: Fe^{3+}-complexes > dissolved (Fe^{3+}) species > Fe^{3+} in oxide form (Tan, 2003; Trovó and Nogueira, 2011). The same results were observed for degradation of organic compounds (Silva *et al.*, 2007; Trovó and Nogueira, 2011; Batista and Nogueira, 2012) where a higher efficiency with iron citrate was found as compared to iron salt.

The inactivation of *E. coli* by a homogeneous photo-Fenton process may be explained by:

(i)   Internal process, where endogenous photo-sensitizers and internal iron sources synergistically coupled to external UV and Fenton reactants (Fe^{2+}, H_2O_2) lead to oxidative stress through the intracellular Fenton's reaction, generating highly toxic $HO^\bullet$ that can directly attack DNA and other intracellular components leading to bacterial growth inhibition,

(ii) Contribution of external pathways, where exogenous short-living reactive oxygen species (ROS) formed outside of the cell, such as $^1O_2$, H_2O_2 and $HO^\bullet$, directly attack the external cell membrane and initiate lipid peroxidation chain reactions. This increases membrane permeability and subsequently alters normal cell functions and affects cell viability (Cabiscol *et al.*, 2000). However, we consider that the internal (photo)Fenton mechanism represents a key contribution to the overall inactivation process, since the photo-Fenton treatment at neutral pH induces only slight lipid peroxidation and cell permeability changes, as reported in our previous paper (Ruales-Lonfat *et al.*, 2014).
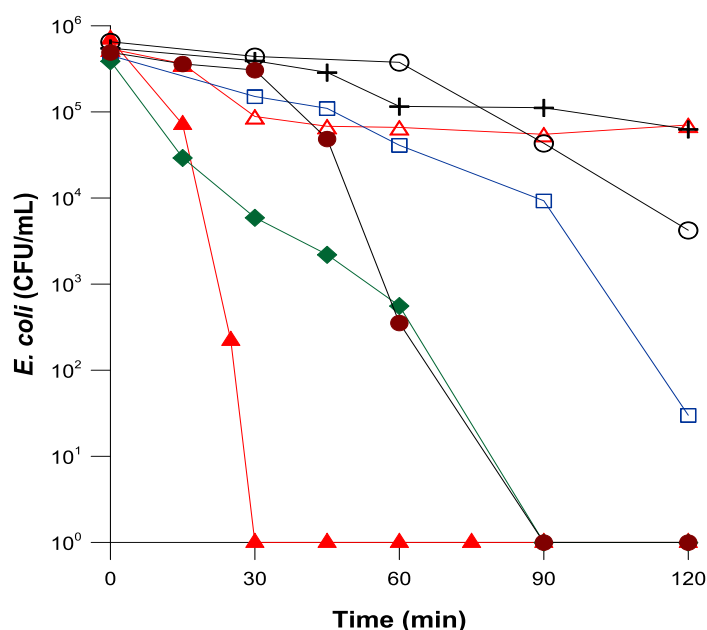
Figure 5-6: *E. coli* inactivation during photo-Fenton process mediated by different iron sources. (▲) Fe–citrate/H_2O_2/light; (◆) FeSO$_4$/H_2O_2/light and (●) goethite/H_2O_2/light. Control experiments: (△) Fe–citrate/light; (+) Fe–citrate/H_2O_2/dark; (○) light alone; (□) H_2O_2/light. Fe–citrate or FeSO$_4$ or goethite concentration: 0.6 mg/L relative to the Fe content, [H_2O_2]: 10 mg/L, pH 6.5. Irradiated with simulated solar light. Experiments were conducted in triplicate and standard error was found to be approximately 5%.

The mechanism involved in goethite-based heterogeneous photo Fenton process can be summarized by two mechanisms:

(i) Photo-reduction of $> Fe^{3+}OH$ to $> Fe^{2+}$ on the surface of iron-bearing particles, under Vis irradiation (Leland and Bard, 1987), which subsequently reacts with H_2O_2 generating $HO^{\bullet}$ radicals at the particle surface. Then, the generated $HO^{\bullet}$ radicals attacked the bacteria adsorbed on the surface of the iron oxide particles. ($>Fe^{3+}OH$ and $> Fe^{2+}$ represent the iron species in solid or solution phase),

(ii) Photocatalytic action of goethite, which possesses semiconductor properties with a band gap of 2.0–2.3 eV, typical to iron oxide semiconductors. Electrons and hole that are photogenerated in the goethite particles are scavenged by surface sites ($> FeOH$) to produce $HO^{\bullet}$ radicals and $> Fe^{2+}$. Also, conduction band electrons could react with O_2 to form $O_2^{\bullet-}$ and generate $HO^{\bullet}$ by several subsequent steps (Xu *et al.*, 2013). Furthermore, the photo-generated holes in the valence-band of goethite can directly react with bacteria (Xu *et al.*, 2013; Ruales-Lonfat *et al.*, 2015). Therefore, the reactive $HO^{\bullet}$ radicals formed during these processes at the goethite and/or from direct oxidation of bacteria by surface holes could contribute to achieving complete bacterial inactivation after 90 min of treatment for the goethite/H_2O_2/light system (Figure 5-6, trace (●)).

To get a better insight into the Fe–citrate complex–mediated bacterial inactivation through the formation of hydroxyl radicals, we compared the $HO^{\bullet}$ formation during the photo-Fenton process using different iron sources. The results shown in Figure 5-7 indicate that $HO^{\bullet}$ radicals were not detected before illumination. This finding suggests that exposure to the simulated solar light was essential for generation of ROS for the photo-Fenton process using different iron sources. From the results shown in Figure 5-7 (traces (▲), (◆) and (●)) it can be seen that the trend of $HO^{\bullet}$ radicals formation agreed well with the trend of bacterial inactivation during photo-Fenton treatment with different iron sources (Figure 5-6, traces (▲), (◆) and (●)). This indicates that the bacterial inactivation is due to the production of $HO^{\bullet}$ and that Fe–citrate can enhance the $HO^{\bullet}$ formation in the photo-Fenton process compared to $FeSO_4$- and goethite-based photo-Fenton treatments. This result is consistent with previous findings, which suggested that $HO^{\bullet}$ radical was the main species responsible for inactivating *E. coli* in the photoferrioxalate system under slightly acidic and near-neutral pH conditions (Cho *et al.*, 2004b).
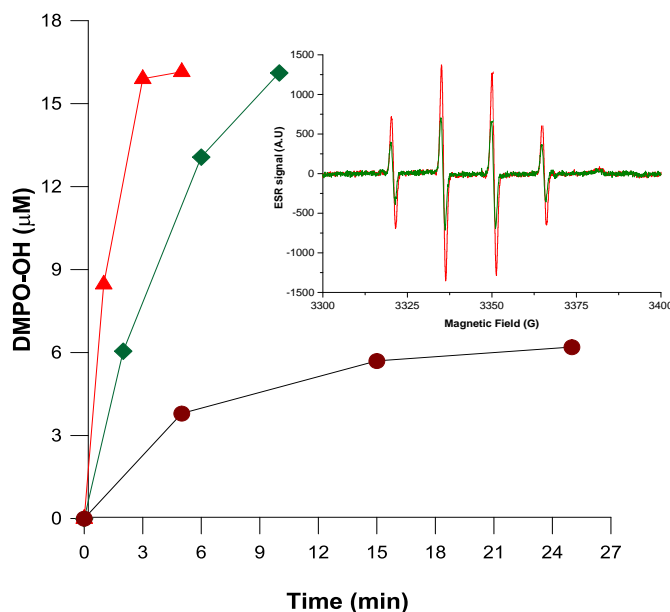
Figure 5-7: The ESR-measured formation of hydroxyl radical (HO$^{\bullet}$) during photo-Fenton process mediated by different iron sources. (▲) Fe–citrate; (◆) FeSO$_4$ and (●) goethite. Concentration: 0.6 mg/L relative to the Fe content, [H$_2$O$_2$]: 10 mg/L, irradiated with simulated solar light. *Insert*: a typical ESR spectrum of the Fe–citrate/H$_2$O$_2$/light (red), FeSO$_4$ /H$_2$O$_2$/light (green) systems.

The results of the photo-activity of Fe–citrate complex evaluated in the absence of H$_2$O$_2$ are shown in Figure 5-6. In particular, the trace (△) in Figure 5-6 shows 1.0 log$_{10}$ reduction of the number of live bacteria during the first 30 min of treatment. This could be attributed to a combined action of HO$_2^{\bullet}$/O$_2^{\bullet-}$ radicals formed during the photo-reduction of Fe–citrate *via* reactions (Eqs. (5.11) and (5.12)). The photo-generation of O$_2^{\bullet-}$ from Fe–citrate solution was detected only qualitatively, by electron spin resonance spectroscopy (ESR) and was not sufficient for the quantitative analysis. Furthermore, the possibility of the involvement of a ligand radical, 3–hydroxyglutaric acid, (3–HGA$^{2\bullet-}$), in inactivating *E. coli* cannot be excluded. These radical species are generated in the photo-reduction of Fe–citrate, as highlighted in Eq. (5.8). Nevertheless, due to the instantaneous decarboxylation and oxidation of HGA$^{2\bullet-}$ (Eq. (5.11)), the chance of inactivating *E. coli* by Citrate$^{2\bullet-}$ is minimal. Beyond 30 min of treatment a plateau was observed (Figure 5-6, traces (△)), possibly due to the Fe-citrate complex degradation. A similar result was observed by Cho *et al.*, (2004b) who detected a slight photo-inactivation of *E. coli* for ferrioxalate complex in the absence of H$_2$O$_2$ dose at near-neutral pH. Fe-citrate complex absorbs in the UV and near-visible light (Figure 5-1(a)) producing a light screening effect, hindering its penetration in the water, and thus, protecting the bacteria. The negative screen effect was observed with regard to the control experiment

under light alone (Fig. 7, traces (Δ) and (○)).

In the absence of light, the Fe–citrate/H_2O_2 system (Fenton-like process) resulted in 0.5 log_{10} reduction of the initial *E. coli* concentration during 60 min of reaction time (Figure 5-6, trace (+)). The absence of light limits Fe^{2+} regeneration (Eqs. (5.8) and (5.9)), and the catalytic cycle is, therefore, limited. Another control experiment under light alone (Figure 5-6, trace (○)) shows that the sunlight affects bacteria, although not immediately. The curve has a shoulder, which corresponds to first resistance phenomenon due to the self-defence and auto-repair mechanisms of *E. coli* (Helali *et al.*, 2014). After that, the inactivation rate increases considerably reached 2 log reductions of bacteria at 420 min of treatment. It is the resulted from alteration in the bacterial metabolism through UV-A radiation. As the deleterious action of UV-A radiation was indirect, its effect on bacterial cultivability mainly resulted from photosensitization of endogenous chromophores such as co-enzymes or cytochromes, which could damage enzymes essential to bacteria growth (Pigeot-Rémy *et al.*, 2012).

5.3.6 Bacterial inactivation by Fe–citrate–based photo-Fenton process in natural water

In order to evaluate the effect of dissolved organic and mineral matter present in natural drinking water sources on the activity of Fe–citrate–based photo-Fenton process during bacterial inactivation, water samples originating from Lake Geneva were used and compared with ultrapure water. As can be seen in Figure 5-8 (traces (Δ) and (●)), for the Fe–citrate/H_2O_2/light system, at the pH of 8.5, a complete *E. coli* inactivation was achieved before 60 and 30 min of treatment in both natural and ultrapure water, respectively. The inactivation rate constants presented in Table 5-1, confirm that the chemical components of the natural water do not enhance the Fe–citrate complex–mediated inactivation of bacteria through the homogeneous photo-Fenton action. Even if dissolved organic matter (DOM) had a positive effect on the complexation and solubilisation of iron resulting from photolysis of Fe–citrate complex (Pignatello *et al.*, 2006) (Table 5-1), DOM can react with $HO^•$ and thus disfavour the inactivation of bacteria. DOM substances can also absorb the UV–vis light producing a light screening effect that limit the light absorption of the Fe–citrate to inactivate bacteria. Furthermore, the presence of bicarbonates ions in lake water (Table 5-1) probably affects the photo-Fenton system due to the scavenging the $HO^•$ radicals, since HCO_3^- react

with HO⁺ radicals to produce less reactive radicals, $^{\bullet}CO_3^{-}$. The radical $^{\bullet}CO_3^{-}$ is an electrophilic species reacting slower compared to HO⁺. Also, HCO_3^{-} absorbs light hindering its penetration in the water, thus protecting the bacteria (Rubio *et al.*, 2013).

Control experiments Fe–citrate/H_2O_2 and Fe–citrate/light, in natural water did not yield inactivation, indicating that neither homogeneous Fenton processes nor photo-reduction of Fe–citrate complex contributed to bacterial inactivation under our experimental conditions (Figure 5-8, traces (＋) and (△)). A negative screen effect was observed for Fe-citrate/light system, with regard to the control experiment under light alone, due to the absorption of Fe-citrate complex in the UV and near-visible light (Fig. 1), hindering its penetration in the water, thus protecting the bacteria (Figure 5-8, traces (◆) and (•). For H_2O_2/light system control, complete bacterial inactivation was achieved before 120 min of treatment (Figure 5-8, trace (□).
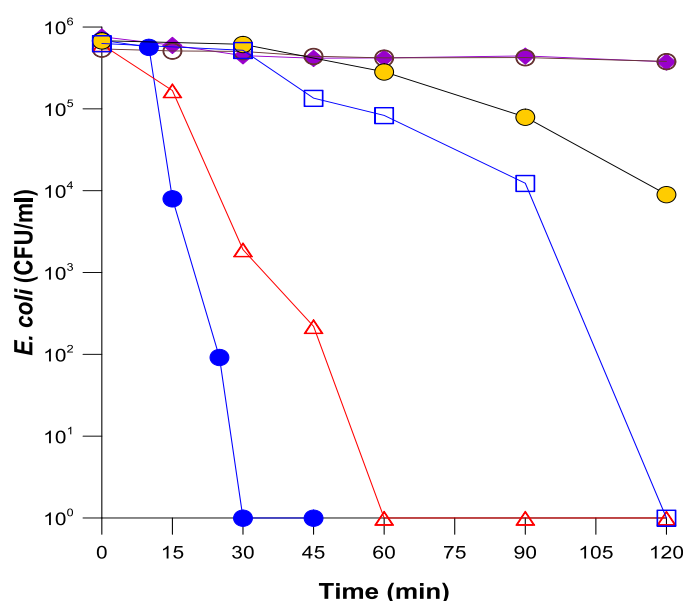
Figure 5-8: *E. coli* inactivation during photo-Fenton process. *E. coli* were suspended in natural water and ultrapure water having the characteristics described in Table 5-1. (◆) Fe–citrate/light, Lake water; (○) Fe–citrate/H_2O_2/dark, Lake water; (△) Fe–citrate/H_2O_2/light, Lake water (•) Fe–citrate/H_2O_2/light, ultrapure water (pH 8.5); (□) H_2O_2/light; (○) light alone. Fe-citrate concentration: 0.6 mg/L relative to the Fe content, [H_2O_2]: 10 mg/L. Irradiated with simulated solar light. Experiments were conducted in triplicate and standard error was found to be approximately 5%.

The pH of the solution of Lake Geneva water remains constant during the treatment (the final pH was of 8.2, Table 5-1), thus revealing a strong buffer capacity. This is due to the presence of carbonate, hydrocarbonate and phosphate ions in solution as shown in the composition of

the natural water (Table 5-1). Instead, the pH in ultrapure water for the system Fe–citrate/H_2O_2/simulated solar light decreased to the final pH value of 7.4. In each experiment, a residual peroxide concentration was detected at the end of the experiments ensuring the photo-Fenton reaction took place along of the treatment.

To be sure that the bacteria appearing as not-cultivable were inactivated, rather than slightly damaged, when using the photo-Fenton reaction, bacterial reactivation and/or growth of bacteria were verified. No bacterial reactivation and/or growth were observed at various pH values, different Fe-citrate concentrations and type of irradiations for the Fe–citrate–mediated photo-Fenton treatment (data not shown). The same results were observed when using samples of natural water. Furthermore, no bacterial reactivation and/or growth were observed when Fe^{3+}-citrate, $FeSO_4$ and goethite were used as iron sources during the photo-Fenton process. This evidenced irreversible inactivation of bacteria by the homogeneous photo-Fenton process at near-neutral and alkaline pH for all the iron sources and experimental conditions tested in this work.

5.4 Conclusions

Iron citrate-mediated intensification of the solar photo-Fenton process showed promising results for bacterial inactivation at near-neutral and alkaline pH conditions, with using low iron concentration (Fe–citrate concentration: 0.6 mg/L relative to the Fe content) and avoiding precipitation of ferric hydroxides. Positive results were also obtained while applying this treatment for bacterial inactivation in natural water samples from Lake Geneva (Switzerland) at pH 8.5. Additionally, no bacterial reactivation and/or growth were observed after photo-Fenton treatment. This suggested irreversible inactivation, which is advantageous for environmental applications.

The homogeneous photo-Fenton process at near-neutral pH, with using Fe–citrate complex as a source of iron, markedly improved the efficiency of bacterial inactivation as compared to the heterogeneous photo-Fenton treatment ($FeSO_4$ and goethite as sources of iron). The bacterial inactivation rate increased in the order of goethite < $FeSO_4$ < Fe-citrate, which agreed well with the trend for the $HO^{\bullet}$ radicals formation. The key reason has been attributed to the higher solubility and stabilization of iron in aqueous solution and a relatively high quantum yield of Fe-citrate complex.

This study reports the first application of Fe–citrate–based photo-Fenton chemistry for inactivation of *E. coli*. Another promising application of this system is related to the treatment of rural sites, where surface water or groundwater is frequently contaminated by agricultural chemicals and microorganisms. This type of application is promising, considering the simplicity of the installations and procedures, the possibility of using solar light and the low concentration of reagents used. Studies investigating larger-scale and field applications of the Fe–citrate–based photo-Fenton AOP are highly recommended.

6. Mechanistic interpretation of bacterial inactivation by photo-Fenton process at near-neutral pH.

Based on these experimental observations and an exhaustive revision of the literature, a mechanistic interpretation of the inactivation of *E. coli* in the presence of the photo-Fenton reagents at near-neutral pH under simulated solar radiation is proposed. An overview is presented in Figure 6-1. The processes are subdivided in two groups: internal or external processes.

6.1 Intensification of internal (photo)Fenton processes by the synergistic action of UV-A and external Fenton reactants

(1) UV-A light can damage iron-containing proteins such as ferritin, leading to the intracellular release of Fe^{2+} and enzymes, such as catalase or superoxide dismutase (SOD), which constitute a cellular self-defense against ROS (Eisenstark, 1998). Their disfunction can lead to increased intracellular concentrations of long living ROS such as H_2O_2 and $O_2^{\cdot-}$ (Imlay, 2003).

(2) Added Fe^{2+} has a lower charge density than Fe^{3+} and can diffuse across the outer membrane and is transported by specific proteins *via* a FeO (ferrous iron-transport) system across the cytoplasmic membrane (Cartron *et al.*, 2006; Ruales-Lonfat *et al.*, 2014).

(3) Part of the added Fe^{2+} in the bulk of the solution precipitates as iron (hydr)oxides at near-neutral pH and can not move freely into the cell. Thus, siderophores produced by bacteria (enterobactin, aerobactin, and ferrichrome) can chelate iron to manage the Fe^{3+} transport inside the cell *via* siderophores (metabolic Fe^{3+} chelating agents) (Köster, 2001; Upritchard *et al.*, 2007).

(4) H_2O_2 is a long living ROS, thus relatively stable (unlike $HO^\bullet$) and uncharged (unlike $O_2^{\bullet-}$). When added to the bulk of the solution, H_2O_2 can penetrate bacterial membrane and diffuses into cells; therefore, H_2O_2 stress arises inside cells (Imlay, 2008).

(5)   Endogenous cell photosensitizers (PS) such as porphyrins, cytochromes, aromatic amino acids, flavins, tryptophan, chlorophyll, and other absorb solar light in the UV-A and visible spectrum. The excited PS can either directly attack biomolecules or react with surrounding oxygen generating ROS (Reed, 2004).

The formation or penetration of H_2O_2 and Fe^{2+} in the cytoplasm by these systems (1-4) and endogenous photo-sensitizers lead to oxidative stress through the intracellular Fenton's reaction (Imlay, 2003, 2008), generating highly toxic $HO^\bullet$ that can directly attack DNA, thus causing DNA deactivation primarily *via* pyrimidine dimerization and, consequently, cell growth inhibition (Zepp *et al.*, 1992).

6.2   Contribution of external pathways to bacteria inactivation

Considering that the cell wall is a protective barrier against environmental stress to microorganisms, the following external events could occur in which the ROS generated leads to membrane peroxidation and increases in the permeability of bacterial cell walls.

(6) Fe^{3+} can be adsorbed or absorbed on proteins of the bacterial membrane and their carboxylic endgroups, thus leading to the formation of Fe^{3+}-bacteria exciplexes. The photosensitization of these forms by UV-A and visible light might result in direct oxidation of the membrane, initiation of lipid peroxidation chains, and generation of Fe^{2+} and $HO^\bullet$ in spitting distance of the target microorganism (Feng and Nansheng, 2000).

(7)   Highly reactive short-living $HO^\bullet$ and other ROS are formed in the bulk of the solution by a homogeneous process through the contribution of the following routes:

    (a)   Iron ions can forms complexes with by-products (generated from bacterial inactivation) and with siderophores which absorb UVA and visible light, leading to the regeneration of Fe^{2+}, which subsequently reacts with H_2O_2 generating $HO^\bullet$ in the bulk via the homogeneous photo-Fenton reagent (Pignatello *et al.*, 2006). The

formation of Fe^{3+}-organo complexes allows the photo-Fenton reactions to take place at near neutral pH (Cho *et al.*, 2004b; Rodriguez-Chueca *et al.*, 2013; Ortega-Gómez *et al.*, 2014b; Rodríguez-Chueca *et al.*, 2014b; Ruales-Lonfat *et al.*, 2014; Ruales-Lonfat *et al.*, 2015).

(b) At near-neutral pH, Fe^{2+} is oxidized by O_2 and H_2O_2 and precipitates as ferric (hydr)oxide. Siderophores secreted by bacteria increase the light-induced dissolution of ferric (hydr)oxide by forming bacteria Fe^{3+}-siderophore complex (Andrews *et al.*, 2003; Borer *et al.*, 2005; Upritchard *et al.*, 2007). Additionally, by-products generated from bacterial inactivation can be polydentate ligands that form complexes with ferric ions (Fe^{3+}-by-products), allowing their solubilization. The photo-reduction of these complexes under UV-A and visible radiation, produce $HO^\bullet$ and regenerating Fe^{2+} *via* LMCT (Feng and Nansheng, 2000).

(c) The radical formed by the photosensitization of Fe^{3+}-complexes react with O_2 leading to the formation of the radicals such as $O_2^{\bullet-}/HO_2^\bullet$, that can attack the membrane.

(8) The iron (hydr)oxide particles under illumination at near-neutral pH participate in bacterial inactivation by the following routes:

(a) As semiconductor photocatalysis, leading to the formation of $> Fe^{2+}$ and $HO^\bullet$, followed by reaction between hole and superoxide radical to form singlet oxygen. Holes in the excited surface of iron (hydr)oxides can directly react with bacteria.

(b) As catalysts of the heterogeneous photo-Fenton process by promoting the photo-reduction of $> Fe^{3+}OH$ to $> Fe^{2+}$, which subsequently reacts with H_2O_2 generating $HO^\bullet$ radicals at the particle surface.
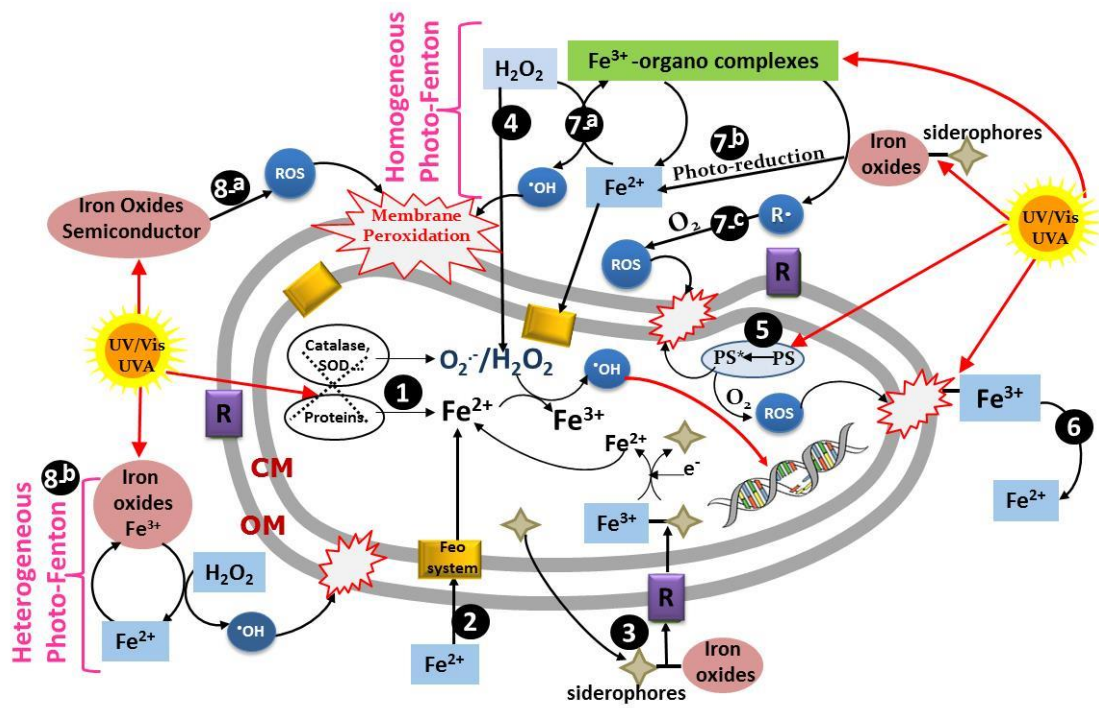
Figure 6-1: Mechanistic representation of possible pathways involved in photo-inactivation of *E. coli* in the presence of Fe^{2+}, Fe^{3+} and H_2O_2 at near-neutral pH. R: receptor proteins, CM: cytoplasmatic membrane, OM: outer membrane, PS: photosensitizers.

7. General conclusions and perspectives

7.1 Conclusions

Heterogeneous and homogeneous photo-Fenton processes catalyzed by low concentration of iron are an efficient alternative for waterborne bacteria disinfection in natural water. Other types of bacteria such as *Salmonella, Shigella, etc.* may also be inactivated by this approach.

Iron (hydr)oxides act as photocatalytic semiconductors and catalysts in the heterogeneous photo-Fenton process at near-neutral pH with the exception of magnetite, which needs H_2O_2 as electron acceptors. Other iron (hydr)oxides were photoactive under sunlight in the absence of H_2O_2 using only oxygen as electron acceptors. Therefore, the iron (hydr)oxide particles, even those already present in environmental waters, represent low-cost photocatalysts for solar water disinfection.

In the case of the homogeneous photo-Fenton process at neutral pH conditions using Fe–citrate complex as a source of iron, improved bacterial inactivation compared to heterogeneous photo-Fenton treatment ($FeSO_4$ and goethite as sources of iron). The bacterial inactivation rate increased in the order of goethite < $FeSO_4$ < Fe-citrate, which agreed with the trend for the $HO^{\bullet}$ radicals formation, due to the higher solubility and stabilization of iron in aqueous solution and a relatively high quantum yield of Fe-citrate complex.

The bacterial inactivation by photo-Fenton process at near-neutral pH is mediated by both internal and external processes that occur in the bacteria. Internal (photo)Fenton processes are mediated by the synergistic action of UV-A and presence of the Fenton reactants. For external events, homogeneous and heterogeneous photocatalytic actions contributed to efficient bacterial inactivation.

Positive results were also obtained when homogeneous or heterogeneous photo-Fenton processes for bacterial inactivation in natural water samples from Lake Geneva (Switzerland) at pH 8.5 were applied. Additionally, no bacterial reactivation and/or growth were observed, suggesting irreversible inactivation. This type of application is promising, considering the

simplicity of the installations and procedures, the possibility of using solar light, the low concentration of reagents and the does not produce toxic waste.

7.2 Perspectives

In this work, ultrapure water and natural water were used during the investigation of bacterial inactivation by photo-Fenton processes at near-neutral pH. Further studies should be conducted to completely assess the effectiveness of these AOPs, heterogeneous and homogeneous photo-Fenton processes as disinfection methods. In this context, the following points should be considered:

- Scaling up of the heterogeneous and homogeneous photo-Fenton processes.
- The detailed inactivation kinetics for other type of bacteria and pathogens by these processes.
- The effect of the NOM and the chemical composition of natural water especially HCO_3^- contents on the photo-Fenton process, followed by the evaluation of their impact on the pH evolution during the photo-disinfecting treatment.
- To compare the inactivation efficiency by Fe-citrate-based photo-Fenton process with others chelating agents (*e.g.* oxalate, EDDS, isolated or synthetic siderophores, *etc*.).
- To further in the understanding of post irradiation events to elucidate the mechanism which leads damaged cells to death in the dark.
- The efficiency of photo-Fenton processes at near-neutral pH in comparison with the conventional disinfection methods.

To better understand the mechanisms involved in bacterial inactivation may address:

- The effect of substances released during the bacterial inactivation.
- The bacteria damage by ROS on the cell wall integrity and size can be followed by electron microscopy techniques (HRTEM, SEM).
- The ad- and absorption of Fe^{2+} and Fe^{3+} by bacteria and to identify the nature of the parameters controlling the absorption.

- Address fluorescent probes to determine bacterial enzyme activity and damage by cytometry.
- Determination of the membrane integrity by capillary cytometry, in the presence of SOD to show whether the generated $O_2^{\bullet-}$ and $HO^{\bullet}$ are responsible for cell membrane damage.

Finally, a socio-economic evaluation for the sustainable application of these processes as a disinfection method in developing countries may be conducted. The following points should be considered:

- The economic feasibility of using photo-Fenton processes as a disinfection method.
- The design of the treatment plant to incorporate a photo-Fenton -type system.
- The maintenance services necessary in order to maintain an efficient inactivation by these processes over longer times of handling.
- The possible sources of H_2O_2 production at point-of-use level as well as the conception and production of hydrogen peroxide pellets in easily usable dose for photo-Fenton treatment.

References

A. Safarzadeh-Amiri, Bolton, J.R., Cater, S.R., 1996. The Use of Iron in Advanced Oxidation Processes. Journal Adv. Oxidation Technol. 1, 18-26.

Abida, O., Kolar, M., Jirkovsky, J., Mailhot, G., 2012. Degradation of 4-chlorophenol in aqueous solution photoinduced by Fe(iii)-citrate complex. Photochem Photobiol Sci 11, 794-802.

Abrahamson, H.B., Rezvani, A.B., Brushmiller, J.G., 1994. Photochemical and spectroscopic studies of complexes, of iron(III) with citric acid and other carboxylic acids. Inorganica Chimica Acta 226, 117-127.

Acra, A., Ayoub, G., 1997. Experimental evaluation of a novel photodynamic water disinfection technique. Journal of Water Supply Research and Technology-Aqua 46, 218-223.

Acra, A., Jurdi, M., Allem, H.M., Karahagopian, Y., Raffoul, Z., 1989. Sunlight as disinfectant. Lancet 1, 280-280.

Acra, A., Karahagopian, Y., Raffoul, Z., Dajani, R., 1980. Disinfection of oral rehydration solutions by sunlight. Lancet 2, 1257-1258.

Agulló-Barceló, M., Polo-López, M.I., Lucena, F., Jofre, J., Fernández-Ibáñez, P., 2013. Solar Advanced Oxidation Processes as disinfection tertiary treatments for real wastewater: Implications for water reclamation. Applied Catalysis B: Environmental 136–137, 341-350.

Aldhous, P., 2003. The world's forgotten crisis. Nature 422, 251-251.

Amin, S.A., Green, D.H., Küpper, F.C., Carrano, C.J., 2009. Vibrioferrin, an Unusual Marine Siderophore: Iron Binding, Photochemistry, and Biological Implications. Inorganic Chemistry 48, 11451-11458.

Andreozzi, R., Caprio, V., Marotta, R., 2003. Iron(III) (hydr)oxide-mediated photooxidation of 2-aminophenol in aqueous solution: A kinetic study. Water Res 37, 3682-3688.

Andrews, S.C., Robinson, A.K., Rodriguez-Quinones, F., 2003. Bacterial iron homeostasis. Fems Microbiology Reviews 27, 215-237.

Antonini, E., Vidic, H.-J., 1994. Complejo de hierro-citrato, procedimiento para su fabricación y su aplicación farmacéutica. In: marca, O.e.d.p.y. (Ed.), Spanish

Asadishad, B., Ghoshal, S., Tufenkji, N., 2013. Short-term inactivation rates of selected gram-positive and gram-negative bacteria attached to metal oxide mineral surfaces: role of solution and surface chemistry. Environmental Science & Technology 47, 5729-5737.

Balmer, M.E., Sulzberger, B., 1999. Atrazine degradation in irradiated iron/oxalate systems: Effects of pH and oxalate. Environmental Science and Technology 33, 2418-2424.

Bandala, E.R., Gonzalez, L., Sanchez-Salas, J.L., Castillo, J.H., 2012. Inactivation of Ascaris eggs in water using sequential solar driven photo-Fenton and free chlorine. Journal of Water and Health 10, 20-30.

Barbeau, K., Rue, E.L., Trick, C.G., Bruland, K.W., Butler, A., 2003. Photochemical reactivity of siderophores produced by marine heterotrophic bacteria and cyanobacteria based on characteristic Fe(III) binding groups. Limnology and Oceanography 48, 1069-1078.

Batista, A.P.S., Nogueira, R.F.P., 2012. Parameters affecting sulfonamide photo-Fenton degradation - Iron complexation and substituent group. Journal of Photochemistry and Photobiology A: Chemistry 232, 8-13.

Bekbölet, M., Balcioglu, I., 1996. Photocatalytic degradation kinetics of humic acid in aqueous TiO2 dispersions: The influence of hydrogen peroxide and bicarbonate ion. Water Science and Technology 34, 73-80.

Benabbou, A.K., Derriche, Z., Felix, C., Lejeune, P., Guillard, C., 2007. Photocatalytic inactivation of Escherischia coli: Effect of concentration of TiO2 and microorganism, nature, and intensity of UV irradiation. Applied Catalysis B: Environmental 76, 257-263.

Benabbou, A.K., Guillard, C., Pigeot-Rémy, S., Cantau, C., Pigot, T., Lejeune, P., Derriche, Z., Lacombe, S., 2011. Water disinfection using photosensitizers supported on silica. Journal of Photochemistry and Photobiology A: Chemistry 219, 101-108.

Bernabeu, A., Vicente, R., Peribáñez, M.A., Arques, A., Amat, A.M., 2011. Exploring the applicability of solar driven photocatalytic processes to control infestation by zebra mussel. Chemical Engineering Journal 171, 490-494.

Berney, M., Weilenmann, H.U., Ihssen, J., Bassin, C., Egli, T., 2006. Specific growth rate determines the sensitivity of Escherichia coli to thermal, UVA, and solar disinfection. Appl Environ Microbiol 72, 2586-2593.

Beydoun, D., Amal, R., Low, G., McEvoy, S., 2002. Occurrence and prevention of photodissolution at the phase junction of magnetite and titanium dioxide. Journal of Molecular Catalysis a-Chemical 180, 193-200.

Beydoun, D., Amal, R., Low, G.K.C., McEvoy, S., 2000. Novel photocatalyst: Titania-coated magnetite. Activity and photodissolution. Journal of Physical Chemistry B 104, 4387-4396.

Binder, B., 1971. Mixed-valence complexes of iron(III) with iron(II) and mixed-metal complexes of iron(III) with tin(II) in aqueous citrate media. Inorganic Chemistry 10, 2146-2150.

Borer, P.M., Sulzberger, B., Reichard, P., Kraemer, S.M., 2005. Effect of siderophores on the light-induced dissolution of colloidal iron(III) (hydr)oxides. Marine Chemistry 93, 179-193.

Brame, J., Li, Q., Alvarez, P.J.J., 2011. Nanotechnology-enabled water treatment and reuse: Emerging opportunities and challenges for developing countries. Trends in Food Science and Technology 22, 618-624.

Brasca, M., Morandi, S., Lodi, R., Tamburini, A., 2007. Redox potential to discriminate among species of lactic acid bacteria. Journal of Applied Microbiology 103, 1516-1524.

Braun, V., 2001. Iron uptake mechanisms and their regulation in pathogenic bacteria. International Journal of Medical Microbiology 291, 67-79.

Buettner, G.R., Mason, R.P., 1990. Spin-trapping methods for detecting superoxide and hydroxyl free-radicals in-vitro and in-vivo. Methods in Enzymology 186, 127-133.

Buzmakov, V.M., Pshenichnikov, A.F., 1996. On the structure of microaggregates in magnetite colloids. Journal of Colloid and Interface Science 182, 63-70.

Byrne, J.A., Fernandez-Ibanez, P.A., Dunlop, P.S.M., Alrousan, D.M.A., Hamilton, J.W.J., 2011. Photocatalytic Enhancement for Solar Disinfection of Water: A Review. International Journal of Photoenergy.

Cabiscol, E., Tamarit, J., Ros, J., 2000. Oxidative stress in bacteria and protein damage by reactive oxygen species. Int. Microbiol 3, 3-8.

Cambier, P., 1986. Infrared study of goethites of varying crystallinity and particle size: I. Interpretation of hydroxyl and lattice vibration frequencies. Clay Miner 21, 191-200.

Candan, N.T., N., 2008. Very rapid quantification of malondialdehyde (MDA) in rat brain exposed to lead, aluminium and phenolic antioxidants by high-performance liquid chromatography-fluorescence detection. NeuroToxicology 29, 708-713.

Canonica, S., Jans, U., Stemmler, K., Hoigne, J., 1995. Transformation kinetics of phenols in water - photosensitization by dissolved natural organic material and aromatic ketones. Environmental Science & Technology 29, 1822-1831.

Cartron, M.L., Maddocks, S., Gillingham, P., Craven, C.J., Andrews, S.C., 2006. Feo - Transport of ferrous iron into bacteria. Biometals 19, 143-157.

Catastini, C., Sarakha, M., Mailhot, G., Bolte, M., 2002. Iron (III) aquacomplexes as effective photocatalysts for the degradation of pesticides in homogeneous aqueous solutions. Science of the Total Environment 298, 219-228.

Chen, Y., Liu, Z., Wang, Z., Xue, M., Zhu, X., Tao, T., 2011. Photodegradation of propranolol by Fe(III)–citrate complexes: Kinetics, mechanism and effect of environmental media. Journal of Hazardous Materials 194, 202-208.

Chen, Y., Wu, F., Lin, Y., Deng, N., Bazhin, N., Glebov, E., 2007. Photodegradation of glyphosate in the ferrioxalate system. Journal of Hazardous Materials 148, 360-365.

Cho, M., Chung, H., Choi, W., Yoon, J., 2004a. Linear correlation between inactivation of E. coli and OH radical concentration in TiO2 photocatalytic disinfection. Water research 38, 1069-1077.

Cho, M., Kim, J., Kim, J.Y., Yoon, J., Kim, J.H., 2010. Mechanisms of Escherichia coli inactivation by several disinfectants. Water Res 44, 3410-3418.

Cho, M., Lee, Y., Chung, H., Yoon, J., 2004b. Inactivation of Escherichia coli by photochemical reaction of ferrioxalate at slightly acidic and near-neutral pHs. Appl Environ Microbiol 70, 1129-1134.

Chou, J.C., Lin, S.A., Lee, C.Y., Gan, J.Y., 2013. Effect of bulk doping and surface-trapped states on water splitting with hematite photoanodes. Journal of Materials Chemistry A 1, 5908-5914.

Chueca, J.R., Mosteo, R., Ormad, M.P., Miguel, N., Ovelleiro, J.L., 2012. Heterogeneous fenton and photofenton processes for disinfection of treated urban wastewater. Tecnologia del Agua 32, 72-77.

Cieśla, P., Kocot, P., Mytych, P., Stasicka, Z., 2004. Homogeneous photocatalysis by transition metal complexes in the environment. Journal of Molecular Catalysis A: Chemical 224, 17-33.

Cornell, R.M., Schewetmann, U., 2003. The iron oxides: structure, properties, reactions, ocurrences and uses. ISBN: 3-527-30274-3., British.

Cornell, R.M., Schwertmann, 2000. Iron Oxides in the Laboratory: Preparation and Characterization. ISBN: 3527296697.

Cory, R.M., Cotner, J.B., McNeill, K., 2008. Quantifying Interactions between Singlet Oxygen and Aquatic Fulvic Acids. Environmental Science & Technology 43, 718-723.

Costa, R.C.C., Lelis, M.F.F., Oliveira, L.C.A., Fabris, J.D., Ardisson, J.D., Rios, R.R.V.A., Silva, C.N., Lago, R.M., 2006. Novel active heterogeneous Fenton system based on Fe3−xMxO4 (Fe, Co, Mn, Ni): The role of M2+ species on the reactivity towards H2O2 reactions. Journal of hazardous materials 129, 171-178.

Curtis, T.P., Mara, D.D., Silva, S.A., 1992. INFLUENCE OF PH, OXYGEN, AND HUMIC SUBSTANCES ON ABILITY OF SUNLIGHT TO DAMAGE FECAL-COLIFORMS IN WASTE STABILIZATION POND WATER. Appl Environ Microbiol 58, 1335-1343.

Dalrymple, O.K., Isaacs, W., Stefanakos, E., Trotz, M.A., Goswami, D.Y., 2011. Lipid vesicles as model membranes in photocatalytic disinfection studies. Journal of Photochemistry and Photobiology A: Chemistry 221, 64-70.

Davies, M.J., 2003. Singlet oxygen-mediated damage to proteins and its consequences. Biochemical and Biophysical Research Communications 305, 761-770.

Davies, M.J., 2005. The oxidative environment and protein damage. Biochimica et Biophysica Acta (BBA) - Proteins and Proteomics 1703, 93-109.

de Lima Perini, J.A., Perez-Moya, M., Nogueira, R.F.P., 2013. Photo-Fenton degradation kinetics of low ciprofloxacin concentration using different iron sources and pH. Journal of Photochemistry and Photobiology A: Chemistry 259, 53-58.

Dendy, J.S., 1968. Determination of Depletion of Dissolved Oxygen Content in Water. United States.

Doerrler, W.T., 2006. Lipid trafficking to the outer membrane of Gram-negative bacteria. Molecular Microbiology 60, 542-552.

Downes, A., Blunt, T.P., 1877. Researches on the Effect of Light upon Bacteria and other Organisms. Proceedings of the Royal Society of London 26, 488-500.

Durães, L., Costa, B.F.O., Vasques, J., Campos, J., Portugal, A., 2005. Phase investigation of as-prepared iron oxide/hydroxide produced by sol–gel synthesis. Materials Letters 59, 859-863.

Eisenstark, A., 1998. Bacterial gene products in response to near-ultraviolet radiation. Mutation Research-Fundamental and Molecular Mechanisms of Mutagenesis 422, 85–95.

Esterbauer, H., Cheeseman, K.H., 1990. Determination of aldehydic lipid-peroxidation products - malonaldehyde and 4-hydroxynonenal. Methods in Enzymology 186, 407-421.

Faraldo-Gomez, J.D., Sansom, M.S.P., 2003. Acquisition of siderophores in Gram-negative bacteria. Nat Rev Mol Cell Biol 4, 105-116.

Farré, M.J., Doménech, X., Peral, J., 2007. Combined photo-Fenton and biological treatment for Diuron and Linuron removal from water containing humic acid. Journal of Hazardous Materials 147, 167-174.

Faust, B.C., Zepp, R.G., 1993. Photochemistry of aqueous iron(III)-polycarboxylate complexes: roles in the chemistry of atmospheric and surface waters. Environmental Science & Technology 27, 2517-2522.

Feng, W., Nansheng, D., 2000. Photochemistry of hydrolytic iron (III) species and photoinduced degradation of organic compounds. A minireview. Chemosphere 41, 1137-1147.

Feng, X., Wang, Z., Chen, Y., Tao, T., Wu, F., Zuo, Y., 2012. Effect of Fe(III)/Citrate Concentrations and Ratio on the Photoproduction of Hydroxyl Radicals: Application on the Degradation of Diphenhydramine. Industrial & Engineering Chemistry Research 51, 7007-7012.

Fenton, H.J.H., 1894. Oxidation of tartaric acid in presence of iron. Journal of the Chemical Society, Transactions 65, 899-910.

Field, T.B., McCourt, J.L., McBryde, W.A.E., 1974. Composition and Stability of Iron and Copper Citrate Complexes in Aqueous Solution. Canadian Journal of Chemistry 52, 3119-3124.

Foster, H.A., Ditta, I.B., Varghese, S., Steele, A., 2011. Photocatalytic disinfection using titanium dioxide: Spectrum and mechanism of antimicrobial activity. Applied Microbiology and Biotechnology 90, 1847-1868.

Francis, A.J., Dodge, C.J., 1993. Influence of Complex Structure on the Biodegradation of Iron-Citrate Complexes. Applied and environmental microbiology 59, 109-113.

Fridovich, I., 2011. Superoxide Dismutases: Anti-Versus Pro- Oxidants? Anti-Cancer Agents in Medicinal Chemistry 11, 175-177.

García-Fernández, I., Polo-López, M.I., Oller, I., Fernández-Ibáñez, P., 2012. Bacteria and fungi inactivation using Fe3+/sunlight, H2O2/sunlight and near neutral photo-Fenton: A comparative study. Applied Catalysis B: Environmental 121-122, 20-29.

Garrido-Ramírez, E.G., Theng, B.K.G., Mora, M.L., 2010. Clays and oxide minerals as catalysts and nanocatalysts in Fenton-like reactions — A review. Applied Clay Science 47, 182-192.

Gautier-Luneau, I., Merle, C., Phanon, D., Lebrun, C., Biaso, F., Serratrice, G., Pierre, J.-L., 2005. New Trends in the Chemistry of Iron(III) Citrate Complexes: Correlations between X-ray Structures and Solution Species Probed by Electrospray Mass Spectrometry and Kinetics of Iron Uptake from Citrate by Iron Chelators. Chemistry – A European Journal 11, 2207-2219.

Geeraerd, A.H., Valdramidis, V.P., Van Impe, J.F., 2005. GInaFiT, a freeware tool to assess non-log-linear microbial survivor curves. International Journal of Food Microbiology 102, 95-105.

Gernjak, W., Maldonado, M.I., Malato, S., Cáceres, J., Krutzler, T., Glaser, A., Bauer, R., 2004. Pilot-plant treatment of olive mill wastewater (OMW) by solar TiO2 photocatalysis and solar photo-Fenton. Solar Energy 77, 567-572.

Gogniat, G., Thyssen, M., Denis, M., Pulgarin, C., Dukan, S., 2006. The bactericidal effect of TiO2 photocatalysis involves adsorption onto catalyst and the loss of membrane integrity. FEMS Microbiology Letters 258, 18-24.

Gourmelon, M., Cillard, J., Pommepuy, M., 1994a. Visible-light damage to Escherichia-Coli in seawater - Oxidative stress hypothesis. Journal of Applied Bacteriology 77, 105-112.

Gourmelon, M., Cillard, J., Pommepuy, M., 1994b. Visible light damage to Escherichia coli in seawater: oxidative stress hypothesis. Journal of Applied Microbiology 77, 105-112.

Guillard, C., Bui, T.-H., Felix, C., Moules, V., Lina, B., Lejeune, P., 2008. Microbiological disinfection of water and air by photocatalysis. Comptes Rendus Chimie 11, 107-113.

Gumy, D., Morais, C., Bowen, P., Pulgarin, C., Giraldo, S., Hajdu, R., Kiwi, J., 2006a. Catalytic activity of commercial of TiO2 powders for the abatement of the bacteria (E. coli) under solar simulated light: Influence of the isoelectric point. Applied Catalysis B: Environmental 63, 76-84.

Gumy, D., Rincon, A., Hajdu, R., Pulgarin, C., 2006b. Solar photocatalysis for detoxification and disinfection of water: Different types of suspended and fixed TiO2 catalysts study. Solar Energy 80, 1376-1381.

Gurol, M.D., Lin, S.-S., 2002. Hydrogen Peroxide/Iron Oxide - Induced Catalytic Oxidation of Organic Compounds. Journal of Advanced Oxidation Technologies 5, 147-154.

Gutteridge, J.M.C., 1982. The role of superoxide and hydroxyl radicals in phospholipid peroxidation catalysed by iron salts. Febs Letters 150, 454-458.

Haag, W.R., Hoigné, J., 1985. Photo-sensitized oxidation in natural water via .OH radicals. Chemosphere 14, 1659-1671.

Haber, F., Weiss, J., 1934. The Catalytic Decomposition of Hydrogen Peroxide by Iron Salts. Proceedings of the Royal Society of London. Series A, Mathematical and Physical Sciences 147, 332-351.

Halliwell, B., Chirico, S., 1993. LIPID-PEROXIDATION - ITS MECHANISM, MEASUREMENT, AND SIGNIFICANCE. American Journal of Clinical Nutrition 57, S715-S725.

Halliwell, B., Gutteridge, J.M.C., 1992. BIOLOGICALLY RELEVANT METAL ION-DEPENDENT HYDROXYL RADICAL GENERATION - AN UPDATE. Febs Letters 307, 108-112.

Han, S.K., Hwang, T.M., Yoon, Y., Kang, J.W., 2011. Evidence of singlet oxygen and hydroxyl radical formation in aqueous goethite suspension using spin-trapping electron paramagnetic resonance (EPR). Chemosphere 84, 1095-1101.

Harris, G.D., Adams, V.D., Sorensen, D.L., Curtis, M.S., 1987. Ultraviolet inactivation of selected bacteria and viruses with photoreactivation of the bacteria. Water Res 21, 687-692.

Hartman, P.S., Eisenstark, A., 1978. SYNERGISTIC KILLING OF ESCHERICHIA-COLI BY NEAR-UV RADIATION AND HYDROGEN-PEROXIDE - DISTINCTION BETWEEN RECA-REPAIRABLE AND RECA-NONREPAIRABLE DAMAGE. Journal of Bacteriology 133, 769-774.

He, J., Ma, W., Song, W., Zhao, J., Qian, X., Zhang, S., Yu, J.C., 2005. Photoreaction of aromatic compounds at -FeOOH/H2O interface in the presence of H2O2: evidence for organic-goethite surface complex formation. Water Res 39, 119-128.

He, J., Tao, X., Ma, W.H., Zhao, J.C., 2002. Heterogeneous photo-fenton degradation of an azo dye in aqueous H2O2/iron oxide dispersions at neutral pHs. Chemistry Letters, 86-87.

Helali, S., Polo-López, M.I., Fernández-Ibáñez, P., Ohtani, B., Amano, F., Malato, S., Guillard, C., 2014. Solar photocatalysis: A green technology for E. coli contaminated water disinfection. Effect of concentration and different types of suspended catalyst. Journal of Photochemistry and Photobiology A: Chemistry 276, 31-40.

Henle, E.S., Linn, S., 1997. Formation, prevention, and repair of DNA damage by iron hydrogen peroxide. Journal of Biological Chemistry 272, 19095-19098.

Herrera, F., Pulgarin, C., Nadtochenko, V., Kiwi, J., 1998. Accelerated photo-oxidation of concentrated p-coumaric acid in homogeneous solution. Mechanistic studies, intermediates and precursors formed in the dark. Applied Catalysis B: Environmental 17, 141-156.

Hoerter, J., Pierce, A., Troupe, C., Epperson, J., Eisenstark, A., 1996. Role of Enterobactin and Intracellular Iron in Cell Lethality During Near-UV Irradiation in Escherichia coli. Photochemistry and photobiology 64, 537-541.

Hoerter, J.D., Arnold, A.A., Ward, C.S., Sauer, M., Johnson, S., Fleming, T., Eisenstark, A., 2005. Reduced hydroperoxidase (HPI and HPII) activity in the Δfur mutant contributes to increased sensitivity to UVA radiation in Escherichia coli. Journal of Photochemistry and Photobiology B: Biology 79, 151-157.

Huang, H.-H., Lu, M.-C., Chen, J.-N., 2001. Catalytic Decomposition of Hydrogen Peroxide and 2-chlorophenol with iron oxides. Water Res 35, 2291-2299.

Huang, Z., Maness, P.-C., Blake, D.M., Wolfrum, E.J., Smolinski, S.L., Jacoby, W.A., 2000. Bactericidal mode of titanium dioxide photocatalysis. Journal of Photochemistry and Photobiology A: Chemistry 130, 163-170.

Hutchins, D.A., Witter, A.E., Butler, A., Luther, G.W., 1999. Competition among marine phytoplankton for different chelated iron species. Nature 400, 858-861.

Imlay, J.A., 2003. Pathways of oxidative damage. Annual Review of Microbiology 57, 395-418.

Imlay, J.A., 2008. Cellular defenses against superoxide and hydrogen peroxide. Annual Review of Biochemistry, pp. 755-776.

Ireland, J.C., Klostermann, P., Rice, E.W., Clark, R.M., 1993. Inactivation of Escherichia coli by titanium dioxide photocatalytic oxidation. Applied and environmental microbiology 59, 1668-1670.

Janero, D.R., 1990. Malondialdehyde and thiobarbituric acid-reactivity as diagnostic indices of lipid peroxidation and peroxidative tissue injury. Free Radical Biology & Medicine, 515-540.

Jiménez-Hernández, M.E., Manjón, F., García-Fresnadillo, D., Orellana, G., 2006. Solar water disinfection by singlet oxygen photogenerated with polymer-supported Ru(II) sensitizers. Solar Energy 80, 1382-1387.

Jolivet, J.P., Chaneac, C., Tronc, E., 2004. Iron oxide chemistry. From molecular clusters to extended solid networks. Chem Commun (Camb) 338, 481-487.

Karatas, F., Karatepe, M., Baysar, A., 2002. Determination of free malondialdehyde in human serum by high-performance liquid chromatography. Analytical Biochemistry 311, 76-79.

Katsumata, H., Kaneco, S., Suzuki, T., Ohta, K., Yobiko, Y., 2006. Photo-Fenton degradation of alachlor in the presence of citrate solution. Journal of Photochemistry and Photobiology A: Chemistry 180, 38-45.

Kehoe, S.C., Joyce, T.M., Ibrahim, P., Gillespie, J.B., Shahar, R.A., McGuigan, K.G., 2001. Effect of agitation, turbidity, aluminium foil reflectors and container volume on the inactivation efficiency of batch-process solar disinfectors. Water Res 35, 1061-1065.

Kellogg, E.W., Fridovich, I., 1975. SUPEROXIDE, HYDROGEN-PEROXIDE, AND SINGLET OXYGEN IN LIPID PEROXIDATION BY A XANTHINE-OXIDASE SYSTEM. Journal of Biological Chemistry 250, 8812-8817.

Kenfack, S., Sarria, V., Wethe, J., Cisse, G., Maiga, A.H., Klutse, A., Pulgarin, C., 2009. From Laboratory Studies to the Field Applications of Advanced Oxidation Processes: A Case Study of Technology Transfer from Switzerland to Burkina Faso on the Field of Photochemical Detoxification of Biorecalcitrant Chemical Pollutants in Water. International Journal of Photoenergy.

Khaengraeng, R., Reed, R.H., 2005. Oxygen and photoinactivation of Escherichia coli in UVA and sunlight. Journal of Applied Microbiology 99, 39-50.

Kiwi, J., Gratzel, M., 1987. Light-induced hydrogen formation and photo-uptake of oxygen in colloidal suspensions of α-FE2O3. Journal of the Chemical Society-Faraday Transactions I 83, 1101-1108.

Kiwi, J., Lopez, A., Nadtochenko, V., 2000. Mechanism and Kinetics of the OH-Radical Intervention during Fenton Oxidation in the Presence of a Significant Amount of Radical Scavenger (Cl-). Environmental Science & Technology 34, 2162-2168.

Kiwi, J., Nadtochenko, V., 2004. New evidence for TiO2 photocatalysis during bilayer lipid peroxidation. Journal of Physical Chemistry B 108, 17675-17684.

Klamerth, N., Malato, S., Agüera, A., Fernández-Alba, A., 2013. Photo-Fenton and modified photo-Fenton at neutral pH for the treatment of emerging contaminants in wastewater treatment plant effluents: A comparison. Water research 47, 833-840.

Klamerth, N., Malato, S., Agüera, A., Fernández-Alba, A., Mailhot, G., 2012. Treatment of Municipal Wastewater Treatment Plant Effluents with Modified Photo-Fenton As a Tertiary Treatment for the Degradation of Micro Pollutants and Disinfection. Environmental Science & Technology 46, 2885-2892.

Klamerth, N., Malato, S., Maldonado, M.I., Agüera, A., Fernández-Alba, A., 2011. Modified photo-Fenton for degradation of emerging contaminants in municipal wastewater effluents. Catalysis Today 161, 241-246.

Kong, S.-H., Watts, R.J., Choi, J.-H., 1998. Treatment of petroleum-contaminated soils using iron mineral catalyzed hydrogen peroxide. Chemosphere 37, 1473-1482.

Königsberger, L.-C., Königsberger, E., May, P.M., Hefter, G.T., 2000. Complexation of iron(III) and iron(II) by citrate. Implications for iron speciation in blood plasma. Journal of Inorganic Biochemistry 78, 175-184.

Köster, W., 2001. ABC transporter-mediated uptake of iron, siderophores, heme and vitamin B12. Res. Microbiol 152 291–301.

Krishnamurti, G.S.R., Huang, P.M., 1991. Influence of citrate on the kinetics of Fe(II) oxidation and the formation of iron oxyhydroxides. Clays and Clay Minerals 39, 28-34.

Kwan, W.P., Voelker, B.M., 2003. Rates of Hydroxyl Radical Generation and Organic Compound Oxidation in Mineral-Catalyzed Fenton-like Systems. Environmental Science & Technology 37, 1150-1158.

Kwon, S.-K., Suzuki, S., Saito, M., Waseda, Y., 2006. Atomic-scale structure and morphology of ferric oxyhydroxides formed by corrosion of iron in various aqueous media. Corrosion Science 48, 3675-3691.

Lau, C.K.Y., Ishida, H., Liu, Z.H., Vogel, H.J., 2013. Solution Structure of Escherichia coli FeoA and Its Potential Role in Bacterial Ferrous Iron Transport. Journal of Bacteriology 195, 46-55.

Lee, S., Oh, J., Park, Y., 2006. Degradation of phenol with fenton-like treatment by using heterogeneous catalyst (modified iron oxide) and hydrogen peroxide. Bulletin of the Korean Chemical Society 27, 489-494.

Leland, J.K., Bard, A.J., 1987. Photochemistry of Colloidal Semiconducting Iron-Oxide Polymorphs. Journal of Physical Chemistry 91, 5076-5083.

Liang, C., Bruell, C.J., Marley, M.C., Sperry, K.L., 2004. Persulfate oxidation for in situ remediation of TCE. II. Activated by chelated ferrous ion. Chemosphere 55, 1225-1233.

Liu, P., Duan, W., Wang, Q., Li, X., 2010. The damage of outer membrane of Escherichia coli in the presence of TiO2 combined with UV light. Colloids and Surfaces B: Biointerfaces 78, 171-176.

Lv, X., Xu, Y., Lv, K., Zhang, G., 2005. Photo-assisted degradation of anionic and cationic dyes over iron(III)-loaded resin in the presence of hydrogen peroxide. Journal of Photochemistry and Photobiology A: Chemistry 173, 121-127.

Malato, S., Fernández-Ibáñez, P., Maldonado, M.I., Blanco, J., Gernjak, W., 2009. Decontamination and disinfection of water by solar photocatalysis: Recent overview and trends. Catalysis Today 147, 1-59.

Maness, P.C., Smolinski, S., Blake, D.M., Huang, Z., Wolfrum, E.J., Jacoby, W.A., 1999. Bactericidal activity of photocatalytic TiO2 reaction: Toward an understanding of its killing mechanism. Applied Environmental Microbiology 65, 4094-4098.

Marugan, J., van Grieken, R., Sordo, C., Cruz, C., 2008. Kinetics of the photocatalytic disinfection of Escherichia coli suspensions. Applied Catalysis B-Environmental 82, 27-36.

Matta, R., Hanna, K., Chiron, S., 2007. Fenton-like oxidation of 2,4,6-trinitrotoluene using different iron minerals. Science of the Total Environment 385, 242-251.

Mäusezahl, D., Christen, A., Pacheco, G.D., Tellez, F.A., Iriarte, M., Zapata, M.E., Cevallos, M., Hattendorf, J., Cattaneo, M.D., Arnold, B., Smith, T.A., Colford, J.M., Jr., 2009. Solar Drinking Water Disinfection (SODIS) to Reduce Childhood Diarrhoea in Rural Bolivia: A Cluster-Randomized, Controlled Trial. Plos Medicine 6.

Mazellier, P., Bolte, M., 2000. Heterogeneous light-induced transformation of 2,6-dimethylphenol in aqueous suspensions containing goethite. Journal of Photochemistry and Photobiology A: Chemistry 132, 129-135.

Mazille, F., Moncayo-Lasso, A., Spuhler, D., Serra, A., Peral, J., Benítez, N.L., Pulgarin, C., 2010. Comparative evaluation of polymer surface functionalization techniques before iron oxide deposition. Activity of the iron oxide-coated polymer films in the photo-assisted degradation of organic pollutants and inactivation of bacteria. Chemical Engineering Journal 160, 176-184.

McGuigan, Joyce, Conroy, Gillespie, Elmore, M., 1998. Solar disinfection of drinking water contained in transparent plastic bottles: characterizing the bacterial inactivation process. Journal of Applied Microbiology 84, 1138-1148.

McGuigan, K.G., Conroy, R.M., Mosler, H.J., du Preez, M., Ubomba-Jaswa, E., Fernandez-Ibanez, P., 2012. Solar water disinfection (SODIS): a review from bench-top to roof-top. Journal of hazardous materials 235-236, 29-46.

Meierhofer, R., Wegelin, M., 2002. Solar Water Disinfection: A Guide for the Application of SODIS. Eawag/Sandec, Dübendorf, p. 88.

Michael T. Madigan, John M. Martinko, Parker, J., 2003. Brock Biology of Microorganisms. Prentice Hall-Pearson Education, USA.

Mills, A., Le Hunte, S., 1997. An overview of semiconductor photocatalysis. Journal of Photochemistry and Photobiology A: Chemistry 108, 1-35.

Moncayo-Lasso, A., Mora-Arismendi, L.E., Rengifo-Herrera, J.A., Sanabria, J., Benítez, N., Pulgarin, C., 2012. The detrimental influence of bacteria (E. coli, Shigella and Salmonella) on the degradation of organic compounds (and vice versa) in TiO2 photocatalysis and near-neutral photo-Fenton processes under simulated solar light. Photochemical and Photobiological Sciences 11, 821-827.

Moncayo-Lasso, A., Sanabria, J., Pulgarin, C., Benítez, N., 2009. Simultaneous E. coli inactivation and NOM degradation in river water via photo-Fenton process at natural pH in solar CPC reactor. A new way for enhancing solar disinfection of natural water. Chemosphere 77, 296-300.

Moncayo-Lasso, A., Torres-Palma, R.A., Kiwi, J., Benítez, N., Pulgarin, C., 2008. Bacterial inactivation and organic oxidation via immobilized photo-Fenton reagent on structured silica surfaces. Applied Catalysis B: Environmental 84, 577-583.

Morgan, B., Lahav, O., 2007. The effect of pH on the kinetics of spontaneous Fe(II) oxidation by O2 in aqueous solution – basic principles and a simple heuristic description. Chemosphere 68, 2080-2084.

Murray, C.A., Parsons, S.A., 2004. Removal of NOM from drinking water: Fenton's and photo-Fenton's processes. Chemosphere 54, 1017-1023.

N. Seraghni, S.B., Y. Mameri, N. Debbache, and T. Sehili, 2012. Fe(III)-Citrate-Complex-Induced Photooxidation of 3-Methylphenol in Aqueous Solution. International Journal of Photoenergy 2012.

Nadtochenko, V., Denisov, N., Sarkisov, O., Gumy, D., Pulgarin, C., Kiwi, J., 2006. Laser kinetic spectroscopy of the interfacial charge transfer between membrane cell walls of E. coli and TiO2. Journal of Photochemistry and Photobiology A: Chemistry 181, 401-407.

Nansheng, D., Feng, W., Fan, L., Mei, X., 1998. Ferric citrate-induced photodegradation of dyes in aqueous solutions. Chemosphere 36, 3101-3112.

Ndounla, J., Kenfack, S., Wéthé, J., Pulgarin, C., 2014. Relevant impact of irradiance (vs. dose) and evolution of pH and mineral nitrogen compounds during natural water disinfection by photo-Fenton in a solar CPC reactor. Applied Catalysis B: Environmental 148–149, 144-153.

Ndounla, J., Pulgarin, C., 2014. Evaluation of the efficiency of the photo Fenton disinfection of natural drinking water source during the rainy season in the Sahelian region. Science of the Total Environment 493, 229-238.

Ndounla, J., Spuhler, D., Kenfack, S., Wéthé, J., Pulgarin, C., 2013. Inactivation by solar photo-Fenton in pet bottles of wild enteric bacteria of natural well water: Absence of re-growth after one week of subsequent storage. Applied Catalysis B: Environmental 129, 309-317.

Nieto-Juarez, J.I., Kohn, T., 2013. Virus removal and inactivation by iron (hydr)oxide-mediated Fenton-like processes under sunlight and in the dark. Photochemical & photobiological sciences 12, 1596-1605.

Nieto-Juarez, J.I., Pierzchała, K., Sienkiewicz, A., Kohn, T., 2010. Inactivation of MS2 coliphage in Fenton and Fenton-like systems: role of transition metals, hydrogen peroxide and sunlight. Environmental Science & Technology 44, 3351-3356.

Nogueira, R.F.P., Silva, M.R.A., Trovó, A.G., 2005. Influence of the iron source on the solar photo-Fenton degradation of different classes of organic compounds. Solar Energy 79, 384-392.

Nosaka, Y., Nakamura, M., Hirakawa, T., 2002. Behavior of superoxide radicals formed on TiO2 powder photocatalysts studied by a chemiluminescent probe method. Physical Chemistry Chemical Physics 4, 1088-1092.

Ortega-Gómez, E., Ballesteros Martín, M.M., Carratalà, A., Fernández Ibañez, P., Sánchez Pérez, J.A., Pulgarín, C., 2015. Principal parameters affecting virus inactivation by the solar photo-Fenton process at neutral pH and μM concentrations of H2O2 and Fe2+/3+. Applied Catalysis B: Environmental 174–175, 395-402.

Ortega-Gómez, E., Ballesteros Martín, M.M., Esteban García, B., Sánchez Pérez, J.A., Fernández Ibáñez, P., 2014a. Solar photo-Fenton for water disinfection: An investigation of the competitive role of model organic matter for oxidative species. Applied Catalysis B: Environmental 148–149, 484-489.

Ortega-Gómez, E., Esteban García, B., Ballesteros Martín, M.M., Fernández Ibáñez, P., Sánchez Pérez, J.A., 2013. Inactivation of Enterococcus faecalis in simulated wastewater treatment plant effluent by solar photo-Fenton at initial neutral pH. Catalysis Today 209, 195-200.

Ortega-Gómez, E., Esteban García, B., Ballesteros Martín, M.M., Fernández Ibáñez, P., Sánchez Pérez, J.A., 2014b. Inactivation of natural enteric bacteria in real municipal wastewater by solar photo-Fenton at neutral pH. Water Res 63, 316-324.

Ortega-Gómez, E., Fernández-Ibáñez, P., Ballesteros Martín, M.M., Polo-López, M.I., Esteban García, B., Sánchez Pérez, J.A., 2012. Water disinfection using photo-Fenton: Effect of temperature on Enterococcus faecalis survival. Water Res 46, 6154-6162.

Paciolla, M.D., Davies, G., Jansen, S.A., 1999. Generation of Hydroxyl Radicals from Metal-Loaded Humic Acids. Environmental Science & Technology 33, 1814-1818.

Panias, D., Taxiarchou, M., Paspaliaris, I., Kontopoulos, A., 1996. Mechanisms of dissolution of iron oxides in aqueous oxalic acid solutions. Hydrometallurgy 42, 257-265.

Papoutsakis, S., Brites-Nóbrega, F.F., Pulgarin, C., Malato, S., 2015a. Benefits and limitations of using Fe(III)-EDDS for the treatment of highly contaminated water at near-neutral pH. Journal of Photochemistry and Photobiology A: Chemistry.

Papoutsakis, S., Miralles-Cuevas, S., Oller, I., Garcia Sanchez, J.L., Pulgarin, C., Malato, S., 2015b. Microcontaminant degradation in municipal wastewater treatment plant secondary effluent by EDDS assisted photo-Fenton at near-neutral pH: An experimental design approach. Catalysis Today.

Paul, A., Hackbarth, S., Vogt, R.D., Roder, B., Burnison, B.K., Steinberg, C.E.W., 2004. Photogeneration of singlet oxygen by humic substances: comparison of humic substances of aquatic and terrestrial origin. Photochemical & photobiological sciences 3, 273-280.

Pecson, B.M., Decrey, L., Kohn, T., 2012. Photoinactivation of virus on iron-oxide coated sand: Enhancing inactivation in sunlit waters. Water Res 46, 1763-1770.

Pérez, M., Torrades, F., García-Hortal, J.A., Domènech, X., Peral, J., 2002. Removal of organic contaminants in paper pulp treatment effluents under Fenton and photo-Fenton conditions. Applied Catalysis B: Environmental 36, 63-74.

Peter Schroeder, Krutmann, J., 2010. Textbook of Aging Skin. Springer Berlin Heidelberg.

Pham, A.N., Waite, T.D., 2008. Oxygenation of Fe(II) in the presence of citrate in aqueous solutions at pH 6.0-8.0 and 25 °C: Interpretation from an Fe(II)/citrate speciation perspective. Journal of Physical Chemistry A 112, 643-651.

Pichat, P., Guillard, C., Amalric, L., Renard, A.-C., Plaidy, O., 1995. Assessment of the importance of the role of H2O2 and O2o− in the photocatalytic degradation of 1,2-dimethoxybenzene. Solar Energy Materials and Solar Cells 38, 391-399.

Pigeot-Rémy, S., Simonet, F., Atlan, D., Lazzaroni, J.C., Guillard, C., 2012. Bactericidal efficiency and mode of action: A comparative study of photochemistry and photocatalysis. Water research 46, 3208-3218.

Pigeot-Rémy, S., Simonet, F., Errazuriz-Cerda, E., Lazzaroni, J.C., Atlan, D., Guillard, C., 2011. Photocatalysis and disinfection of water: Identification of potential bacterial targets. Applied Catalysis B: Environmental 104, 390-398.

Pignatello, J.J., Oliveros, E., MacKay, A., 2006. Advanced oxidation processes for organic contaminant destruction based on the Fenton reaction and related chemistry. Critical Reviews in Environmental Science and Technology 36, 1-84.

Pinto, I.S.X., Pacheco, P.H.V.V., Coelho, J.V., Lorençon, E., Ardisson, J.D., Fabris, J.D., de Souza, P.P., Krambrock, K.W.H., Oliveira, L.C.A., Pereira, M.C., 2012. Nanostructured δ-FeOOH: An efficient Fenton-like catalyst for the oxidation of organics in water. Applied Catalysis B: Environmental 119–120, 175-182.

Polo-López, M.I., Castro-Alférez, M., Oller, I., Fernández-Ibáñez, P., 2014. Assessment of solar photo-Fenton, photocatalysis, and H2O2 for removal of phytopathogen fungi spores in synthetic and real effluents of urban wastewater. Chemical Engineering Journal 257, 122-130.

Polo-Lopez, M.I., Garcia-Fernandez, I., Velegraki, T., Katsoni, A., Oller, I., Mantzavinos, D., Fernandez-Ibanez, P., 2012. Mild solar photo-Fenton: An effective tool for the removal of Fusarium from simulated municipal effluents. Applied Catalysis B-Environmental 111, 545-554.

Polo-López, M.I., Oller, I., Fernández-Ibáñez, P., 2013. Benefits of photo-Fenton at low concentrations for solar disinfection of distilled water. A case study: Phytophthora capsici. Catalysis Today 209, 181-187.

Pourzand, C., Watkin, R.D., Brown, J.E., Tyrrell, R.M., 1999. Ultraviolet A radiation induces immediate release of iron in human primary skin fibroblasts: The role of ferritin. Proceedings of the National Academy of Sciences 96, 6751-6756.

Pulgarin, C., Kiwi, J., Nadtochenko, V., 2012. Mechanism of photocatalytic bacterial inactivation on TiO2 films involving cell-wall damage and lysis. Applied Catalysis B: Environmental 128, 179-183.

Quici, N., Morgada, M.E., Gettar, R.T., Bolte, M., Litter, M.I., 2007. Photocatalytic degradation of citric acid under different conditions: TiO2 heterogeneous photocatalysis against homogeneous photolytic processes promoted by Fe(III) and H2O2. Applied Catalysis B: Environmental 71, 117-124.

Raetz, C.R.H., Whitfield, C., 2002. Lipopolysaccharide endotoxins Annual Review of Biochemistry 71, 635-700.

Rajendran, M., Gandhidasan, R., Murugesan, R., 2004. Photosensitisation and photoinduced DNA cleavage by four naturally occurring anthraquinones. Journal of Photochemistry and Photobiology A: Chemistry 168, 67-73.

Reed, R.H., 2004. The inactivation of microbes by sunlight: Solar disinfection as a water treatment process. Advances in Applied Microbiology, Vol 54 54, 333-365.

Reed, R.H., Mani, S.K., Meyer, V., 2000. Solar photo-oxidative disinfection of drinking water: preliminary field observations. Letters in Applied Microbiology 30, 432-436.

Rengifo-Herrera, J.A., Pierzchała, K., Sienkiewicz, A., Forró, L., Kiwi, J., Pulgarin, C., 2009. Abatement of organics and Escherichia coli by N, S co-doped TiO2 under UV and visible light. Implications of the formation of singlet oxygen (1O2) under visible light. Applied Catalysis B: Environmental 88, 398-406.

Rey, F., Calle, E., Casado, J., 1998. Study of the effects of concentration and pH on the dissociation kinetics of Fe(II)-fulvic acid complexes. International Journal of Chemical Kinetics 30, 63-67.

Rincón, A.-G., Pulgarin, C., 2006. Comparative evaluation of Fe3+ and TiO2 photoassisted processes in solar photocatalytic disinfection of water. Applied Catalysis B: Environmental 63, 222-231.

Rincón, A.-G., Pulgarin, C., 2007a. Absence of E. coli regrowth after Fe3+ and TiO2 solar photoassisted disinfection of water in CPC solar photoreactor. Catalysis Today 124, 204-214.

Rincón, A.-G., Pulgarin, C., 2007b. Fe3+ and TiO2 solar-light-assisted inactivation of E. coli at field scale. Catalysis Today 122, 128-136.

Rincon, A.G., Pulgarin, C., Adler, N., Peringer, P., 2001. Interaction between E-coli inactivation and DBP-precursors - dihydroxybenzene isomers - in the photocatalytic process of drinking-water disinfection with TiO2. Journal of Photochemistry and Photobiology a-Chemistry 139, 233-241.

Robertson, P.K.J., Robertson, J.M.C., Bahnemann, D.W., 2012. Removal of microorganisms and their chemical metabolites from water using semiconductor photocatalysis. Journal of Hazardous Materials 211-212, 161-171.

Rodríguez-Chueca, J., Mediano, A., Ormad, M.P., Mosteo, R., Ovelleiro, J.L., 2014a. Disinfection of wastewater effluents with the Fenton-like process induced by electromagnetic fields. Water Res 60, 250-258.

Rodriguez-Chueca, J., Morales, M., Mosteo, R., Ormad, M.P., Ovelleiro, J.L., 2013. Inactivation of Enterococcus faecalis, Pseudomonas aeruginosa and Escherichia coli present in treated urban wastewater by coagulation-flocculation and photo-Fenton processes. Photochemical & photobiological sciences 12, 864-871.

Rodríguez-Chueca, J., Polo-López, M.I., Mosteo, R., Ormad, M.P., Fernández-Ibáñez, P., 2014b. Disinfection of real and simulated urban wastewater effluents using a mild solar photo-Fenton. Applied Catalysis B: Environmental 150-151, 619-629.

Ruales-Lonfat, C., Barona, J.F., Sienkiewicz, A., Bensimon, M., Vélez-Colmenares, J., Benítez, N., Pulgarín, C., 2015. Iron oxides semiconductors are efficients for solar water disinfection: A comparison with photo-Fenton processes at neutral pH. Applied Catalysis B: Environmental 166–167, 497-508.

Ruales-Lonfat, C., Benítez, N., Sienkiewicz, A., Pulgarín, C., 2014. Deleterious effect of homogeneous and heterogeneous near-neutral photo-Fenton system on Escherichia coli. Comparison with photo-catalytic action of TiO2 during cell envelope disruption. Applied Catalysis B: Environmental 160–161, 286-297.

Ruales-Lonfat, C., Varón, A., Barona, J., Moncayo-Lasso, A., Benítez, N., Pulgarìn, C., 2013. Iron-catalyzed low cost solar activated process for drinking water disinfection in Colombian rural areas. Technologies for Sustainable Development, pp. 1-16.

Rubio, D., Nebot, E., Casanueva, J.F., Pulgarin, C., 2013. Comparative effect of simulated solar light, UV, UV/H2O2 and photo-Fenton treatment (UV–Vis/H2O2/Fe2+,3+) in the Escherichia coli inactivation in artificial seawater. Water research 47, 6367-6379.

S.Sunglin., M.G., 1998. Catalytic Decomposition of Hydrogen Peroxide on Iron Oxide: Kinetics, Mechanism, and Implications. Environ. Sci. Technol. 32, 1417-1423.

Saito, T., Iwase, T., Horie, J., Morioka, T., 1992. Mode of photocatalytic bactericidal action of powdered semiconductor TIO2 on mutans streptococci. Journal of Photochemistry and Photobiology B-Biology 14, 369-379.

Sandvik, S.L.H., Bilski, P., Pakulski, J.D., Chignell, C.F., Coffin, R.B., 2000. Photogeneration of singlet oxygen and free radicals in dissolved organic matter isolated from the Mississippi and Atchafalaya River plumes. Marine Chemistry 69, 139-152.

Santilli, C.V., Onillon, M., Bonnet, J.P., 1990. Influence of the elaboration and dehydration conditions of Fe(III) hydrous oxides on the characteristics of resulting α-Fe2O3 powders. Ceramics International 16, 89-97.

Sciacca, F., Rengifo-Herrera, J.A., Wéthé, J., Pulgarin, C., 2010. Dramatic enhancement of solar disinfection (SODIS) of wild Salmonella sp. in PET bottles by H2O2 addition on natural water of Burkina Faso containing dissolved iron. Chemosphere 78, 1186-1191.

Sciacca, F., Rengifo-Herrera, J.A., Wéthé, J., Pulgarin, C., 2011. Solar disinfection of wild Salmonella sp. in natural water with a 18L CPC photoreactor: Detrimental effect of non-sterile storage of treated water. Solar Energy 85, 1399-1408.

Shin, S., Yoon, H., Jang, J., 2008. Polymer-encapsulated iron oxide nanoparticles as highly efficient Fenton catalysts. Catalysis Communications 10, 178-182.

Sillanpaa, M., Pirkanniemi, K., 2001. Recent Developments in Chelate Degradation. Environmental technology 22, 791-801.

Silva, M.R.A., Trovó, A.G., Nogueira, R.F.P., 2007. Degradation of the herbicide tebuthiuron using solar photo-Fenton process and ferric citrate complex at circumneutral pH. Journal of Photochemistry and Photobiology A: Chemistry 191, 187-192.

Smith, K.C., Wang, T.-C.V., Sharma, R.C., 1987. recA-Dependent DNA repair in UV-irradiated Escherichia coli. Journal of Photochemistry and Photobiology B: Biology 1, 1-11.

Soboleva, N.M., Saprykina, M.N., Kosinova, V.N., Nosonovich, A.A., Goncharuk, V.V., 2012. Inactivation of Candida albicans in the photo-fenton system. Journal of Water Chemistry and Technology 34, 96-102.

Spuhler, D., Andrés Rengifo-Herrera, J., Pulgarin, C., 2010. The effect of Fe2+, Fe3+, H2O2 and the photo-Fenton reagent at near neutral pH on the solar disinfection (SODIS) at low temperatures of water containing Escherichia coli K12. Applied Catalysis B: Environmental 96, 126-141.

Stefaniak, A.B., Harvey, C.J., Bukowski, V.C., Leonard, S.S., 2010. Comparison of free radical generation by pre- and post-sintered cemented carbide particles. Journal of Occupational and Environmental Hygiene 7, 23-34.

Sulzberger, B., Laubscher, H., 1995. Reactivity of various types of iron(III) (hydr)oxides towards light-induced dissolution. Marine Chemistry 50, 103-115.

Sun, D.D., Tay, J.H., Tan, K.M., 2003. Photocatalytic degradation of E. coliform in water. Water research 37, 3452-3462.

Sun, Y., Pignatello, J.J., 1992. Chemical treatment of pesticide wastes. Evaluation of iron(III) chelates for catalytic hydrogen peroxide oxidation of 2,4-D at circumneutral pH. Journal of Agricultural and Food Chemistry 40, 322-327.

Sun, Y., Pignatello, J.J., 1993. Activation of hydrogen peroxide by iron(III) chelates for abiotic degradation of herbicides and insecticides in water. Journal of Agricultural and Food Chemistry 41, 308-312.

Sun, Z.-X., Su, F.-W., Forsling, W., Samskog, P.-O., 1998. Surface characteristics of magnetite in aqueous suspension. Journal of Colloid and Interface Science 197, 151-159.

Sunada, K., Kikuchi, Y., Hashimoto, K., Fujishima, A., 1998. Bactericidal and Detoxification Effects of TiO2 Thin Film Photocatalysts. Environmental Science & Technology 32, 726-728.

Sunada, K., Watanabe, T., Hashimoto, K., 2003. Studies on photokilling of bacteria on TiO2 thin film. Journal of Photochemistry and Photobiology A: Chemistry 156, 227-233.

Swetha, S., Kumari Singh, M., Minchitha, K.U., Geetha Balakrishna, R., 2012. Elucidation of cell killing mechanism by comparative analysis of photoreactions on different types of bacteria. Photochemistry and photobiology 88, 414-422.

Sychev, Y.A., Isak, G.V., 1995. Iron compounds and the mechanisms of the homogeneous catalysis of the activation of O_2 and H_2O_2 and of the oxidaiton of organic substrates. Russian Chemical Reviews 64, 1105–1129.

Tabet, D., Saidi, M., Houari, M., Pichat, P., Khalaf, H., 2006. Fe-pillared clay as a Fenton-type heterogeneous catalyst for cinnamic acid degradation. Journal of Environmental Management 80, 342-346.

Tan, K.H., 2003. Humic matter in soil and the environment. Principles and controversies. New York, NY, USA

Thabet, S., Weiss-Gayet, M., Dappozze, F., Cotton, P., Guillard, C., 2013. Photocatalysis on yeast cells: Toward targets and mechanisms. Applied Catalysis B: Environmental 140–141, 169-178.

TitanPE Technologies, I., 2011. http://www.naprotec.be/uploaded/Sterilization%20by%20Titanium%20and%20Silver%20coatings.pdf . Shanghai.

Trovó, A.G., Nogueira, R.F.P., 2011. Diclofenac abatement using modified solar photo-fenton process with ammonium iron(III) citrate. Journal of the Brazilian Chemical Society 22, 1033-1039.

Tsaknis, J., Lalas, S., Tychopoulos, V., Hole, M., Smith, G., 1998. Rapid high-performance liquid chromatographic method of determining malondialdehyde for evaluation of rancidity in edible oils. The Analyst 123, 325-327.

Tyrrell, R.M., Pourzand, C.A., Brown, J., Hejmadi, V., Kvam, V., Ryter, S., Watkin , R.D., 2000. Cellular Studies with UVA Radiation: A Role for Iron. Radiation Protection Dosimetry 91, 37-39.

UNICEF, WHO, 2012. Progress on Drinking water and Sanitation 2012 update. WHO/UNICEF Joint Monitoring Programme for Water Supply and Sanitation. WHO, United States of America, p. 66.

UNICEF, WHO, 2013. Progress on sanitation and drinking-water - 2013 update. World Health Organization and UNICEF, France, p. 40.

Upritchard, H.G., Yang, J., Bremer, P.J., Lamont, I.L., McQuillan, A.J., 2007. Adsorption to metal oxides of the pseudomonas aeruginosa siderophore pyoverdine and implications for bacterial biofilm formation on metals. Langmuir 23, 7189-7195.

Veréb, G., Manczinger, L., Bozsó, G., Sienkiewicz, A., Forró, L., Mogyorósi, K., Hernádi, K., Dombi, A., 2013. Comparison of the photocatalytic efficiencies of bare and doped rutile and anatase TiO2 photocatalysts under visible light for phenol degradation and E. coli inactivation. Applied Catalysis B: Environmental 129, 566-574.

Vikesland, P.J., Heathcock, A.M., Rebodos, R.L., Makus, K.E., 2007. Particle size and aggregation effects on magnetite reactivity toward carbon tetrachloride. Environmental Science & Technology 41, 5277-5283.

Vukosav, P., Mlakar, M., Tomišić, V., 2012. Revision of iron(III)–citrate speciation in aqueous solution. Voltammetric and spectrophotometric studies. Analytica Chimica Acta 745, 85-91.

Vukosav, P., Tomišić, V., Mlakar, M., 2010. Iron(III)-Complexes Engaged in the Biochemical Processes in Seawater. II. Voltammetry of Fe(III)-Malate Complexes in Model Aqueous Solution. Electroanalysis 22, 2179-2186.

Waite, T.D., Morel, F.M.M., 1984. Photoreductive dissolution of colloidal iron oxides in natural waters. Environmental Science & Technology 18, 860-868.

Wang, C., Liu, H., Sun, Z., 2012. Heterogeneous photo-Fenton reaction catalyzed by nanosized iron oxides for water treatment. International Journal of Photoenergy 2012, 1-10.

Wang, Z., Guo, Y., Liu, Z., Feng, X., Chen, Y., Tao, T., 2015. Catechin as a new improving agent for a photo-Fenton-like system at near-neutral pH for the removal of inderal. Photochem Photobiol Sci 14, 473-480.

Wang, Z., Liu, Z., Yu, F., Zhu, J., Chen, Y., Tao, T., 2013. Siderophore-modified Fenton-like system for the degradation of propranolol in aqueous solutions at near neutral pH values. Chemical Engineering Journal 229, 177-182.

Wegelin, M., Canonica, S., Meschner, K., Fleishmann, T., Pesaro, F., Metzler, A., 1994. Solar water disinfection: scope of the process and analysis of radiation experiments. Journal of Water Supply: Research and Technology-AQUA 43, 154-169.

Wenk, J., Von Gunten, U., Canonica, S., 2011. Effect of dissolved organic matter on the transformation of contaminants induced by excited triplet states and the hydroxyl radical. Environmental Science and Technology 45, 1334-1340.

Whitelam, G.C., Codd, G.A., 1982. A rapid whole-cell assay for superoxide dismutase. Analytical Biochemistry 121, 207-212.

WHO, 2007. Combating waterborne disease at the household level. In: WHO (Ed.), The International Network to Promote Household Water Treatment and Safe Storage. World Health Organization, Geneva, Switzerland, p. 35.

WHO, W.H.O., 2011. Guidelines for Drinking-Water Quality. In: ed.), t. (Ed.), Geneva

WHO/UNICEF, 2013. Ending Preventable Child Deaths from Pneumonia and Diarrhoea by 2025. The integrated Global Action Plan for Pneumonia and Diarrhoea (GAPPD), Geneva.

Widdel, F., Schnell, S., Heising, S., Ehrenreich, A., Assmus, B., Schink, B., 1993. Ferrous iron oxidation by anoxygenic phototrophic bacteria. Nature 362, 834-836.

Wu, F., Deng, N.S., 2000. Photochemistry of hydrolytic iron (III) species and photoinduced degradation of organic compounds. A minireview. Chemosphere 41, 1137-1147.

Xu, J., Sahai, N., Eggleston, C.M., Schoonen, M.A.A., 2013. Reactive oxygen species at the oxide/water interface: Formation mechanisms and implications for prebiotic chemistry and the origin of life. Earth and Planetary Science Letters 363, 156-167.

Xu, P., Zeng, G.M., Huang, D.L., Feng, C.L., Hu, S., Zhao, M.H., Lai, C., Wei, Z., Huang, C., Xie, G.X., Liu, Z.F., 2012. Use of iron oxide nanomaterials in wastewater treatment: a review. The Science of the total environment 424, 1-10.

Xu, Y., Schoonen, M.A.A., 2000. The absolute energy positions of conduction and valence bands of selected semiconducting minerals. American Mineralogist 85, 543-556.

Xue, X., Hanna, K., Deng, N., 2009. Fenton-like oxidation of Rhodamine B in the presence of two types of iron (II, III) oxide. Journal of hazardous materials 166, 407-414.

Yuan, B., Xu, J., Li, X., Fu, M.-L., 2013. Preparation of Si–Al/α-FeOOH catalyst from an iron-containing waste and surface–catalytic oxidation of methylene blue at neutral pH value in the presence of H2O2. Chemical Engineering Journal 226, 181-188.

Zepp, R.G., Faust, B.C., Hoigne, J., 1992. Hydroxyl Radical Formation in Aqueous Reactions (pH 3-8) of Iron(II) with Hydrogen-Peroxide - The Photo-Fenton Reaction. Environmental Science & Technology 26, 313-319.

Zepp, R.G., Wolfe, N.L., Baughman, G.L., Hollis, R.C., 1977. SINGLET OXYGEN IN NATURAL-WATERS. Nature 267, 421-423.

Zhan, M., 2009. Determination of photochemically-generated reactive oxygen species in natural water. Journal of Environmental Sciences 21, 303-306.

Zhan, M., Yang, X., Xian, Q., Kong, L., 2006. Photosensitized degradation of bisphenol A involving reactive oxygen species in the presence of humic substances. Chemosphere 63, 378-386.

Zhang, C., Wang, L., Wu, F., Deng, N., 2006. Quantitation of Hydroxyl Radicals from Photolysis of Fe(III)-Citrate Complexes in Aerobic Water (5 pp). Env Sci Poll Res Int 13, 156-160.

Zhangl, Z., Boxall, C., Kelsall, G.H., 1993. Photoelectrophoresis of colloidal iron oxides 1. Hematite (α-Fe2O3). Colloids and Surfaces A: Physicochemical and Engineering Aspects 73 145-163.

Curriculum vitae

LONFAT Cristina
Rue de la Dixence 6
1950 Sion
Tél. 078 656 68 77
Email: cris.lonfat@gmail.com

Formation académique

2011-2015	**Doctorat ès sciences** à l'Ecole polytechnique fédérale de Lausanne (EPFL). Sujet: «Les oxydes de fer et le citrate de fer comme nouveaux photocatalyseurs pour l'inactivation d'*Escherichia coli* dans l'eau: aspects mécanistiques» ;
2008-2010	**Master en sciences chimiques** à l'Université de Valle, Colombie. Titre du Mémoire: «Suivi et évaluation des pesticides présents dans différentes matrices (eau, sol et poissons) de la ville de Cali et impact sur l'apparition des malformations congénitales» ;
2002-2007	**Licence en chimie** à l'Université de Cauca, Colombie. Sujet du Mémoire: «Identification, séparation et quantification par chromatographie en phase liquide à haute performance (CLHP) de Stevioside et Rebaudioside présents dans le miel de Stevia».

Formation continue

2014	Introduction au traitement de l'eau au domicile et au stockage sûr. Cours organisé par l'EPFL en collaboration avec SANDEC EAWAG (réussi avec mention) ;
2013	Formation en correspondante de sécurité d'unité (COSEC), dispensée par le domaine sécurité, prévention et santé (DSPS), EPFL ;
2011	Décontamination et désinfection de l'eau et de l'air par des procédés d'oxydation avancée. Cours organisé par le Centre de l'Energie, de l'Environnement et de la Technologie (CIEMAT), Madrid Espagne ;
2007	Formation sur la norme ISO 9000:2000. Systèmes de contrôle de qualité. Cours organisé par le Service national d'apprentissage SENA, Popayán, Colombie ;
2007	Système de Management Environnemental (SME), Certification ISO 14001, SENA, Popayán, Colombie ;
2007	Gestion de projets, SENA, Popayán, Colombie.

Expériences professionnelles

2011-2014   Assistante de recherche à l'Institut des sciences et ingénierie chimiques de l'EPFL ;

2012-2014   Coordinatrice de sécurité d'unité et de prévention de la santé à l'EPFL, Institut des sciences et ingénierie chimiques ;

2009-2011   Séjour de recherche à l'EPFL, *Id* ;

2008-2008   Séjour de recherche à l'EPFL, laboratoire central environnemental ;

2007-2009   Assistante d'enseignement au département de chimie de l'Université de Valle, Colombie ;

2004-2006   Responsable du laboratoire des analyses physico-chimiques et du contrôle qualité en chimie des produits naturels à l'Université de Cauca, Colombie.

Projets de recherche

- Développement d'un processus solaire bon marché catalysé par le fer pour la désinfection de l'eau potable dans les zones rurales de Colombie. Programme de collaboration entre l'Université de Valle et l'EPFL soutenu par le Fond National Suisse (FNS, projet No IZ70Z0_131312/1-2) ;

- Estimation et analyse spatiale des émissions de polluants dans le sol et l'eau à partir d'un site d'enfouissement sanitaire à Cali (Colombie) : polluants organiques et métaux. Programme de collaboration entre l'Université de Valle et l'EPFL («Seed Money Project») ;

- Développement de nouvelles alternatives de l'apiculture: validation des méthodes analytiques pour analyser le miel fait avec le sirop à base de fruits, de stevia, d'eucalyptus et de soja", Université de Cauca, Colombie.

Bourses obtenues

2009-2011   Bourse de la Confédération suisse, séjour de recherche dans l'Institut des sciences et ingénierie chimiques, EPFL ;

2008-2008   Séjour de recherche à l'EPFL, laboratoire central environnemental, financé par le project: «Seed Money Project» ;

2007-2009   Bourse offerte par l'Université de Valle, Colombie, lors de la réalisation du Master.

Publications

1. **C. Ruales-Lonfat,** J.F. Barona N. Benítez, A. Sienkiewicz, C. Pulgarín. Iron oxides semiconductors are efficient for solar water disinfection: A comparison with photo-Fenton processes at neutral pH, Applied Catalysis B: Environmental, 166–167 (2015) 497-508 ;

2. **C. Ruales-Lonfat,** N. Benítez, A. Sienkiewicz, C. Pulgarín, Deleterious effect of homogeneous and heterogeneous near-neutral photo-Fenton system on *Escherichia coli*. Comparison with photo-catalytic action of TiO_2 during cell envelope disruption, Applied Catalysis B: Environmental, 160–161 (2014) 286-297 ;

3. **C. Ruales-Lonfat,** A. Varón, J. Barona, A. Moncayo-Lasso, N. Benítez, C. Pulgarìn, Iron-catalyzed low cost solar activated process for drinking water disinfection in Colombian rural areas, Technologies for Sustainable Development, (2013) 1-16 ;

4. L.A. Lenis, **C. Ruales C**., R. Benitez B., Determination of glycosides, in express honey of stevia (Stevia rebaudiana) by liquid chromatography, Biotecnología en el Sector Agropecuario y Agroindustrial, 11 (2013) 85-91 ;

5. O. Baghriche, **C. Ruales**, R. Sanjines, C. Pulgarin, A. Zertal, I. Stolitchnov, J. Kiwi, Ag-surfaces sputtered by DC and pulsed DC-magnetron sputtering effective in bacterial inactivation: Testing and characterization, Surface and Coatings Technology, 206 (2012) 2410-2416 ;

6. Osorio-Vargas, R. Sanjines, **C. Ruales**, C. Castro, C. Pulgarin, A.J. Rengifo-Herrera, J.C. Lavanchy, J. Kiwi, Antimicrobial Cu-functionalized surfaces prepared by bipolar asymmetric DC-pulsed magnetron sputtering (DCP), Journal of Photochemistry and Photobiology A: Chemistry, 220 (2011) 70-76 ;

7. A. Torres, **C. Ruales**, C. Pulgarin, A. Aimable, P. Bowen, V. Sarria, J. Kiwi, Innovative High-Surface-Area CuO Pretreated Cotton Effective in Bacterial Inactivation under Visible Light, ACS Applied Materials & Interfaces, 2 (2010) 2547-2552 ;

8. **C. Ruales-Lonfat**, J.F. Barona N. Benítez, A. Sienkiewicz, C. Pulgarín, Bacterial inactivation with iron citrate complex: a new source of dissolved iron in solar photo-Fenton process at neutral and alkaline pH. Applied Catalysis B: Environmental, summited ;

9. **C. Ruales-Lonfat**, J. J. Vélez-Colmenares, J. Ndounla C. Pulgarín. Enhancement of Solar disinfection by Fenton reactants ($Fe^{2+, 3+}$, H_2O_2) at neutral and alkaline pH on natural water from Colombia, Burkina Faso, and Switzerland. Influence of Irradiance, Turbidity and type of Microorganisms. Liter of Light Switzerland, summited ;

10. Stefanos Giannakis, **Cristina Ruales-Lonfat**, Sana Thabet, Pascale Cotton, César Pulgarin. Internal photo-Fenton leads the solar inactivation of *Saccharomyces cerevisiae* in hv/H_2O_2/Fe systems at neutral pH. Applied Catalysis B: Environmental, summited.